Characterization of uterine activity by electrohysterography

Document Version:
Publisher's PDF, also known as Version of Record (includes final page, issue and volume numbers)

Please check the document version of this publication:

• A submitted manuscript is the version of the article upon submission and before peer-review. There can be important differences between the submitted version and the official published version of record. People interested in the research are advised to contact the author for the final version of the publication, or visit the DOI to the publisher's website.
• The final author version and the galley proof are versions of the publication after peer review.
• The final published version features the final layout of the paper including the volume, issue and page numbers.

Link to publication

Characterization of uterine activity by electrohysterography

PROEFSCHRIFT

ter verkrijging van de graad van doctor aan de Technische
Universiteit Eindhoven, op gezag van de rector magnificus,
prof.dr.ir. C.J. van Duijn, voor een commissie aangewezen door
het College voor Promoties in het openbaar te verdedigen op
maandag 26 april 2010 om 16.00 uur

door

Chiara Rabotti

geboren te Florence, Italië

Dit proefschrift is goedgekeurd door de promotoren:

prof.dr.ir. J.W.M. Bergmans
en
prof.dr. S.G. Oei

Copromotor:
dr.ir. M. Mischi

To Luigi and to my father, the 'men of science' that I love the most

Summary

Characterization of uterine activity by electrohysterography

A growing number of pregnancies is complicated by miscarriage, preterm delivery, and birth defects, with consequent health problems later in life. It is therefore increasingly important to monitor the health status of mother and fetus, so as to permit timely medical intervention when acute health risks are detected. For timely recognition of complications, quantitative assessment of uterine activity can be fundamental during both pregnancy and delivery.

During pregnancy, timely prediction of preterm delivery can improve the effectiveness of the required treatments. Unfortunately, the prognostic techniques employed in current obstetrical practice, namely, uterine contraction measurements using an elastic belt (external tocography), cervical change evaluation, and the use of biomarkers like fetal fibronectin, have been demonstrated to be inaccurate for the prediction of preterm delivery. In the last stage of pregnancy and during labor, contractions are routinely monitored. Especially when complications occur, e.g., when labor shows poor progress, quantitative assessment of uterine activity can guide the physician to choose a uterine contraction induction or augmentation, a cesarean section, or other therapies. Furthermore, monitoring the fetal heart response to the uterine activity (cardiotography) is widely used as a screening test for timely recognition of fetal distress (e.g. asphyxia). However, in current obstetrical practice, accurate quantitative assessment of the uterine contractions can be provided only invasively and during labor. The current golden standard for contraction monitoring, which is based on the direct internal uterine pressure (IUP) measurement by an intrauterine catheter, can be risky and its use is generally limited to very complicated deliveries.

The contractile element of the uterus is the myometrium, which is composed of smooth muscle cells. Uterine contractions are caused by electrical activity in the form of action potentials (AP) that propagate through the myometrium cells. Electrohysterography is the measurement of the uterine electrical activity and can be performed by electrodes placed on the abdomen. Electrohysterographic (EHG) measurements

are inexpensive and noninvasive. Moreover, it has been demonstrated that the non-invasively recorded EHG signal is representative of those APs that, by propagating from cell to cell, are the root cause of a uterine contraction. Therefore, in view of the limitation of current obstetrical practice, significant benefits could be expected from the introduction of EHG signal analysis for routine contraction monitoring.

Previous studies highlighted the potential prognostic and diagnostic value of EHG signal analysis, but did not investigate the possibility of accurately estimating the IUP from noninvasive EHG recordings. Moreover, important issues like the effect of the tissues interposed between the uterus and the skin (volume conductor) on EHG recordings have not been studied. Besides, EHG signal interpretation has been typically based on single-channel measurements, while the use of multiple electrodes conveys additional information (e.g., distribution and dynamics of the electrical activation) that can possibly be predictive of delivery.

In this thesis, we focus on the analysis of the EHG signal as an alternative to existing techniques for predicting preterm delivery and monitoring uterine contractions during both pregnancy and delivery. The main goal of this work is to contribute to the technical basis which is required for the introduction of electrohysterography in everyday clinical practice.

A major part of this thesis investigates the possibility of using electrohysterography to replace invasive IUP measurements. A novel method for IUP estimation from EHG recordings is developed in the first part of this thesis. The estimates provided by the method are compared to the IUP invasively recorded on women during delivery and result in a root mean squared error (RMSE) with respect to the reference invasive IUP recording as low as 5 mmHg, which is comparable to the accuracy of the invasive golden standard.

Another important objective of this thesis work is to contribute to the introduction of novel techniques for timely prediction of preterm delivery. As the spreading of electrical activity at the myometrium is the root cause of coordinated and effective contractions, i.e., contractions that are capable of pushing the fetus down into the birth canal ultimately leading to delivery, a multichannel analysis of the spatial propagation properties of the EHG signal could provide a fundamental contribution for predicting delivery. A thorough study of the EHG signal propagation properties is therefore carried out in this work. Parameters related to the EHG that are potentially predictive of delivery, such as the uterine area where the contraction originates (pacemaker area) or the distribution and dynamics of the EHG propagation vector, can be derived from the delay by which the signal is detected at multiple locations over the whole abdomen.

To analyze the propagation of EHG signals on a large scale (cm), a method is designed for calculating the detection delay among the EHG signals recorded by multiple electrodes. Relative to existing interelectrode delay estimators, this method

improves the accuracy of the delay estimates for interelectrode distances larger than 5-10 cm. The use of a large interelectrode distance aims at the assessment of the EHG propagation properties through the whole uterine muscle using a limited number of sensors. The method estimates values of velocity within the physiological range and highlights the upper part of the uterus as the most frequent (65%) pacemaker area during labor. Besides, our study suggests that more insight is needed on the effect that tissues interposed between uterus and skin (volume conductor) have on the EHG signal.

With the aim of improving the current interpretation and measurement accuracy of EHG parameters with potential clinical relevance, such as the conduction velocity (CV), a volume conductor model for the EHG signal is introduced and validated. The intracellular AP at the myometrium is analytically modeled in the spatial domain by a 2-parameter exponential in the form of a Gamma variate function. The unknown atomical parameters of the volume conductor model are the thicknesses of the biological tissues interposed between the uterus and the abdominal surface. These model parameters can be measured by echography for validation. The EHG signal is recorded by an electrode matrix on women with contractions. In order to increase the spatial resolution of the EHG measurements and reduce the geometrical and electrical differences among the tissues below the recording locations, electrodes with a reduced surface and smaller interelectrode distance are needed relative to the previous studies on electrohysterography. The EHG signal is recorded, for the first time, by a 64-channel (8×8) high-density electrode grid, comprising 1 mm diameter electrodes with 4 mm interelectrode distance. The model parameters are estimated in the spatial frequency domain from the recorded EHG signal by a least mean square method. The model is validated by comparing the thickness of the biological tissues recorded by echography to the values estimated using the mathematical model. The agreement between the two measures (RMSE = 1 mm and correlation coefficient, $R = 0.94$) suggests the model to be representative of the underlying physiology.

In the last part of this dissertation, the analysis of the EHG signal propagation focuses on the CV estimation of single surface APs. As on a large scale this parameter cannot be accurately derived, the propagation analysis is here carried out on a small scale (mm). Also for this analysis, the EHG signal is therefore recorded by a 3×3 cm^2 high-density electrode grid containing 64 electrodes (8×8). A new method based on maximum likelihood estimation is then applied in two spatial dimensions to provide an accurate estimate of amplitude and direction of the AP CV. Simulation results prove the proposed method to be more robust to noise than the standard techniques used for other electrophysiological signals, leading to over 56% improvement of the RMS CV estimate accuracy. Furthermore, values of CV between 2 cm/s and 12 cm/s, which are in agreement with invasive and *in-vitro* measurements described in the literature, are obtained from real measurements on ten women in labor.

In conclusion, this research provides a quantitative characterization of uterine contractions by EHG signal analysis. Based on an extensive validation, this thesis indicates that uterine contractions can be accurately monitored noninvasively by dedicated analysis of the EHG signal. Furthermore, our results open the way to new clinical studies and applications aimed at improving the understanding of the electrophysiological mechanisms leading to labor, possibly reducing the incidence of preterm delivery and improving the perinatal outcome.

List of abbreviations

AP	Action potential
CCF	Cross-correlation function
CV	Conduction velocity
DFT	Discrete Fourier transform
DRL	Driven right leg (electrode)
ECG	Electrocardiogram
EHG	Electrohysterography
EMG	Electromyography
FHR	Fetal heart-rate
FIR	Finite impulse response
FM	Frequency modulation
HD	High-density (electrode)
HR	Heart-rate
IUP	Internal uterine pressure
MECG	Maternal electrocardiogram
ML	Maximum likelihood
PD	Phase difference
REF	Reference (electrode)
RMS	Root mean square
RMSE	Root mean squared error
SD	Standard deviation
SNR	Signal-to-noise ratio
TF	Time-frequency
TFD	Time-frequency distribution
WT	Wavelet transform

Contents

Chapter 1

Introduction

> *I numeri primi sono divisibili soltanto per 1 e per se stessi. Se ne stanno al loro posto nell' infinita serie dei numeri naturali, schiacciati come tutti fra due, ma un passo in là rispetto agli altri. Sono numeri sospettosi e solitari... (P. Giordano)* [1]

Preterm birth, i.e., birth before completing the 37th week of gestation, is still a major cause of infant mortality and morbidity. In the last decades, a better understanding of risk factors and mechanisms related to preterm birth has led to the introduction of several measures to reduce its incidence. However, in most industrialized countries the preterm birth rate is still 12% and it accounts for 75% of perinatal mortality and more than 50% of long term morbidity [1], with an associated annual societal economic cost that, in the United States alone, was estimated to amount to 26.2 billion US dollars in 2005 [2].

About 30% of preterm births are the result of indicated preterm delivery, i.e., labor is induced or the baby is delivered by prelabor Cesarean section before completing the 37th week of gestation. Common reasons for indicated preterm delivery include hypertension accompanied by protein in the urine (pre-eclampsia), mother's seizures (eclampsia), and uterine growth restriction. In up to 70% of preterm births, the obstetric precursor is spontaneous preterm labor in the form of preterm uterine contractions with intact membranes (40-45% of spontaneous preterm labor) or premature membrane rupture (25-30% of spontaneous preterm labor) [1].

The pathogenesis of spontaneous preterm labor is not well understood: spontaneous preterm contractions might be caused by an early activation of the normal labor process or by other (unknown) pathological causes [1, 3, 4]. Most obstetric interventions to reduce the incidence of spontaneous preterm delivery have been focused

---

[1] 'Prime numbers are divisible only by 1 and by themselves. They stand in their place in the infinite series of natural numbers, squashed in between two others, like all other numbers, but a step further on than the rest. They are suspicious and solitary...'. From 'La solitudine dei numeri primi' (published in English as 'The solitude of prime numbers').

on inhibiting premature contractions by tocolytic agents in order to temporarily delay delivery, therefore permitting the administration of antenatal steroids along with mother's transfer to a hospital where appropriate care can be provided. However, the effectiveness of tocolytic agents requires early introduction of the therapy. The onset of active labor, leading eventually to the delivery of the fetus, is the result of a preparatory phase which induces in the uterus the electrophysiological changes required to produce forceful and coordinated contractions [5]. At a certain point of the preparatory phase, this process becomes irreversible; after this point, even with the latest tocolytics, delivery cannot be delayed for more than few days [5].

Although an early treatment improves the effectiveness of tocolytics [6, 7], their indiscriminate use at the first signs of preterm delivery can be risky for mother and fetus [8]. Therefore, timely recognition of the process leading to labor is of prime importance to discriminate preterm physiological contractions that are unproductive, i.e., will not soon lead to delivery, from efficient contractions, i.e., contractions that will induce a progressive cervical dilatation and soon lead to delivery. Besides symptomatic self monitoring and cervical change evaluation, current methods employed in clinical practice during pregnancy are based on uterine contraction monitoring. The use of biomarkers, such as fibronectin, has also been recently proposed as a screening test for preterm labor prediction. Unfortunately, none of these methods can reliably discriminate between unproductive and efficient uterine contractions probably because the method analysis is based on parameters that are independent of the irreversible uterine preparatory stage necessary for active labor to take place [5, 9, 10].

During delivery, contractions are routinely and constantly monitored. Especially when complications occur, e.g., when labor shows poor progress, quantitative assessment of uterine contraction efficiency can guide the physician to choose a uterine contraction induction or augmentation, a Cesarean section, or other therapies. Furthermore, monitoring the response of the fetal heart to the uterine activity (cardiotocography) is widely used in clinical practice as a screening test for timely recognition of fetal distress (e.g., asphyxia) [11].

The first result of a contraction is an increase of the internal uterine pressure (IUP). The techniques used in clinical practice for uterine contraction monitoring mainly rely on the direct (internal) or indirect (external) measurement of the IUP. External tocography is currently the most widely used technique to monitor the uterus during pregnancy and delivery [12]. A tocodynamometer consists of a strain gauge transducer placed around the external surface of the abdomen and has the primary advantage of being noninvasive. However, due to the fact that it is an indirect mechanical measurement of the pressure increase, the signal provided by external tocography is characterized by a low sensitivity. Poor sensitivity can affect the estimation accuracy of contraction amplitude and duration [5, 13, 14]. Since external tocography only conveys accurate information on the contraction rate, it is well established that

this technique is neither accurate for prediction of preterm delivery during pregnancy, nor for quantification of uterine efficiency during labor.

During delivery, quantitative information concerning uterine efficiency can be provided invasively, by measuring the amniotic IUP with an internal uterine pressure catheter (IUPC). However, the employment of an IUPC requires the rupture of the membranes and, due to its invasiveness, this device can increase the risk of infections and even cause damages to the fetus [15, 16]. Therefore, the use of an IUPC is usually limited to complicated cases.

The contractile element of the uterus is the myometrium, which is a smooth muscle. Smooth muscle is an involuntary, non striated muscle, which presents significant anatomical and physiological differences relative to (striated) skeletal muscle [17]. The physiological basis of uterine contractions is the cyclic depolarization and repolarization of the smooth muscle cells composing the myometrium [18]. Early in pregnancy, the poor electrical coupling among the cells is responsible for the quiescent status of the uterus. As delivery approaches, the formation of low resistance electrical paths (gap junctions) allows the propagation of electrical activity from cell to cell in the form of action potentials (APs) [19]. The propagation of APs through an adequate number of cells results in a coordinated mechanical contraction of the myometrium, capable of inducing progressive cervical dilatation and producing an increase of the IUP acting towards the expulsion of the fetus at the end of delivery [18, 20, 21]. Usually, APs occur in groups (bursts) and each electrical burst corresponds to a uterine contraction.

Electrohysterography (EHG) is the noninvasive measurement the electrical activity underlying uterine contractions. The first EHG signal ever reported in the literature was measured in 1931 as the deflection of a galvanometric needle during a uterine contraction [22]. This pioneering measurement unveiled a signal with great potentials, since EHG measurements are inexpensive and noninvasive. Moreover, as it is indicative of the root cause of a contraction [12, 15, 18, 23], EHG may not only replace the invasive or inaccurate methods that are currently employed for contraction monitoring during labor, but could also be an alternative tool for predicting delivery.

Due to the need for a noninvasive and reliable method aimed at following the evolution of the uterine activity, predicting the delivery time, and understanding the processes underlying the onset of labor, the interest in EHG has progressively increased. At the same time, since the pioneering measurements in the early 30s, the recording techniques have significantly advanced and computer technology has opened new possibilities for signal analysis. Nevertheless, EHG measurements are not yet adopted in obstetric practice.

The numerous unsolved issues related to EHG analysis and interpretation make the introduction of EHG measurements in routine clinical practice still a challenging objective for both scientists and physicians. Besides the need for establishing a more

solid knowledge of the physiology underlying uterine contractions, a prerequisite for such a challenging objective is the development of dedicated signal analysis techniques that permit detection and interpretation of parameters of potentially clinical relevance. Moreover, extensive clinical studies are required for understanding the link between the parameters derived from the EHG signal and the processes leading to labor.

Over the years it has been scientifically established that the EHG signal is representative of the electrical changes occurring in the myometrial cells and initiating a contraction [18]. Several studies investigated the use of the noninvasively recorded EHG signal for predicting labor and discriminating effective contractions leading to preterm delivery from unproductive physiological uterine activity. Overall, many parameters derived from the EHG signal have been considered, both in time [18, 24–26] and in frequency domain [4, 18, 24, 25, 27, 28]. Typically, EHG signal interpretation has been based on single-channel measurements. The shift of the EHG burst frequency components from lower frequencies, during pregnancy, to higher frequencies, during labor, seems the most significant variation and one of the earliest observable characteristics, observed in both term and preterm delivery by several studies [28, 29]. Despite these promising observations, a proper frequency threshold for an accurate contraction discrimination and delivery prediction over a broad range of patients could not be determined [29].

It has been suggested that the spectral changes of the EHG signal observed during the progression of pregnancy may be due to the increased cell excitability and improved electrical coupling [4]. Only few studies have recorded the intracellular electrical activity of the human myometrium, and the current knowledge of uterine physiology was mainly obtained by animal studies [21, 30–32]. The role of gap junctions for the propagation of the electrical activity, their presence and necessity during parturition, and their hormone-dependent regulation were also scientifically established by animal investigation [33–36]. Modeling techniques mainly focused on the intracellular AP. The temporal evolution of the AP was modeled as a function of a large number of electrophysiological parameters related to ionic concentrations [37, 38].

There are several important aspects related to the EHG signal interpretation that have not been addressed by previous studies. The possibility of replacing invasive IUPC by noninvasive EHG measurements was suggested only very recently [39, 40]. However, a poor accuracy of the estimation [39] and the required use of the IUPC signal [40], hamper the feasibility of the previously proposed methods in a clinical environment.

The spreading of electrical activity in the myometrium is the first cause of a coordinated and effective contraction and could therefore represent a fundamental parameter to follow the process leading to labor and to accurately predict the time to deliv-

ery [18, 36]. However, the propagation properties of the EHG signal have received little attention and have been mostly investigated *in-vitro* or in animals [36, 41]. Noticeably, most of the previous studies were based on single-channel measurements, with only few exceptional studies on animals employing multichannel grid electrodes [42]. Besides, the conduction pattern of electrical activation at the myometrium and the effect of the tissues interposed between the uterus and the skin (volume conductor) are key aspects of the EHG measurement and interpretation that are not yet fully understood [41]. In general, possibly due to these unexplained aspects, most of the previous literature on EHG signal analysis has investigated the properties of the whole burst of APs [43] and only little attention has been dedicated to the analysis of single surface APs extracted from the EHG burst [41]. In the context of surface recordings, by surface AP, or simply AP, we refer to a single spike extracted from a single channel EHG burst that, being recorded noninvasively, is the weighted average of the electrical activity of all the underlying excited cells [44, 45].

In this context, important advances for improving the current interpretation and measurement accuracy of EHG parameters with potential clinical relevance, e.g., the AP conduction velocity (CV), could be achieved by the introduction and validation of mathematical models that can reliably describe the cellular AP and the EHG volume conductor. The models of the cellular AP previously proposed [37, 38] provide an accurate representation of the biochemical processes underlying the generation of APs; however, for clinical applications, a significant reduction of the number of parameters is required. Furthermore, the myometrium-skin volume conductor has been only partially investigated and it is typically considered as a homogeneous infinite layer [37, 46]. A complete understanding of the volume conductor effect operated by the different tissue layers is fundamental to support the EHG signal measurement and interpretation and, ultimately, for the development of accurate prognostic and diagnostic tools based on EHG.

In this thesis, we focus on the analysis of the EHG signal as an alternative to existing techniques for characterizing the uterine activity, predicting preterm delivery, and monitoring uterine contractions during both pregnancy and delivery. The goal of this work is to contribute to the technical basis which is required for the introduction of the EHG signal analysis in clinical practice. To this end, we propose dedicated models and methods to improve the current measurement and interpretation accuracy of EHG parameters with established or potential clinical relevance for pregnancy monitoring. Our contribution is structured in four main objectives:

1. Proposing an accurate method for the noninvasive estimation of the IUP;

2. Designing a dedicated method for estimating the spatial propagation of EHG bursts on a large scale (cm) as a potential parameter for contraction assessment and delivery prediction;

3. Introducing and validating a 4-layer mathematical model of the volume conductor and a two-parameter analytical representation of the myometrium AP;

4. Analyzing the EHG propagation on a small scale (mm) and proposing a new method for noninvasive estimation of the CV of single surface APs extracted from the EHG signal.

An additional novelty relatively to previous studies is the employment, in some of the methods proposed in this thesis, of an improved spatial resolution (high-density) electrode grid.

The EHG measurement and analysis methods proposed in this thesis are tightly linked to background physiology. As the knowledge of smooth muscle physiology is not as well established as that of the other muscles, the physiology underlying uterine contractions is described in the first part of Chapter 2 as a synthesis of previous studies. In order to position the proposed methods in a clinical context, the methods that are currently employed in clinical practice for contraction monitoring and delivery prediction are reported and discussed in the second part of Chapter 2.

In Chapter 3, we propose a new method for assessing noninvasively the uterine mechanical activity as measured by an invasive IUPC. Only recently, few studies focused on EHG analysis as an alternative to existing methods for a quantitative estimation of the uterine mechanical activity [39, 40]. The physiological assumptions underlying these previous methods can be summarized in the use of only the EHG amplitude as indicative of the mechanical tension produced by the contracting myometrium. The proposed method is fundamentally conceived on the basis of the physiologic phenomena underling the generation of the recorded signals and regards the IUP increase as the result of the joint contribution of frequency and amplitude of the EHG signal. Simultaneous recordings by an IUP catheter confirm that the proposed method, probably due to the physiology-based approach, outperforms those previously proposed with an accuracy which is comparable to that of the golden standard.

Another important objective of this thesis work is to contribute to the introduction of novel techniques for timely prediction of preterm delivery. As the spreading of electrical activity at the myometrium is the root cause of coordinated and effective contractions, a multichannel analysis of the spatial propagation properties of the EHG signal could provide a fundamental contribution for predicting delivery. In Chapter 4, a thorough study of the EHG signal propagation properties is carried out on a large scale (cm). Parameters related to the EHG that are potentially predictive of delivery, such as the uterine area where the contraction originates (pacemaker area) or the distribution and dynamics of the EHG propagation vector, can be derived from the delay by which the EHg burst is detected at multiple locations over the whole abdomen. In this Chapter, a method is therefore designed for estimating the detection delay

among the EHG signals recorded by multiple electrodes. Relative to existing inter-electrode delay estimators, this method has an improved estimation accuracy when interelectrode distances larger than 5-10 cm are used. The use of a large interelectrode distance aims at the assessment of the EHG propagation properties through the whole uterine muscle using a limited number of sensors. Measurements by eight electrodes on women in labor confirm the feasibility of the method for clinical practice and highlight the upper part of the uterus as the most frequent location of the pacemaker area.

In order to improve the current interpretation and measurement accuracy of EHG parameters with potential clinical relevance, such as the CV, a volume conductor model for the EHG signal is introduced and validated in Chapter 5. A myometrium-skin conduction model is developed which consists of a four-layer model obtained by extension of previous studies reported in the literature for the skeletal electromyogram, which were based on simulations [47]. The volume conductor effect is formalized in the spatial-frequency domain by a transfer function that accounts for the physical and geometrical properties of the biological tissues interposed between the myometrium and the recording site on the skin. The unknown anatomical parameters of the volume conductor model are reduced to the thicknesses of these biological tissues. The tissue thicknesses can be measured by echography for validation. The intracellular AP at the myometrium is analytically modeled in the spatial domain by a 2-parameter exponential in the form of a Gamma variate function [48]. The EHG signal is recorded by an electrode matrix on women with contractions. In order to increase the spatial resolution of the EHG measurements and reduce the geometrical and electrical differences among the tissues below the recording locations, electrodes with a reduced surface and smaller interelectrode distance are needed relative to the previous studies on EHG. The EHG signal is recorded, for the first time, by a high-density electrode grid. The model parameters are estimated in the spatial frequency domain from the recorded EHG signal by a least mean square method. The model is validated by comparing the thickness of the biological tissues recorded by echography to the values estimated using the mathematical model.

In Chapter 6, the analysis of the EHG signal propagation focuses on the CV estimation of single surface APs. As on a large scale this parameter cannot be accurately derived, the propagation analysis is here carried out on a small scale (mm). Also for this analysis, the EHG signal is therefore recorded by a 3×3 cm^2 high-density electrode grid containing 64 electrodes (8×8). New methods based on maximum likelihood estimation are then applied in two spatial dimensions to provide an accurate estimate of amplitude and direction of the AP CV. Simulation results prove the proposed method to be more robust to noise than the standard techniques used for other electrophysiological signals. Recordings on women in labor confirm the clinical feasibility of the methods.

The concluding remarks of this thesis are given in Chapter 7 with some suggestions for possible future work.

The methods and results reported in this thesis have been published in several journal articles and conference proceedings. In particular, with reference to the section *List of author's publications*, Chapter 3 integrates [JP-6] and [IC-3]. Chapter 4 and Chapter 5 have been published as [JP-5] and [JP-3], respectively, and Chapter 6 has been submitted as [JP-2].

List of author's publications

Journal Papers

[JP-1] P. G. C. Vinken, C. Rabotti, M. Mischi, J. O. E. H. van Laar and S. G. Oei, "Nifedipine-induced changes in the electrohysterogram of preterm contractions: feasibility in clinical practice," submitted to Obstetrics and Gynecology International.

[JP-2] C. Rabotti, M. Mischi, S. G. Oei, J. W. M. Bergmans, "Noninvasive estimation of the electrohysterographic action-potential conduction velocity," IEEE Trans. Biomed. Eng., conditional acceptance.

[JP-3] C. Rabotti, M. Mischi, L.Beulen, S. G. Oei, J. W. M. Bergmans, "Modeling and identification of the electrohysterographic volume conductor by high-density electrodes," IEEE Trans. Biomed. Eng., vol.57 , pp. 519 - 527, 2010.

[JP-4] P. G. C. Vinken, C. Rabotti, M. Mischi, S. G. Oei, "Accuracy of frequency-related parameters of the electrohysterogram for predicting preterm delivery: a review of the literature," Obstet. Gynecol. Surv., vol. 64, n. 8, 529 - 541, 2009.

[JP-5] C. Rabotti, M. Mischi, J. O. E. H. van Laar, S. G. Oei, J. W. M. Bergmans, "Inter-electrode delay estimators for electrohysterographic propagation analysis," Physiol. Meas., vol. 30, pp.745 - 761, 2009.

[JP-6] C. Rabotti, M. Mischi, J. O. E. H. van Laar, S. G. Oei, J. W. M. Bergmans, "Estimation of internal uterine pressure by joint amplitude and frequency analysis of electrohysterographic signals," Physiol. Meas., vol. 29, pp. 829 - 841, 2008.

[JP-7] S. M. M. Martens, C. Rabotti, M. Mischi, and R.J. Sluijter, "A robust fetal ECG detection method for abdominal recordings," Physiol. Meas., vol. 28, pp. 373 - 388, 2007. **Martin Black prize for best paper in Physiological Measurement in 2007.**

International conferences proceedings

[IC-1] C. Rabotti, M. Mischi, S. G. Oei, and J. W. M. Bergmans, "Electrohysterographic volume conductor model validation by high-density electrodes," 18th Congress of the International Society of Electrophysiology and Kinesiology, Aalborg, Denmark, October 16 - 19, 2010.

[IC-2] C. Rabotti, M. Mischi, L. Beulen, J. W. M. Bergmans, and S. G. Oei, "Mathematical modeling of the electrohysterogram: understanding the origin of uterine contractions for preterm delivery prediction," 9th World Congress of perinatal medicine, Berlin, Germany, October 24 - 28, 2009.

[IC-3] M. Mischi, C. Rabotti, L. P. J. Vosters, S. G. Oei, and J. W. M. Bergmans, "Electrohysterographic conduction velocity estimation," IEEE-EMBS Proc. on the 31st Annual International Conference, Minneapolis, USA, Sep. 2 - 7, 2009, pp. 6934 - 6939.

[IC-4] C. Rabotti, M. Mischi, J. O. E. H. van Laar, S. G. Oei, and J. W. M. Bergmans, "Myometrium electromechanical modeling for internal uterine pressure estimation by electrohysterography," IEEE-EMBS Proc. on the 31st Annual International Conference, Minneapolis, USA, Sept. 2 - 7, 2009, pp. 6259 - 6262.

[IC-5] C. Rabotti, M. Mischi, M. Gamba, M. Vinken, S. G. Oei, and J. W. M. Bergmans, "Identification of the electrohysterographic volume conductor by high-density electrodes," 4th European Congress for Medical and Biomedical Engineering, Antwerp, Belgium, 23 - 27 November 2008, pp. 235 - 238.

[IC-6] C. Rabotti, M. Mischi, J. O. E. H. van Laar, S. G. Oei, and J. W. M. Bergmans, "On the propagation analysis of electrohysterographic signals," IEEE-EMBS Proc. on the 30th Annual International Conference, Vancouver, Canada, August 20 - 24, 2008, pp. 3868 - 3871.

[IC-7] P. G. C. Vinken, C. Rabotti, S. G. Oei, "Accuracy of frequency-related parameters of the EHG for predicting preterm delivery: a review of the literature," 35th annual meeting of the fetal and neonatal physiological society, Maastricht, the Netherlands, 22 - 25 June 2008, p132.

[IC-8] P. G. C. Vinken, C. Rabotti, S. G. Oei, "Effects of tocolytics on the electrohysterographic signal of preterm contractions," 35th annual meeting of the fetal and neonatal physiological society, Maastricht, the Netherlands, 22 - 25 June 2008, p. 39.

[IC-9] C. Rabotti, M. Mischi, J. O. E. H. van Laar, S. G. Oei, and J. W. M. Bergmans, "Non-invasive estimation of the uterine pressure by electrohysterography," 8th

world congress of perinatal medicine, Florence, Italy, 9 - 13 September, 2007, Journal of Perinatal Medicine, vol. 35, supplement II, p. s85.

[IC-10] C. Rabotti, M. Mischi, S. G. Oei, and J. W. M. Bergmans, "Electrohysterographic analysis of uterine contraction propagation with labor progression: a preliminary study," IEEE-EMBS Proc. on the 29th Annual International Conference, Lyon, France, Aug. 23 - 26, 2007, pp. 4135 - 4138.

[IC-11] C. Rabotti, M. Mischi, J. O. E. H. van Laar, P. Aelen, S. G. Oei, and J. W. M. Bergmans, "Relationship between electrohysterogram and internal uterine pressure: a preliminary study," IEEE-EMBS Proc. on the 28th Annual International Conference, New York, USA, 30 Aug. - 3 Sep., 2006, pp. 1661 - 1664.

Regional conferences proceedings

[RC-1] C. Rabotti, M. Mischi, L. Beulen, S. G. Oei, and J. W. M. Bergmans, "Electrohysterographic volume conductor modeling," 4th Annual symposium of the IEEE-EMBS Benelux Chapter, Twente, Nov. 9 - 10, 2009.

[RC-2] C. Rabotti, M. Mischi, J. O. E. H. van Laar, S. G. Oei, and J. W. M. Bergmans, "Intrauterine pressure estimation by Time-Frequency analysis of electrohysterograms," 1st IEEE/EMBS Benelux Symposium, Brussels, Dec. 7 - 8, 2006, pp. 72 - 75.

[RC-3] P. Aelen, C. Rabotti, M. Mischi, B. De Vries, J. O. E. H. van Laar, S. G. Oei, and J. W. M. Bergmans, "Electrohysterographic estimation of intra uterine pressure," IEEE SPS DARTS Symposium, Antwerpen, March 28 - 29, 2006.

Technical reports

[TR-1] C. Rabotti and M. Mischi, "Fetal monitoring: state of the art", Internal Report SPS Group, Eindhoven University of Technology, 2006.

Bibliography

[1] R.L. Goldenberg, J.F. Culhane, J.D. Jams, and R. Romero, "Epidemiology and causes of preterm birth," *Lancet*, vol. 371, pp. 75–84, 2008.

[2] R.E. Behrman and A.S Butler, *Preterm Birth: Causes, Consequences, and Prevention*, The National Academy Press, Washington, DC, 2007.

[3] H. Leman, C. Marque, and J. Gondry, "Use of the electrohysterogram signal for characterization of contractions during pregnancy," *IEEE Trans. Biomed. Eng.*, vol. 46, pp. 1222–1229, 1999.

[4] W.L. Maner, R.E. Garfield, H. Maul, G. Olson, and G. Saade, "Predicting term and preterm delivery with transabdominal uterine electromyography," *Obstet. Gynecol.*, vol. 101, pp. 1254–1260, 2003.

[5] R.E. Garfield, H. Maul, L. Shi, W. Maner, C. Fittkow, G. Olsen, and G.R. Saade, "Methods and devices for the management of term and preterm labor," *Ann. NY Acad.Sci.*, vol. 943, pp. 203–224, 2001.

[6] M. Mclean, A. Walters, and R. Smith, "Prediction and early diagnosis of preterm labour: a critical review," *Obstet. Gynecol. Surv.*, vol. 48, pp. 209–225, 1993.

[7] E. Amon, C. Midkiff, H. Winn, W. Holcomb, J. Shumway, and R. Artal, "Tocolysis with advanced cervical dilatation," *Obstet. Gynecol.*, vol. 95, pp. 358–362, 2000.

[8] N. M. Fisk and J. Chan, "The case for tocolysis in threatened preterm labour," *BJOG*, vol. 110, no. s20, pp. 98–102, 2003.

[9] J.D. Iams, "Prediction and early detection of preterm labor," *Obstet. Gynecol.*, vol. 101, pp. 402–412, 2003.

[10] H.M. McNamara, "Problems and challenges in the management of preterm labor," *BJOG*, vol. 110, pp. 79–85, 2003.

[11] R.K. Freeman, T.J. Garite, and M.P. Nageotte, *Fetal heart rate monitoring*, Lippincott William & Wilkins, Philadelphia, PA, 2003.

[12] R.E. Garfield, G. Saade, C. Buhimschi, I. Buhimschi, L. Shi, S.Q. Shi, and K. Chwalisz, "Control and assessment of the uterus and cervix during pregnancy and labor," *Hum. Reprod. Update*, vol. 4, pp. 673–695, 1998.

[13] H. Eswaran, J.D. Wilson, P. Murphy an H. Preissl, and C.L. Lowery, "Application of Wavelet tranform to uterine electromyographic signals recorded using abdominal surface electrodes," *J. Matern.-Fetal Neonatal Med.*, vol. 11, pp. 158–166, 2002.

[14] A.M. Miles, M. Monga, and K.S. Richeson, "Correlation of external and internal monitoring of uterine activity in a cohort of term patients," *Am. J. Perinatol.*, vol. 18, pp. 137–140, 2001.

[15] R.E. Garfield, H. Maul, W. Maner, C. Fittkow, G. Olson, L. Shi, and G. R. Saade, "Uterine electromyography and light-induced fluorescence in the management of term and preterm labor," *J. Soc. Gynecol. Invest.*, vol. 9, pp. 265–275, 2002.

[16] F.A. Wilmink, F.F. Wilms, R Heydanus, B.W. Mol, and D.N. Papatsonis, "Fetal complications after placement of an intrauterine pressure catheter: a report of two cases and review of the literature," *J. Matern. Fetal. Neonatal. Med.*, vol. 21, pp. 880–883, 2008.

[17] E. Fischer, "Vertebrate smooth muscle," *Physiol. Rev.*, vol. 24, pp. 467–490, 1944.

[18] C. Buhimschi and R.E. Garfield, "Uterine activity during pregnancy and labor assessed by simultaneous recordings from the myometrium and abdominal surface in the rat," *Am. J. Obstet. Gynecol.*, vol. 178, pp. 811–822, 1998.

[19] C. Buhimschi and R.E. Garfield, "Uterine contractility as assessed by abdominal surface recording of electromyographic activity in rats during pregancy," *Am. J. Obstet. Gynecol.*, vol. 174, pp. 744–753, 1996.

[20] G.M.J.A. Wolfs and M. van Leeuwen, "Electromyographic observations on the human uterus during labour," *Acta Obstet. Gynecol. Scand.*, vol. 58, pp. 1–61, 1979.

[21] T. Chard and J. Grudzinskas, *The uterus*, Cambridge University Press, 1994.

[22] O. Bode, "Das elektrohysterogramm," *Arch. Gyndk.*, vol. 28, pp. 123–128, 1931.

[23] D. Devedeux, C. Marque, S. Mansour, G. Germain, and J. Duchêne, "Uterine electromyography: a critical review," *Am. J. Obstet. Gynecol.*, vol. 169, pp. 1636–1653, 1993.

[24] I. Verdenik, M. Pajntar, and B. Leskošek, "Uterine electrical activity as predictor of preterm birth in women with preterm contractions," *Eur. J. Obstet. Gynecol. Reprod. Biol.*, vol. 95, pp. 149–153, 2001.

[25] C. Marque, J. Duchêne, S. Leclercq, G. Panczer, and J. Chaumont, "Uterine EHG processing for obstetrical monitoring," *IEEE Trans. Biomed. Eng.*, vol. BME-33, pp. 1182–1187, 1986.

[26] J. Duchêne, C. Marque, and S. Planque, "Uterine EMG signal: propagation analysis," in *IEEE EMBS Proc. Int. Conference*, 1990, pp. 831–832.

[27] R.E. Garfield, W.L. Maner, L.B. MacKay, D. Schlembach, and G.R. Saade, "Comparing uterine electromyography activity of antepartum patients versus term labor patients," *Am. J. Obstet. Gynecol.*, vol. 193, pp. 23–29, 2005.

[28] M. Doret, R. Bukowski, M. Longo, H. Maul, W.L. Maner, R.E. Garfield, and G.R. Saade, "Uterine electromyography characteristics for early diagnosis of mifepristone-induced preterm labor," *Obstet. Gynecol.*, vol. 105, pp. 822–830, 2005.

[29] M.P.G.C. Vinken, C. Rabotti, S.G. Oei, and M. Mischi, "Accuracy of frequency-related parameters of the electrohysterogram for predicting preterm delivery: a review of the literature," *Ob. Gyn. Survey*, vol. 64, pp. 529–541, 2009.

[30] J.M. Marshall, "Regulation of activity in uterine smooth muscle," *Physiol. Rev. Suppl.*, vol. 5, pp. 213–227, 1962.

[31] S. Kanda and H. Kuriyama, "Specific features of smooth muscle cells recorded from the myometrium of pregnant rats," *J. Physiol.*, vol. 299, pp. 127–144, 1980.

[32] H. Kuriyama and A. Csapo, "A study of the parturient uterus with the micro-electrode technique," *Endocrinology*, vol. 68, pp. 1010–1025, 1961.

[33] R.E. Garfield, S. Sims, E.E. Daniel, et al., "Gap junctions: their presence and necessity in myometrium during parturition," *Science*, vol. 198, pp. 958–960, 1977.

[34] R.E. Garfield, M.S. Kannan, and E.E. Daniel, "Gap junction formation in myometrium: control by estrogens, progesterone, and prostaglandins," *Am. J. Physiol.*, vol. 238, pp. C81–C89, 1980.

[35] R. E. Garfield and R. H. Hayashi, "Appearance of gap junctions in the myometrium of women during labor," *Am. J. Obstet. Gynecol.*, vol. 140, pp. 254–260, 1981.

[36] S.M. Miller, R.E. Garfield, and E.E. Daniel, "Improved propagation in myometrium associated with gap junctions during parturition," *Am. J. Physiol. Cell. Physiol.*, vol. 256, pp. C130–C141, 1989.

[37] S. Rihana and C. Marque, "Preterm labor-modeling the uterine electrical activity from cellular level to surface recording," in *IEEE EMBS Proc. Int. Conference*, 2008, pp. 3726–3729.

[38] L. Bursztyn, O. Eytan, A. J. Jaffa, and D. Elad, "Mathematical model of excitation-contraction in a uterine smooth muscle cell," *Am. J. Physiol. cell. Physiol.*, vol. 292, pp. C1816–C1829, 2007.

[39] J. Jezewski, K. Horoba, A.Matonia, and J. Wrobel, "Quantitative analysis of contraction patterns in electrical activity signal of pregnant uterus as an alternative to mechanical approach," *Physiol. Meas.*, vol. 26, pp. 753–767, 2005.

[40] M.D. Skowronski, J.G. Harris, D.E. Marossero, R.K. Edwards, and T.Y. Euliano, "Prediction of intrauterine pressure from electrohysterography using optimal linear filtering," *IEEE Trans. Biomed. Eng.*, vol. 53, pp. 1983–1989, 2006.

[41] W.J.E.P. Lammers, H. Mirghani, B. Stephen, S. Dhanasekaran, A. Wahab, and M.A.H. Al Sultan, "Patterns of electrical propagation in the intact guinea pig uterus," *Am. J. Physiol. Regul. Integr. Comp. Physiol.*, vol. 294, pp. R919–R928, 2008.

[42] W.J.E.P. Lammers, K. Arafat, A. El-Kays, and T.Y. El-Sharkawy, "Spatial and temporal variation in local spike propagation in the myometrium of the 17-day pregnant rat," *Am. J. Physiol. Cell. Physiol.*, vol. 267, pp. C1210–C1223, 1994.

[43] J. Planes, J. Morucci, H. Grandjean, and R. Favretto, "External recording and processing of fast electrical activity of the uterus in human parturition," *Med. Biol. Eng. Comput.*, vol. 22, pp. 585–591, 1984.

[44] M.J. Zwarts and D.F. Stegeman, "Multichannel surface EMG: basic aspects and clinical utility," *Muscle Nerve*, vol. 28, pp. 1–17, 2003.

[45] J.P. van Dijk, D.F. Stegeman, and M.J. Lapatki, B.G.and Zwarts, "Evidence of potential averaging over the finite surface of a bioelectric electrode using high-density EMG," in *XVI Congr. of the ISEK*, 2006, p. 62.

[46] C. K. Marque, J. Terrien, S. Rihana, and G. Germain, "Preterm labour detection by use of a biophysical marker: the uterine electrical activity," *BMC Pregnancy Childbirth*, vol. 7 Suppl 1:S5, pp. 2393–7, 2007.

[47] D. Farina and A. Rainoldi, "Compensation of the effect of sub-cutaneous tissue layers on surface EMG: a simulation study," *Med. Eng. Phys.*, vol. 21, pp. 487–496, 1999.

[48] D.F. Stegeman, J.H. Blok, H. J. Hermens, and K. Roeleveld, "Surface EMG models: properties and applications," *J. Electromyogr. Kines.*, vol. 10, pp. 313–326, 2000.

Chapter 2

Uterine contraction and clinical practice

The act of birth is the first experience attended by anxiety, and thus the source and model of the affect of anxiety (S. Freud) [1]

2.1 Introduction

The object of this thesis is the characterization of the uterine contractions during pregnancy. The uterus is a heterogeneous organ composed of many cell types with a predominance of smooth muscle cells. Smooth muscle is an involuntary, non striated muscle. In general, physiologists tend to underline that, differently from striated (skeletal) muscles, for smooth muscles important differences exists between various smooth tissues of the same species and between anatomically and functionally comparable smooth muscles of related species [1]. While striated muscles are all organs with a comparable locomotive function and consist of only muscle tissue, smooth muscles are generally, with few exceptions, only elements contributing together with other tissues to the anatomy of the whole organ.

The smooth muscle is composed of smaller fibers, usually 1 to 5 μm in diameter and 20 to 500 μm in length. Skeletal muscle fibers, by comparison, can be 30 times larger and hundreds of times longer. Furthermore, isolated muscle elements of smooth muscles do not exhibit the functions of the whole organ, like the striated fibers of skeletal muscles, but only those connected with contractility [1]. An additional peculiarity of the uterus with respect to other smooth muscle organs such as the gastrointestinal tract, bladder, airways, and blood vessels, is that the myometrium is normally functional for only brief periods, e.g, following gestation during parturition [2].

Skeletal and cardiac muscles have been studied much more thoroughly and extensively than smooth ones. Relative to the skeletal muscle, the smooth cell structure is fundamentally different and the processes leading to contraction is more complex. Therefore, the physiological properties of smooth muscle cannot be simply derived

---

[1] Sigmund Freud, 'The Interpretation of Dreams', third English edition.

from the well established knowledge on skeletal muscle.

Knowledge of the structure of the myometrium and the factors that regulate uterine contractility during pregnancy is necessary for a thorough comprehension of the mechanisms that maintain the uterus in a quiescent state during pregnancy and then convert it to an active and reactive state during labor. Besides, the EHG measurement and analysis methods proposed in this thesis are tightly linked to the underlying physiological process. The first part of this chapter will therefore be dedicated to the physiology of the uterus and to the factors that regulate the uterine contractility during pregnancy and labor.

The main motivation of this thesis is the need for noninvasive tools for accurately predicting labor and assessment of uterine contractions. This need arises, on the one hand, from the compromise between accuracy and invasiveness imposed by the methods currently used in clinical practice for contraction monitoring, and, on the other hand, from the lack of methods for understanding the process leading to labor and allowing timely treatment of premature labor. Therefore, in order to position this thesis work in a clinical context, the methods currently employed in clinical practice for contraction monitoring and labor prediction will be described and discussed in the second part of this chapter.

2.2 Physiology of contractions

2.2.1 Uterine anatomy

The uterus is a hollow, muscular organ shaped like an inverted pear. In adults the uterus is 7.5 cm long, 5 cm wide, and 2.5 cm thick, but during pregnancy it enlarges by a factor of four to five [3].

The anatomical structure of the nonpregnant uterus is depicted in Fig. 2.1. The narrower, lower end, which projects into the vagina, is named cervix. The cervix is made of fibrous connective tissue and is of a firmer consistency than the body of the uterus. The two fallopian tubes enter the uterus at opposite sides, near its top. The entrances of the tubes divides the uterus in two parts: the fundus (above) and the body (below). The body narrows toward the cervix, and a slight external constriction marks the juncture between the body and the cervix.

As indicated in Fig. 2.1, the uterine wall is composed of three distinct layers in most species: an inner layer, the endometrium, that lines the lumen of the organ, an intermediate layer, the myometrium, and an external layer, the perimetrium. The myometrium, which is the contractile element of the uterus, is composed of two layers: the outer longitudinal muscle layer and the inner circular layer. The longitudinal layer consists of bundles of smooth muscle cells that are generally aligned with the long axis of the uterus. Muscle cells of the circular muscle layer are arranged concentrically around the longitudinal axis of the uterus. The muscle cells in the circular
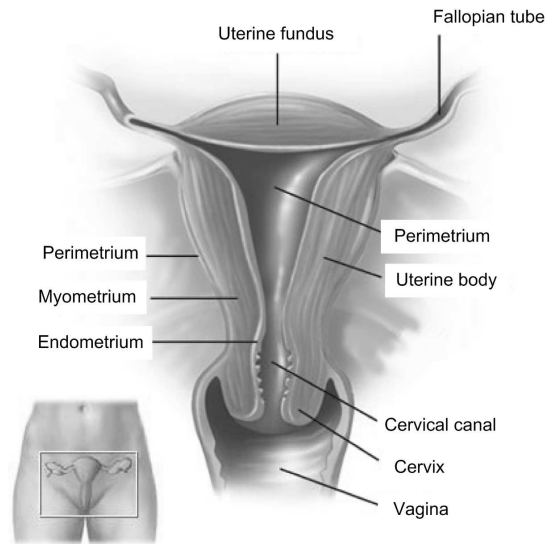
Figure 2.1: *Anatomic structure of the non-pregnant uterus.*

layer are arranged more diffusely and the bundle arrangement, if present, is not as apparent as that of the longitudinal layer [3, 4]. Previous studies indicated that the longitudinal layer is continuous with the circular one [5] and that the two layers usually contract in a coordinated fashion [6]. In some studies, a third intermediate layer of the myometrium is mentioned that is composed of fibers without any organized arrangement [7].

Smooth muscle cells of the myometrium are generally long, spindle shaped cells (see Fig. 2.2(a)), but may also be irregularly shaped. The cells progressively increase in size during the last stage of gestation. Number and size of myometrial smooth muscle cells are mainly regulated by steroid hormones. The size of the myometrial cell is expected to vary considerably among different species. Under the optimal conditions of parturition, for the rabbit, a maximum length of 300 μm and a maximum width of 10 μm have been reported [8].

The type of filaments that have been identified in uterine smooth muscle cells (see Fig. 2.2(b)) include a thick filament (15 nm diameter, myosin), a thin filament (6-8 nm, actin), and an intermediate one (10 nm, desmin or vimentin).

Contraction of smooth muscle cells occurs, as in skeletal muscle, through the interaction of myosin and actin filaments. However, as suggested by Fig. 2.2(b), actin and myosin filaments do not have the same striated arrangement as in skeletal muscles and a large number of actin filaments are attached to dense portions of smooth muscle referred to as dense bodies [3].
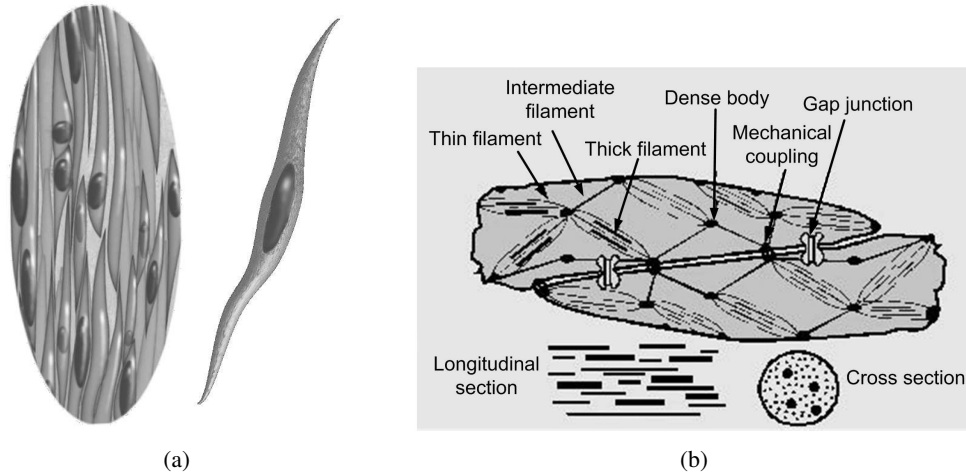
*Figure 2.2: Smooth muscle cell: Muscle fibers and spindle-shape cell (a),
smooth muscle cell filaments (b).*

2.2.2   Cell activation

Basis of activation

Similarly to skeletal muscles, also for smooth muscles, the contraction results from
the propagation of electrical activity through the muscle cells in the form of action
potentials (AP). The intracellular AP results from time-dependent changes in the
membrane ionic permeability, that are caused by hormonal changes or by cell-to-cell
excitation.

The cell membrane potential depends on the distribution of ions across the plasma
membranes. At rest, the ionic distribution in uterine smooth cell is such that the
concentration of sodium (Na^+) and calcium (Ca^{2+}) ions is higher outside the cell
than inside, whereas the concentration of potassium (K^+) ions is higher inside the
cell [3]. This distribution of ions corresponds to the resting membrane potential,
i.e., the value of transmembrane potential at which contraction does not occur and
the myometrium is in a quiescent status. The resting membrane potential of the
myometrial cell usually ranges from -40 to -60 mV but can vary depending on the
hormonal state [9, 10]. In women, the resting myometrial cell membrane potential
ranges between -65 to -80 mV [11].

The muscle cells respond to small changes in permeability by significant move-
ments of ions according to the electrochemical gradients; as a consequence, a trans-
membrane ionic current is established. The contractile event of the uterine smooth
muscle is initiated by a rise in the intracellular Ca^{2+} concentration to approximately
10^{-5} M from a resting level of about 10^{-7} M [12].

The source of Ca^{2+} can be extracellular, intracellular, or a combination of both [3];
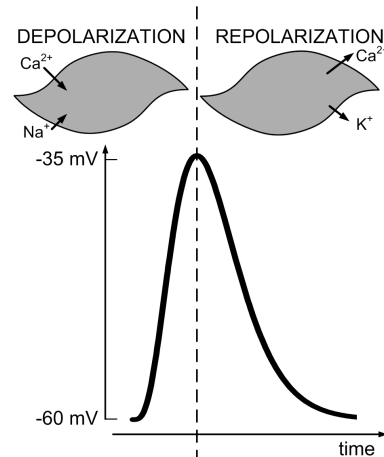
Figure 2.3: Diagram showing the time changes of the membrane potential (bottom) as a function of the efflux and influx of ions (top).

namely, Ca^{2+} ions can flow into the cell following their electrochemical gradient through potential dependent Ca^{2+} channels in response to a change in membrane permeability (extracellular), or they can be released from intracellular storage sites (intracellular). Conversely, a reduction of intracellular free Ca^{2+}, either as a result of efflux into the extracellular space or re-uptake into cellular storage sites, terminates the contraction [3].

Although in smooth muscle, similarly to skeletal muscle, the cell contraction is activated by Ca^{2+}, differently from striated muscle fibres the smooth muscle cell has poorly developed sarcoplasmic reticulum; as a result, the source of Ca^{2+} causing the contraction of smooth muscle cells is mainly extracellular. When the concentration of Ca^{2+} in the extracellular fluid exceeds 10^{-3} M, in comparison with the 10^{-7} M inside the cell, a diffusion of Ca^{2+} into the cell occurs. The time required for the diffusion (latent period) is on average 200-300 ms, and it is approximately 50 times longer than the latent period measured in skeletal muscle fibers [13].

Smooth muscle relaxation is due to the removal of the Ca^{2+} from the intracellular fluids by a calcium pump, which is very slow in comparison to the fast sarcoplasmic reticulum pump that is present in the skeletal muscle.

The diagram in Fig. 2.3 shows the time relationship between the membrane AP and the ion influx and efflux in the cell. The inward current, mainly carried by Ca^{2+}, but also by Na^+, causes a depolarization of the cell. The outward current, carried by potassium ions (K^+) and Ca^{2+}, induces the cell repolarization.

When compared to the skeletal muscle, the smooth muscle cell membrane has far more voltage-gated calcium channels than the skeletal muscle, but fewer voltage-gated sodium channels. Therefore, the generation and propagation of APs in smooth muscle is mainly regulated by Ca^{2+}, while the contraction of skeletal muscle fibers
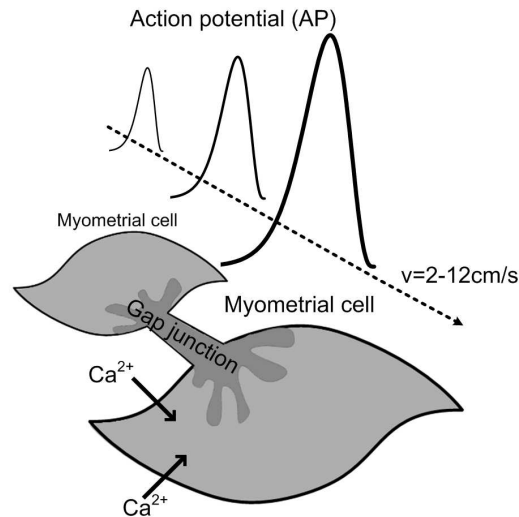
Figure 2.4: *Schematic representation of the cell-to-cell electrical coupling due to the formation of gap-junctions.*

is mainly regulated by sodium channels. Calcium channels open significantly slower than sodium channels and they also remain open longer. This accounts for the slow onset of contraction and relaxation of the smooth muscle tissue in response to the electrical stimulus.

APs usually occur in groups forming a burst [7]. The shape, size, number, and frequency of APs may vary considerably in the uterine muscle under different hormonal conditions. However, little variation is observed from one cell to the next in the parturient uterus [8].

Cell-to-cell coupling

In skeletal muscles, the contraction is initiated by the nervous system. The motoneuron initiates an action potential that propagates through the neuromuscular junction to the muscle end plate, ultimately causing the muscle fiber to contract. Neuromuscular junctions of the highly structured type of skeletal muscle do not occur in smooth muscle [13].

In particular, in the myometrium, the action potential is initiated in pacemaker cells and then propagates to surrounding nonpacemaker cells, opens ion channels and allows the entry into the cell of Ca^{2+} to induce contraction, as schematically represented in Fig. 2.4. There is no evidence for a fixed pacemaker anatomic area in the uterine muscle: any muscle cell can act as pacemaker cell and pacemaker cells can change from one contraction to the other [7]. It has been shown that

non-pacemaker regions can become pacemakers by application of oxytocin, acetylcholine, or prostaglandis [14].

Many studies indicate that myometrial cells are electrically coupled by gap junctions [12, 15, 16], which are also present in other types of tissues, such as the epithelia of the pancreas and liver [17]. A gap-junction is a structure composed of two symmetrical portions of the plasma membrane from two neighboring cells. Gap junction proteins within the opposed cell membrane are thought to align themselves and create channels (of about 1.5 nm) between the cytoplasm of the two cells. These channels are sites of electrical and metabolic coupling between cells. There is evidence that gap junctions form a pathway for the passage of APs by forming a low-resistance electrical contact between the cells (see Fig. 2.4) [12, 15, 16].

Dedicated studies demonstrated that throughout most of the pregnancy the cell-to-cell gap junctions are absent or present in very low density, indicating poor coupling and limited electrical conductance [15]. Conversely, contractile uterine activity during term or pre-term labor is invariably associated with the presence of a large number of gap junctions between the myometrial cells [15, 16]. The presence of gap-junctions is controlled by changing oestrogen and progesterone concentration in the uterus. Progesterone downregulates and progesterone antagonist upregulates the myometrial gap-junction density [12]. It is generally believed that the improved electrical communication among cells can facilitate synchronous excitation of a large number of myometrial fibers and permit the evolution of forceful, coordinated uterine activity, able of effectively terminate pregnancy by helping the fetus to descend into the birth canal [9, 16].

As previously mentioned, the cell depolarization opens voltage-dependent Ca^{2+} channels allowing Ca^{2+} ions to enter the muscle. A single action potential can initiate a quick shortening of a muscle, which is referred to as twitch contraction [18]. Twitch contractions do not develop force. Only when APs are repetitively discharged, as the increments in tension triggered by individual AP can summate, the contraction amplitude is increased as a result of the increase of intracellular free Ca^{2+} [18]. It has been reported that a fused contraction is generated when APs are discharged at a rate higher than about 1 Hz [18].

Recently, another possible mechanism for cell-to-cell communication in the myometrium has been proposed which involves intracellular calcium waves [19] using prostaglandin and paracrine signalling [20]. A model of uterine contractility that comprises a dual mechanism of cell to cell excitation based on APs and calcium waves has been proposed [20]. This model assumes that the functional unit of the uterus is a cylindric bundle of cells, where the cellular AP propagation provides a rapid organ-level propagation and the intercellular calcium wave propagation provide slower coordination within the cylindric bundle. The results reported in [21], where some new three-dimensional structures, including cylindric bundles have been

identified, conceptualizes uterine contractions as the effects of functional units and suggests that the continuity of the network from bundle to bundle supports the hypothesis that AP propagation is fundamental in coordinating uterine contractions and that medications that affect action potential propagation modulate uterine contractility [21].

2.2.3   Cell contraction

Basis of contraction

Contraction of smooth muscle cells occurs through the interaction of myosin and actin filaments. The myosin heads are made up of heavy chains and light protein chains. Contraction and relaxation of the myometrium are regulated by phosphorylation, i.e., acquisition of a phosphate (PO4) group, and dephosphorylation, i.e., removing of a phosphate groups by hydrolysis, of myosin light protein chain. The enzyme that phosphorylates the light chains is called myosin light-chain kinase (MLCK). In order to control the contraction, MLCK is activated by an increase in the intracellular concentration of free Ca^{2+} [22].

Unlike the cardiac and skeletal muscle, the smooth muscle does not contain the calcium-binding protein troponin; instead, calmodulin takes on the regulatory role in smooth muscle. Calcium ions bind to the calmodulin and form a calcium-calmodulin complex. This complex will bind to the MLCK to activate it. Contraction is then initiated by a phosphorylation of myosin where adenosine triphosphate (ATP) is degraded to adenosine diphosphate (ADP) [13, 22].

Phosphorylation of myosin light chain leads to the conformational changes in the myosin head that results, as it is more accurately described in 2.2.3, in the formation of crossbridges, shortening of the muscle, and development of force [22]. Relaxation is affected by low concentration of calcium ions, inactivation of MLCK, and dephosphorylation of myosin light chain by myosin light chain phosphatase (MLCP) [13].

Sliding filament model

Smooth muscle contraction and force development is due to the sliding of myosin and actin filaments over each other. Filament sliding occurs when the globular heads protruding from myosin filaments attach and interact with actin filaments to form crossbridges. The myosin heads tilt and drag the actin filament along a small distance (10-12 nm). The heads then release the actin filament and adopt their original conformation. They can then re-bind to another part of the actin molecule and drag it along further. This process is called crossbridge cycling and is the same for all muscles [22].

Differently from the skeletal muscle, the cross-bridges of most of the myosin filaments in smooth muscle are arranged so that the bridges on one side hinge in one
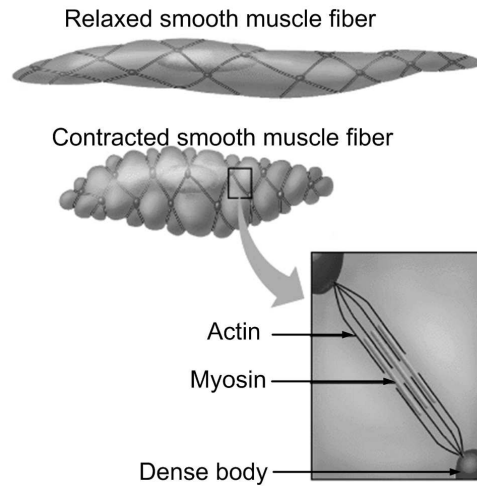
Figure 2.5: *Schematic representation of the smooth cell contraction due to the formation of cross-bridges.*

direction and those on the other side hinge in the opposite direction as schematically represented in Fig. 2.5. This type of cross-bridge allows the myosin to pull an actin filament in one direction on one side while simultaneously pulling another actin filament in the opposite direction on the other side. This organization allows smooth muscle cells to contract as much as 80% of their length instead of less than 30% as in skeletal muscle cells [13].

2.2.4   Uterine contraction

The electrical activity of the smooth muscle cells of the myometrium initiate the mechanical contraction of the uterus. The main function of uterine contractions is, during parturition, shortening the cervix and helping the fetus to descend into the birth canal. In this circumstance, the uterus works under isometric conditions, i.e., it does not shorten. Experiments on rabbits showed that the tension developed by the uterus in isometric conditions as a function of the electric stimulus is nonlinear [4], i.e., increasing the stimulus alters the dynamics of contraction in such a way that there is inhibition of tension development at higher tensions as shown in Fig. 2.6.

In [4], the length-tension relation has been studied for the uterus similarly as it has been done for the skeletal muscle. Results obtained from the rabbit uterus *in-vivo* showed that also for the myometrium the maximum tension is obtained at the resting length. However, as the contractile properties of the uterus are highly dependent on the hormonal status, the shape of the diagrams in [4] were highly dependent on the dominant ovarian hormone as well as on the strength of stimulation.

The tension developed by the uterus is dependent on both strength and duration of
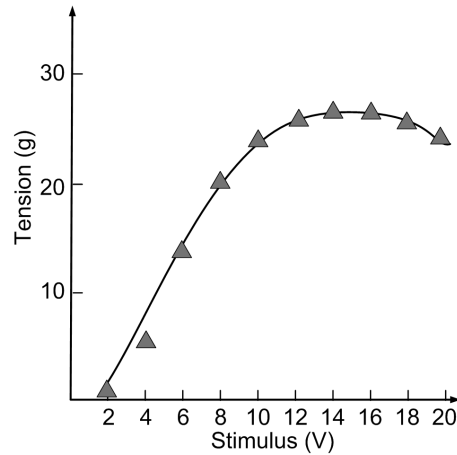
Figure 2.6: *Isometric tension developed by uteri of rabbits as a function of the electric stimulus [4].*

the stimulus [23]. The myometrium requires a relatively long time (5 s) for activation as compared to the skeletal muscle [24]. The slow onset of contraction is mainly due to the speed of cycling of the myosin cross-bridges in smooth muscle, which is 10 to 300 times slower than in the skeletal muscle [13]. However, the fraction of time that the cross-bridges remain attached to the actin filaments, which is a major factor determining the force of contraction, is believed to be significantly increased in smooth muscle. In fact, despite the relatively few myosin filaments in the smooth muscle and the slow cycling time of the cross-bridges, the maximum specific force of contraction of smooth muscles is often greater than that of skeletal muscles and can be as much as 6 Kg/cm^2 of cross sectional area [13].

Furthermore, it was observed that for the uterus as well as for skeletal muscle, the function of the stimulus consists not only of the production but also of the maintenance of a condition, referred to as active state, in which tension can develop. However, differently from skeletal muscles once the muscle has developed a full contraction, negligible energy is required for contraction maintenance [13]. This specific behavior of smooth muscle is generally referred to as latch phenomenon. The most frequently reported theory among the many postulated to explain the latch phenomenon is the following. During muscle contraction, rapidly cycling crossbridges form between activated actin and phosphorylated myosin and generate force. During the sustained phase, the activation of the enzyme decreases. The cross-bridge cycling frequency also decreases. Then the enzyme deactivation allows the myosin heads to remain attached to the actin filaments for a longer period forming slow cycling dephosphorylated crossbridges which act as latch bridges to contribute to force maintenance at a low energy cost [3, 13]. The latch mechanism allows smooth mus-

cles to maintain prolonged tonic contractions for long time (up to hours) with limited energy [25].

2.3 Clinical practice

2.3.1 Contraction monitoring
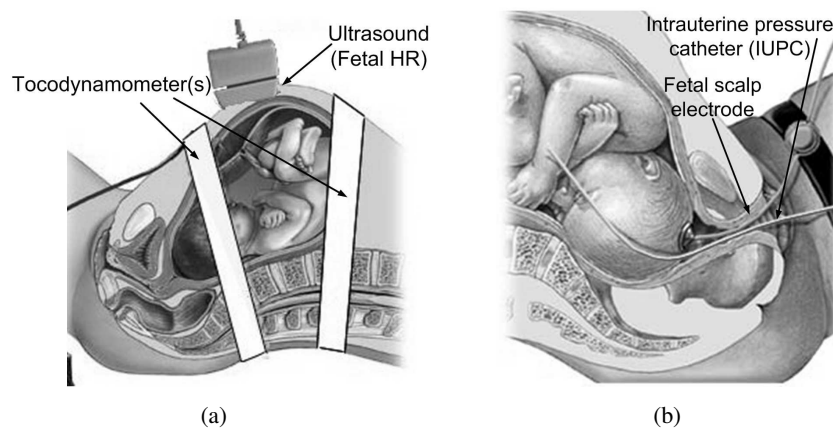
Figure 2.7: *Contraction and fetal heart rate monitoring (cardiotocography): noninvasive recording (a), invasive recording (b).*

The first effect of a uterine contraction is the internal uterine pressure (IUP) increase. The techniques used in clinical practice for contraction monitoring mainly rely on the direct (internal) or indirect (external) measurement of the IUP. Uterine contractions are evaluated in terms of amplitude or peak pressure, duration, and frequency of contractions, which is usually expressed as number of contractions per 10 minutes.

External tocography is currently the most widely used technique to monitor the uterus during pregnancy and delivery [12]. A tocodynamometer, schematically represented in Fig. 2.7(a), consists of a strain gauge transducer placed around the external surface of the abdomen. The primary advantage of a tocodynamometer is its noninvasiveness. However, since it stems from an indirect mechanical measure of the pressure increase, the signal provided by external tocography can be affected by many variables, such as the sensor position and the thickness of the subcutaneous fat tissue. Additionally, body movements, gastric activity, and other nonlabor-induced stresses on the tocodynamometer can be mistaken for labor contractions [26]. As a result, external recordings have an accuracy that is highly dependent on the examiner's skills and are characterized by a low sensitivity. Therefore, the use of external tocodynamometry can only provide information related to the frequency of the con-

tractions while it does not quantify the contraction amplitude and duration, resulting in a poor predictive value for preterm delivery [27, 28].

During delivery, quantitative information concerning the uterine functionality can be provided invasively, by measuring the amniotic IUP with an internal uterine pressure catheter (IUPC). However, the employment of an IUPC requires the rupture of the membranes and, due to the invasiveness of this device, it can increase the risk of infections and even cause damage to the fetus [29, 30]. Therefore, the IUPC is employed exclusively during parturition and its use is usually limited to complicated cases or during labor induction or augmentation.

For the evaluation of amniotic pressure traces obtained by an intrauterine catheter, several units of measurement have been proposed in the literature. Their use in clinical practice is, however, highly controversial [31]. The Montevideo unit [32], which is the product of frequency of contraction and peak contraction (expressed in mmHg), is a commonly used parameter. However, this parameter is insensitive to the duration of each contraction and provides no distinction between a peak pressure maintained for only a brief instant and one maintained for a longer period [31]. Another commonly adopted parameter is the area under the uterine pressure curve [33], which does not distinguish between active pressure and baseline. Conversely, the active pressure, which is obtained by removing the baseline pressure from the total pressure value, can be integrated over a period of 15 minutes to obtain the active pressure area [31].

Uterine contractions can affect the fetal heart rate (HR) by subjecting the fetus to an intermittent hyperbaric state. They also compress the myometrial vessels, may influence the cerebral blood flow, and, depending on the umbilical cord location, they may cause occlusion of the umbilical cord with a consequent decrease in fetal oxygenation [34]. These situations are usually reflected in a deceleration of the fetal HR. Monitoring the fetal HR in combination with the uterine activity is referred to as cardiotocography (CTG). The CTG is widely used in clinical practice as screening test for recognition of fetal distress (e.g., asphyxia) at a sufficiently early stage in order to permit timely obstetric intervention. The most commonly employed parameter is the response time of the fetal HR to a uterine contraction. Non-reassuring features on a CTG trace would include unusually rapid or slow rates, a flat pattern (reduced variability), and specific types of fetal HR decelerations. In particular, late decelerations or severely variable patterns are considered as an indicator of placental insufficiency and fetal hypoxia [35].

The CTG can be obtained either noninvasively, using an external tocodynamometer for contraction monitoring and a ultrasound transducer fixed at the stretch belt to obtain the fetal HR, or invasively by the combined use of an IUPC and an electrode placed on the fetal scalp as depicted in Fig. 2.7. As shown in the example CTG trace in Fig. 2.8, the instantaneous value of the fetal HR is usually plotted above the uterine
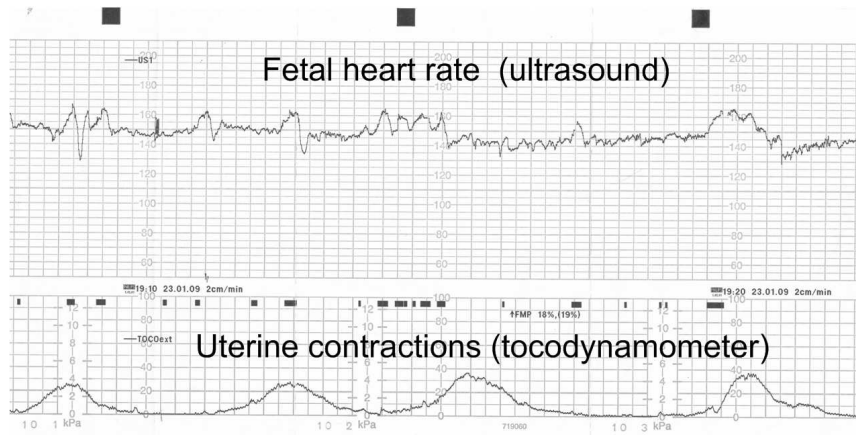
Figure 2.8: *Example of a noninvasively recorded cardiotocographic trace.*

pressure as a function of time.

2.3.2 Prediction and early detection of preterm labor

Premature birth as a consequence of spontaneous preterm labor is still a major cause of fetal mortality and long term morbidity [36, 37]. There are at least two broad areas where early detection of preterm labor might be helpful in clinical practice today. The first area concerns women with symptoms of preterm labor, i.e., preterm uterine contractions possibly accompanied by progressive cervical dilatation. In these cases, in order to avoid unnecessary treatment or ensure accurate and timely intervention to reduce perinatal mortality and morbidity, early diagnosis is important. The second area concerns women with increased risk of preterm labor who need to be identified before clinical signs and symptoms occur [38].

Early detection of preterm labor is difficult because the initial symptoms and signs are often mild and may also occur in normal pregnancies. Thus, many healthy women will report symptoms during routine prenatal visits, whereas others destined to preterm delivery may dismiss the early warning signs as normal in pregnancy [38].

Besides contraction monitoring, digital and ultrasound examination of the cervix, symptomatic self monitoring, and detection of biochemical markers such ad the fetal fibronectin have been used for early detection of preterm labor [26].

Table 2.1 lists the current methods used in clinical practice and their characteristics, which are mainly based on the reviews in [26] and [38]. In general, the performance of each method varies according to its use to reveal a risk of preterm delivery in women without symptoms or predict preterm labor in women with symptoms. As the methods of this thesis are naturally related to the presence of symptoms (i.e., contractions), the performance of the clinical methods is evaluated in Table 2.1 for

detection of labor in women with symptoms. Furthermore, due to the controversial definition of invasiveness, we regard as highly invasive those methods that require tissue cutting, puncturing, or vaginal insertion of a sensor and and whose use is associated with a risk for the health of mother or fetus (for example due to possible infections), moderately invasive those that require only vaginal insertion of sensor but are free of risks, and noninvasive the methods that do not require any insertions.

Contractions can be monitored by an intrauterine pressure catheter, which is accurate, but invasive and requires ruptured membrane, by external tocodynamometer, which is not invasive, but erratic and not predictive of preterm delivery, and by symptomatic patient's self monitoring, which has a very poor accuracy [26–29].

The cervical status in terms of effacement, softening, dilatation and length is also clinically used as a predictor of labor [39–41]. Softening, dilatation and effacement of the cervix, together addressed as cervical changes, are commonly assessed by digital examination and are usually evaluated in combination with other parameters such as the contraction rate [38]. Cervical effacement can also be assessed by ultrasound [41]. The possibility of using ultrasound elastography for characterizing cervix softening was also recently suggested [42]. Parameters derived by assessment of cervical changes, possibly correlated with the contraction frequency, are the most traditional criteria for diagnosis of preterm labor, however their sensitivity and positive predictive value are highly dependent on the adopted threshold values and are, in general, modest [39, 40].

Endovaginal ultrasonography can be used to measure the length of the cervix [43]. The risk of spontaneous preterm birth increases as the length of the cervix decreases [38, 43]. A threshold of 30 mm for the cervix length as measured by endovaginal ultrasonography in symptomatic women was found to be optimal for excluding the diagnosis of preterm labor. A cervical length below 20 mm showed the best predictive value, which is however reported to be as low as 25%. In fact, some values of cervical length may be simply physiologic, early effacement or shortening can be the result of inflammation due to hemorrhage or infection or, less commonly, to biophysical effects of uterine distention or subclinical contractions [44].

Fibronectin is an extracellular matrix protein that attaches the fetal membranes to the underlying uterine endometrium. Fibronectin found in cervicovaginal secretions after 22 weeks is a marker of disruption of the interface between the fetal membranes and the endometrium, and has been associated with a six-fold increased risk of preterm birth before 35 weeks and a 14-fold increased risk of preterm birth before 28 weeks [44]. However, the positive predictive value for delivering within 1 week is reported to be only 18% [38]. Given the 40% rate of false positive diagnosis of preterm labor based on contraction frequency and cervical changes by digital examination, the clinical value of the test in symptomatic women consists primarily in its high negative predictive value (NPV), i.e., in its capability of identifying patients

Table 2.1: Current methods used in clinical practice for prediction of labor

	Accuracy	invasiveness
Intrauterine pressure catheter	High	High
External tocodynamometer	Erratic	No
Symptomatic self monitoring of contractions	Poor	No
Cervical changes (combined with contractions)	Mixed/Moderate	Moderate
Cervical length	Moderate	Moderate
Fetal fibronectin test (or estriol test)	High NPV	Moderate

who are not at risk of preterm delivery. However, studies evaluating the combined use of fibronectin and cervical sonography in symptomatic women showed contradictory results, and it remains unclear whether the accuracy of a diagnosis provided by combination of the two methods is superior to either test alone [45, 46]. An increase in maternal excretion of estriol can also be predictive of labor. The estriol concentration as measured by salivatory test also showed a high NPV for preterm delivery [47].

In summary, the methods currently employed in clinical practice impose a dramatic compromise between reliability and invasiveness that concerns both labor contraction monitoring and preterm delivery prediction. In view of the increasing number of pregnancies complicated by miscarriage, preterm delivery, birth defects, and the growing rate of consequent long term morbidity, novel methods for noninvasive and accurate pregnancy monitoring are urgently needed. Electrohysterography, which is the measurement of the APs propagating through the myometrial cells, is a promising alternative to existing techniques for uterine contraction monitoring because it is representative of the prime cause of a contraction and it can be recorded noninvasively from the abdominal surface. In the following chapters of this thesis, novel methods are proposed for analyzing the electrohysterographic (EHG) signal. These methods aim at paving the way for the introduction in clinical practice of alternative monitoring methods that can accurately characterize uterine activity, follow the evolution of pregnancy and labor, and timely predict preterm delivery.

Bibliography

[1] E. Fischer, "Vertebrate smooth muscle," *Physiol. Rev.*, vol. 24, pp. 467–490, 1944.

[2] E. Bozler, "Conduction, automaticity, and tonus of visceral muscles," *Cell. Mol. Life Sci.*, vol. 4, pp. 213–218, 1948.

[3] T. Chard and J. Grudzinskas, *The uterus*, Cambridge University Press, 1994.

[4] A. Csapo, "Dependence of isometric tension and isotonic shortening of uterine muscle on temperature and on strength of stimulation," *Am. J. Physiol.*, vol. 177, pp. 348–354, 1954.

[5] T. Osa and T. Katase, "Physiological comparison of the longitudinal and circular muscles of the pregnant rat uterus," *Jpn. J. Physiol.*, vol. 25, pp. 153–164, 1975.

[6] B.A. Tomiyasu, C.J. Chen, and J.M. Marshall, "Comparison of the activity of circular and longitudinal myometrium from pregnant rats: co-ordination between muscle layers," *Clin. Exp. Pharmacol. Physiol.*, vol. 15, pp. 647–656, 2007.

[7] D. Devedeux, C. Marque, S. Mansour, G. Germain, and J. Duchêne, "Uterine electromyography: a critical review," *Am. J. Obstet. Gynecol.*, vol. 169, pp. 1636–1653, 1993.

[8] A.I. Csapo, "Smooth muscle as a contractile unit," *Physiol. Rev. Suppl.*, vol. 5, pp. 7–33, 1962.

[9] S.M. Sims, E.E. Daniel, and R.E. Garfield, "Improved electrical coupling in uterine smooth muscle is associated with increased numbers of gap junctions at parturition," *J. Gen. Physiol.*, vol. 80, pp. 353–375, 1982.

[10] H.C. Parkington and H.A. Coleman, "Excitability in uterine smooth muscle," *Front. Horm. Res.*, vol. 27, pp. 179–200, 2001.

[11] C.S. Buhimschi, I.A. Buhimschi, A.M. Malinow, G.R. Saade, R.E. Garfield, and C.P. Weiner, "The forces of labour," *Fetal and Maternal Medicine Review*, vol. 14, pp. 273–307, 2003.

[12] R.E. Garfield, G. Saade, C. Buhimschi, I. Buhimschi, L. Shi, S.Q. Shi, and K. Chwalisz, "Control and assessment of the uterus and cervix during pregnancy and labor," *Hum. Reprod. Update*, vol. 4, pp. 673–695, 1998.

[13] A.C. Guyton and J.E. Hall, *Textbook of medical physiology*, Elsavier Saunders, Philadelphia, 2006.

[14] S. Lodge and J.E. Sproat, "Resting membrane potentials of pacemaker and non pacemaker areas in rat uterus," *Life Sciences*, vol. 28, pp. 2251–2256, 1981.

[15] R.E. Garfield, S. Sims, E.E. Daniel, et al., "Gap junctions: their presence and necessity in myometrium during parturition," *Science*, vol. 198, pp. 958–960, 1977.

[16] S.M. Miller, R.E. Garfield, and E.E. Daniel, "Improved propagation in my-ometrium associated with gap junctions during parturition," *Am. J. Physiol. Cell. Physiol.*, vol. 256, pp. C130–C141, 1989.

[17] D.S. Friend and N.B. Gilula, "Variations in tight and gap junctions in mam-malian tissues," *J. Cell Biol.*, vol. 53, pp. 758–776, 1972.

[18] J.M. Marshall, "Regulation of activity in uterine smooth muscle," *Physiol. Rev. Suppl.*, vol. 5, pp. 213–227, 1962.

[19] R.C. Young and R.O. Hession, "Intra and intercellular calcium waves in cul-tured human myometrium," *J. Muscle Res. Cell. Motil.*, vol. 17, pp. 349–355, 1996.

[20] R.C. Young and R.O. Hession, "Paracrine and intracellular signaling mecha-nisms of calcium waves in cultured human uterine myocytes," *Obstet. Gynecol.*, vol. 90, pp. 928–932, 1997.

[21] R.C. Young and R.O. Hession, "Three-dimensional structure of the smooth muscle in the term-pregnant human uterus," *Obstet. Gynecol.*, vol. 93, pp. 94–99, 1999.

[22] R.A. Word, "Myosin phosphorylation and the control of myometrial contrac-tion/relaxation," *Semin. Perinatol.*, vol. 19, pp. 3–14, 1995.

[23] A.V. Hill, "The abrupt transition from rest to activity in muscle," *Proc. Roy. Soc. B*, vol. 136, pp. 399–420, 1949.

[24] A. Csapo and M. Goodall, "Excitability, length tension relation and kinetics of uterine muscle contraction in relation to hormonal status," *J. Physiol.*, vol. 126, pp. 384–395, 1954.

[25] T.C. Ruch and H.D. Patton, *Physiology and Biophysics*, Saunders Co., Philadel-phia and London, 1965, 19th ed.

[26] R.E. Garfield, H. Maul, L. Shi, W. Maner, C. Fittkow, G. Olsen, and G.R. Saade, "Methods and devices for the management of term and preterm labor," *Ann. NY Acad.Sci.*, vol. 943, pp. 203–224, 2001.

[27] H. Eswaran, J.D. Wilson, P. Murphy an H. Preissl, and C.L. Lowery, "Application of Wavelet tranform to uterine electromyographic signals recorded using abdominal surface electrodes," *J. Matern.-Fetal Neonatal Med.*, vol. 11, pp. 158–166, 2002.

[28] A.M. Miles, M. Monga, and K.S. Richeson, "Correlation of external and internal monitoring of uterine activity in a cohort of term patients," *Am. J. Perinatol.*, vol. 18, pp. 137–140, 2001.

[29] R.E. Garfield, H. Maul, W. Maner, C. Fittkow, G. Olson, L. Shi, and G. R. Saade, "Uterine electromyography and light-induced fluorescence in the management of term and preterm labor," *J. Soc. Gynecol. Invest.*, vol. 9, pp. 265–275, 2002.

[30] F.A. Wilmink, F.F. Wilms, R Heydanus, B.W. Mol, and D.N. Papatsonis, "Fetal complications after placement of an intrauterine pressure catheter: a report of two cases and review of the literature," *J. Matern. Fetal. Neonatal. Med.*, vol. 21, pp. 880–883, 2008.

[31] G.F. Phillips and A.A. Calder, "Units for the evaluation of uterine contractility," *BJOG*, vol. 94, pp. 236–241, 1987.

[32] R. Caldeyro-Barcia and J.J. Poseiro, "Physiology of the uterine contraction," *Clin. Obstet. Gynecol.*, vol. 3, pp. 386–408, 1960.

[33] E.H. Hon and R.H. Paul, "Quantitation of uterine activity," *Obstet. and Gynec.*, vol. 42, pp. 368, 1973.

[34] R.K. Freeman, T.J. Garite, and M.P. Nageotte, *Fetal heart rate monitoring*, Lippincott William & Wilkins, Philadelphia, PA, 2003.

[35] M.L. Murray, "Maternal or fetal heart rate? avoiding intrapartum misidentification," *J. Obstet. Gynecol. Neonatal. Nurs.*, vol. 33, pp. 93–104, 2004.

[36] R.L. Goldenberg, J.F. Culhane, J.D. Jams, and R. Romero, "Epidemiology and causes of preterm birth," *Lancet*, vol. 371, pp. 75–84, 2008.

[37] R.E. Behrman and A.S Butler, *Preterm Birth: Causes, Consequences, and Prevention*, The National Academy Press, Washington, DC, 2007.

[38] J.D. Iams, "Prediction and early detection of preterm labor," *Obstet. Gynecol.*, vol. 101, pp. 402–412, 2003.

[39] W.J. Hueston, "Preterm contractions in community settings: II. predicting preterm birth in women with preterm contractions," *Obstet. Gynecol.*, vol. 92, pp. 43–46, 1998.

[40] J. F. King, A. Grant, M. J. Keirse, and I. Chalmers, "Beta-mimetics in preterm labour: An overview of the randomized clinical trials," *Br. J. Obstet. Gynaecol.*, vol. 95, pp. 211–22, 1988.

[41] M. Zilianti, A. Azuaga, F. Calderon, G. Pages, and G. Mendoza, "Monitoring the effacement of the uterine cervix by transperineal sonography: A new perspective," *J. Ultrasound Med.*, vol. 14, pp. 719–724, 1995.

[42] M. Maanders, R.G.P. Lopata, E.M.H. Bosboom, F.N. van de Vosse, F.K. Lotgering, and C.L. de Korte, "Cervix elastography: a preliminary study," in *IEEE EMBS Benelux Symposium Proc.*, 2007, pp. 64–67.

[43] J.D. Iams, R.L. Goldenberg, P.J. Meis, B.M. Mercer, A.H. Mowad, A. Das, et al., "The length of the cervix and the risk of spontaneous premature delivery," *N. Engl. J. Med.*, vol. 334, pp. 567–572, 1995.

[44] R.L. Goldenberg, J.D. Iams, A. Das, B.M. Mercer, P.J. Meis, A.H. Moawad, M. Miodovnik, J.P. VanDorsten, S.N. Caritis, G.R. Thurnau, M.P. Dombrowski, J.M. Roberts, and D. McNellis, "The preterm prediction study: sequential cervical length and fetal fibronectin testing for the prediction of spontaneous preterm birth," *Am. J. Obstet. Gynecol.*, vol. 182, pp. 636–643, 2000.

[45] G. Rizzo, A. Capponi, A. Arduini, C. Lorido, and C. Romanini, "The value of fetal fibronectin in cervical and vaginal secretions and of ultrasonographic examination of the uterine cervix in predicting premature delivery in patients with preterm labor and intact membranes," *Am. J. Obstet. Gynecol.*, vol. 175, pp. 1146–1151, 1996.

[46] P. Rozenberg, A. Goffinet, L. Malagrida, Y. Giudicelli, M. Perdu, I. Houssin, G. Rizzo, A. Capponi, A Arduini, C Lorido, C. Romanini, Sage-Femme, and I. Nisand, "Evaluating the risk of preterm delivery: A comparison of fetal fibronectin and transvaginal ultrasonographic measurement of cervical length," *Am. J. Obstet. Gynecol.*, vol. 176, pp. 196–199, 1997.

[47] J.A. McGregor, G.M. Jackson, G.C.L. Lachelin, T.M. Goodwin, R. Artal, C. Hastings, and V. Dullien, "Salivary estriol as risk assessment for preterm labor: a prospective trial," *Am. J. Physiol.*, vol. 173, pp. 1337–1342, 1995.

Chapter 3

Internal uterine pressure estimation

> *L'uffizio del muscolo di tirare è non di spingere, eccetto li membri genitali e la lingua (Leonardo da Vinci)* [1]

3.1 Introduction

Premature birth is a major cause of long-term morbidity and it accounts for 69% to 85% of neonatal deaths not caused by congenital malformations [1]. An early prediction of preterm delivery by identification of the risk factors and accurate monitoring of the patients at risk is crucial for the treatment of preterm birth. In particular, an early diagnosis of delivery time can be achieved during pregnancy following the progression of the maternal uterine activity, i.e., frequency, duration, and amplitude of the uterine contractions.

During labor, accurate monitoring of uterine activity is essential to assess the condition of both mother and fetus. In particular, the fetal heart rate (FHR) is monitored in combination with the uterine activity in order to evaluate the fetal response to each contraction [2]. After a uterine contraction, subtle changes of FHR, or a total absence of FHR variability may in fact occur as first signs of fetal distress. Additionally, when complications occur, e.g., poor progress in labor, quantitative assessment of uterine activity can guide the physician to opt for specific medical interventions, such as labor augmentation.

The contractile element of the uterus is the myometrium, which is composed of smooth muscle cells [3]. The uterine contraction is the result of generation and propagation through the muscle cells of electrical activity in the form of action potentials (APs). Myometrial cells can generate APs or can be excited by APs generated by a neighboring cell. The excitation transmission is possible when cells are coupled by

---

[1] 'The function of the muscle is to pull not to push, except in the case of the reproductive organs and the tongue'. From 'De vocie' by Leonardo Da Vinci (quoted by Edmondo Solmi in 'Il trattato di Leonardo da Vinci sul linguaggio *de vocie*', in *Archivio storico lombardo*, VI, 1906).

electronic synapses, which are referred to as gap junctions [4]. During pregnancy, poor coupling and low electrical conductance among the myometrial cells favors the maintenance of pregnancy; at term, gap junctions increase and form a low-resistance electrical path required for the occurrence of effective contractions [5].

The first result of a contraction is the internal uterine pressure (IUP) increase. Besides the traditional methods employing pelvic examination and symptomatic self monitoring, the techniques used in clinical practice for uterine monitoring mainly rely on the direct (internal) or indirect (external) measurement of the IUP. External tocography is currently the most widely used technique to monitor the uterus during pregnancy and delivery [5]. A tocodynamometer consists of a strain gauge transducer placed around the external surface of the abdomen and has the primary advantage of being noninvasive. However, deriving from an indirect mechanical measure of the pressure increase, the signal provided by external tocography is characterized by a low sensitivity, which can affect the estimation accuracy of contraction amplitude and duration [4, 6].

During delivery, quantitative information concerning uterine functionality can be provided invasively, by measuring the amniotic IUP with an internal uterine pressure catheter (IUPC). However, the employment of an IUPC requires the rupture of the membranes and, due to the invasiveness of this device, it can increase the risk of infections and even cause damages to the fetus [7]. Therefore, the IUPC is employed exclusively during parturition and its use is usually limited to complicated cases or during labor induction or augmentation.

An alternative method for monitoring the uterine activity is electrohysterography. The electrohysterographic (EHG) signal is the bioelectrical signal directly associated with the muscular activity of the myometrium. Generation and propagation of APs through an adequate number of cells are the primary causes of the uterine muscle contractions and of the consequent IUP increase. Therefore, the electrical activity recorded from the abdominal surface may provide essential information on the uterine activity and permit the prediction of the IUP associated with each contraction [8].

The possibility of reliable and noninvasive assessment of the uterine activity has generated interest in the EHG analysis. In the literature, extensive research demonstrated the value of external EHG recordings in following the progress of the uterine contractility during pregnancy and parturition [9]. To this end, filtering techniques [10], the Fast Fourier Transform [11], and the Wavelet transform [4] have been employed for EHG analysis; the obtained results were evaluated by visual comparison with the IUP or external tocography traces. However, only few studies focused on EHG analysis as an alternative to existing methods for a quantitative estimation of the uterine mechanical activity [12, 13].

In [12] the contraction pattern estimated by the root mean square (RMS) value of the EHG was compared to the simultaneously recorded external tocogram. As the

estimated contraction pattern was well correlated to the external tocographic signal, previous research could propose a reliable estimation of the contraction frequency, but a validation of amplitude and duration of the detected contractions was not possible. The use of optimal linear filtering for IUP prediction by EHG signal analysis was recently investigated in [13]. In this work, the simultaneously measured IUP was for the first time employed as a quantitative reference for the IUP predicted from the EHG analysis. According to this study, the IUP can be predicted from external EHG signals employing a Wiener filter on the rectified EHG.

In this chapter, a new method for quantitative estimation of the uterine activity by EHG analysis is proposed as a noninvasive alternative technique for IUP monitoring. We consider the EHG signal at each electrode as a nonstationary signal resulting from the summation of several frequency modulation (FM) processes [14]. The IUP increase is determined by the coexistence of two factors which in the myometrium, differently from skeletal muscles, are interrelated. These two factors, namely, propagation of the AP, which is reflected in the spectral properties of the EHG signal, and amount of cells involved in the contraction, which is proportional to the amplitude of the EHG signal, are both taken into account to provide a first IUP estimate.

To further improve the estimate accuracy, the nonlinear relationship between the electrical activation, which is represented by the unnormalized EHG first statistical moment, and the mechanical contraction of the uterus, which is measured in terms of IUP, is modeled by three different functions. In addition to a second-order polynomial model, which is a standard representation of nonlinear relationships, we test a logarithmic function and an exponential function. Simultaneous IUP recordings by an IUPC are employed for a quantitative validation of the pressure estimates.

The proposed method is compared to the methods previously presented in the literature for quantitative estimation of the uterine mechanical activity. For the comparison we employ an improved version of the RMS analysis-based method suggested by [12] and the optimal Wiener filtering proposed in [13].

3.2 Methodology

A schematic description of the proposed method for IUP estimation is shown in Fig. 3.1. The multichannel EHG signal and the invasively measured IUP were first recorded as described in Section 3.2.1. The acquired signals were then preprocessed according to Section 3.2.2; in particular, the EHG signal was made bipolar, downsampled, and analyzed in the Time-Frequency (TF) domain using the spectrogram. From the TF representation $\rho(n, f)$, the unnormalized first statistical moment $\Psi(n)$ was then calculated as the feature providing a first estimation of the contraction pattern. The energy of the EHG is concentrated in a limited frequency interval. Therefore, to optimize the signal-to-noise ratio (SNR), the first statistical moment was
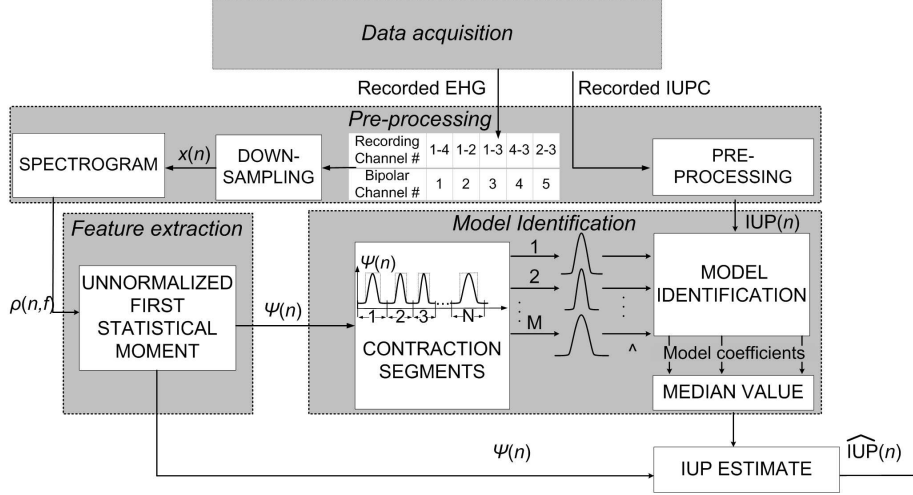
Figure 3.1: *Scheme of the proposed methodology for single channel data analysis.*

calculated in a limited bandwidth $[f_{min}, f_{max}]$, which was experimentally determined.

Each nonlinear model was then identified as described in Section 3.2.4 to provide a better estimation of the IUP.

The model coefficients were initially calculated for each single contraction by minimization of the mean squared error with the invasively measured IUP. Ultimately, for each channel the median value of the coefficients over the available subjects was calculated. The model identified by the median values of the coefficients was finally applied to the unnormalized first EHG statistical moment to provide the IUP estimate, $\widehat{IUP}(n)$.

3.2.1   Data acquisition

The experimental data were collected at the Máxima Medical Center in Veldhoven (the Netherlands). The study was approved by the ethical committee of the hospital. Nine women during labor underwent multichannel electrical EHG recordings after signing an informed consent. Six contact Ag-AgCl electrodes, consisting of four active electrodes, one ground electrode, and one reference electrode, were placed on the subject's abdomen after skin preparation with an abrasive paste for skin impedance reduction. The IUP was simultaneously measured by an IUPC inserted in the uterine cavity due to medical prescription. The total length of data recorded from each subject ranged from 22 to 90 minutes.

In order to identify a suitable electrode configuration, two 15-minute measurements in labor were preliminarily performed with a higher number of active electrodes (11 instead of 4) placed on the abdomen as shown in Fig. 3.2-(a) and a mea-

sure of the average SNR in each electrode was considered. During a contraction, the skeletal muscle EMG can be regarded as the major noise contribution. Considering the higher frequency band of skeletal electromyogram (EMG) energy [11], the SNR was therefore estimated as the ratio of the signal in the frequency band between 0.1 and 5 Hz and that between 5 and 200 Hz during active contractions. In this preliminary study, the highest average SNR was experienced on the lower vertical median line of the abdomen, in particular on the region immediately below the umbilicus. These results have a twofold physiological explanation. On the one hand, in the vertical median line of the abdomen, the distance between the recording site on the skin and the signal source in the myometrium is reduced with respect of the lateral sides [15]. On the other hand, in the region surrounding the umbilicus the position of the uterus relative to the abdominal wall is constant even during contractions [16], resulting in a better SNR.

Based on the results of this preliminary analysis, the recordings employed in the present study were measured by four unipolar contact Ag-AgCl electrodes placed on the abdomen as shown in Fig. 3.2-(b). The common reference for the electrodes was placed on the right hip. In order to obtain an efficient rejection of electromagnetic interference, a driven-right-leg (DRL) electrode was placed below the reference electrode and the cables were actively shielded [17]. The position of the DRL electrode was chosen close to the reference rather than on the limb in order to avoid voltage oscillation due to the induced current flux through the body [17].

A Koala M1333A (Philips Medical Systems, Best, the Netherlands) transducer-tipped IUPC was inserted in the uterine cavity to measure the IUP.

The IUP and the EHG were simultaneously recorded and digitized at 20-bit resolution with an M-PAQ amplifier (Maastricht Instruments Ltd., the Netherlands), a 16-channel system for physiological measurements with programmable gain and sampling frequency. A sampling frequency of 1000 Hz was chosen in order to allow the employment of the recorded signals also by other applications, e.g., fetal electrocardiogram (ECG) detection. Prior to sampling, to avoid aliasing and remove the power-line interference, the analog 500 Hz low-pass and notch filters of the amplifier were employed, respectively.

3.2.2 Preprocessing

The digitized unipolar EHG signal recorded at each active electrode was first made bipolar by subtracting the signals recorded at contiguous electrodes on the abdomen (Fig. 3.1). The employment of bipolar electrical signals has been demonstrated to effectively reduce a large portion of the noise affecting the EHG, e.g., the maternal ECG, part of the movement artifacts, and the electromagnetic noise [18].

The EHG and the IUPC signals, recorded at 1000 Hz, were then down-sampled to 10 Hz, after low-pass anti-aliasing filtering at 5 Hz. The decrease of the sampling fre-
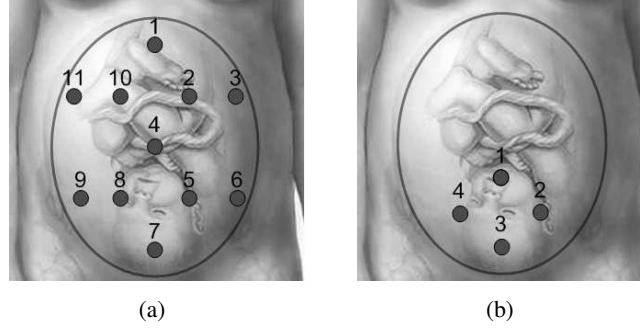
Figure 3.2: Preliminary electrode configuration (a). Final electrode configuration (b).

quency, which reduces the computational time, is made possible by the low-frequency characteristic of the EHG [11, 16, 19–21].

For an easy synchronization with the preprocessed EHG, the IUPC signal was similarly down-sampled to 10 Hz. Additionally, in order to minimize spikes caused by movement artifacts, we employed a non-causal centered median filter of length ± 5 s to remove noise while retaining the IUP peaks [13].

As the EHG is a nonstationary signal [21], the employment of a time frequency distribution (TFD) is a suitable frequency analysis approach. Since we are interested in the electrical energy, which is a quadratic signal, the class of quadratic TFDs was used [22]. In particular, in this study four different quadratic TFDs were tested, namely, the Wigner-Ville Distribution, the Smoothed Wigner-Ville Distribution, the Choi-Williams Distribution, and, finally, the spectrogram, which is obtained by the squared magnitude of the short-time Fourier transform of the time signal $x(n)$ through a limited time-window $w(m)$

$$\rho(n,f) = \left| \sum_{m=-\infty}^{\infty} x(m)w^*(m-n)e^{-j2\pi fm} \right|^2 \tag{3.1}$$

where $(.)^*$ is the conjugate operator.

The Wavelet Transform (WT) can also be employed for the analysis of nonstationary signals [23] and its main advantage over other TFDs, such as the spectrogram, is the capability of performing a multi-resolution analysis in the TF domain [24]. Although the WT is a time-scale representation in the first place, it is also suitable, in fact, for TF interpretation [25] by formally relating the scaling parameter to the center frequency of the employed mother Wavelet [26]. Since we are interested in the analysis of the EHG signal energy distribution, the squared modulus of the WT, namely the Scalogram, was calculated. The adopted mother Wavelet was the Morlet Wavelet, the most commonly used for TF analysis [27].

The most suitable values for the TFDs and the best TF distribution for EHG analysis were singled out by an iterative procedure aiming at the maximization of the average correlation coefficient R between the IUP estimated by the proposed method (before polynomial modeling, see Section 3.2.4) and the IUP measured by the pressure transducer.

According to our experiments, the use of the spectrogram with a 70 s time window $w(m)$ resulted in the best estimation of the IUP. Moreover, with the prospect of on-line applications, the implementation of the spectrogram as the squared magnitude of the short-time Fourier transform results in a lower computational complexity with respect to other TFDs.

3.2.3 Feature extraction

The tension generated by the contracting myometrium and the consequent IUP increase are dependent on the speed of AP propagation from cell to cell and on the amount of muscle cells involved in the contraction [5]; in smooth muscles, these two phenomena are mutually dependent, as propagation requires recruitment of multiple cells. The excitation rate of smooth muscle cells, which is the counterpart of the firing rate for skeletal muscle EMG, is an additional factor which contributes to the IUP increase. All these factors are reflected in the frequency spectrum of the EHG signal, which can be therefore regarded as the result of a FM process. Additionally, the EHG signal at each electrode is the signal generated by the muscular contraction on a macroscopic scale, i.e., a signal originating from the combined contributions of the individual muscle cells activated underneath the electrode. Consequently, the EHG at each electrode is regarded as the result of a FM multi-component signal where the IUP is related to the modulating signal [14]. A first estimate of the contraction pattern can hence be provided by the average frequency. The average frequency $f_1(n)$ of a signal, represented in the TF domain by the spectrogram $\rho(n, f)$ as in (3.1), can be expressed as

$$f_1(n) = \frac{\sum_{f=0}^{\infty} f \rho(n, f)}{\sum_{f=0}^{\infty} \rho(n, f)} \tag{3.2}$$

which also corresponds to the first statistical moment in frequency [28]. The use of (3.2) is common for spectral analysis of the skeletal muscle EMG signals and for assessment of fiber conduction velocity [29]. However, differently from skeletal muscles, the force generated by the uterus is related to both the propagation properties of the APs, which are reflected in the spectral characteristic of the EHG signal, and the amount of cells involved in the contraction, which is proportional to the amplitude

of the EHG signal. A measure of the signal amplitude is provided by its energy [30]

$$E_x(n) = \sum_{f=0}^{\infty} \rho(n,f).$$

(3.3)

The IUP increase is the consequence of the well coordinated contraction of a substantial number of cells. Therefore, the simultaneous increase of both the frequency-related and amplitude-related features of the EHG signal determines the establishment of the IUP wave. By multiplying (3.3) and (3.2) and selecting a frequency band $[f_{min}, f_{max}]$, a first estimation of the IUP can be therefore derived, which corresponds to the unnormalized first statistical moment $\Psi(n)$ of the TF representation $\rho(n, f)$

$$\Psi(n) = \sum_{f_{min}}^{f_{max}} f \, \rho(n,f).$$

(3.4)

Based on our measurements and in agreement with other studies [11, 20, 21, 31, 32], the most suitable integration interval $[f_{min}, f_{max}]$ for IUP estimation resulted the frequency band [0.3 Hz, 0.8 Hz].

3.2.4   Electromechanical activation modeling

The first unnormalized statistical moment obtained by the spectrogram can be further processed in order to increase the accuracy of the estimate. In general, the relationship between the uterine electrical activation, the EHG signal, and the mechanical response, the IUP, can be considered nonlinear. In vitro studies on animal uterine strips [33] highlighted, in fact, during induced isometric contractions, a nonlinear characteristic of the tension developed by the myometrium as a function of the electrical stimulation. Furthermore, the IUP increase is the result of the simultaneous contraction of an adequate number of cells and it is associated with a widespread electrical activity of the whole myometrium. Therefore, electrical activities that are local or poorly coordinated can be recorded without being necessarily followed by a linearly related IUP increase. Furthermore, as the tension generated by the myometrium is the result of the AP spreading in the muscle tissue, the IUP increase is always temporally delayed with respect of the electrical activation. Therefore, the delay τ_k between the IUP recorded by the catheter and the first unnormalized moment calculated in each channel k was also included in the model.

A second-order polynomial model resulted as a suitable representation of the relationship between the unnormalized first statistical moment of the EHG signal TF representation and the simultaneously measured IUP. The use of higher order polynomial models was also investigated, but no improvement was experienced.

We indicate by $\Psi_k(n)$ the unnormalized first EHG statistical moment calculated in each channel k and by IUP(n) the pressure measured by the catheter. An estimate,

$\widehat{\text{IUP}}_k(n+\tau_k)$, of the pressure recorded by the catheter can be derived in each channel by a polynomial expansion of $\Psi_k(n)$ with coefficients a_P, b_P, and $c_P \in R$ as given in (3.5):

$$\widehat{\text{IUP}}_k(n+\tau_k) = a_P + b_P\Psi_k(n) + c_P\Psi_k(n)^2. \qquad (3.5)$$

In (3.5), a_P models the offset, b_P the gain, and c_P the nonlinearities of the relationship between the estimated IUP in each channel k and the IUPC signal.

The model in (3.5) is a standard representation of a nonlinear relationship. However, for values of $\Psi_k(n)$ above the maximum point of the parabola described by (3.5), an IUP decrease is obtained for increasing values of $\Psi_k(n)$; this effect might be not representative of the underlying physiology. Therefore, a logarithmic model, i.e.,

$$\widehat{\text{IUP}}_k(n+\tau_k) = a_L + \log(b_L\Psi_k(n)+1), \qquad (3.6)$$

a_L, b_L, and $c_L \in R$, was considered as a potentially more suitable representation of the electromechanical activation of the myometrium. According to (3.6), an increase of electrical activation, $\Psi_k(n)$, produces always an increase of the mechanical response, $\text{IUP}(n)$.

In order to account for a possible asymptotic behavior of the IUP in response to increasing electrical activation, an exponential model of the form

$$\widehat{\text{IUP}}_k(n+\tau_k) = a_E + b_E(1 - e^{c_E\Psi_k(n)}), \qquad (3.7)$$

with a_E, b_E, and $c_E \in R$, was also tested.

The coefficients a_P, a_L, and a_E in (3.5), (3.6) and (3.7), respectively, represent the offset between the electrical activation and the IUP. In fact, even in the absence of uterine contraction, the IUPC signal gives a value, referred to as baseline tone, which is usually different from zero. Since the IUPC signal baseline tone is affected by factors that are not related to the uterine activity [34], it was detected by the method described in [12] and digitally removed on the basis of the first two minutes of recording. As the same procedure was applied to $\Psi_k(n)$ prior identification of the model coefficients, the constant terms a_P, a_L, and a_E were set to zero.

The other coefficients of the models, in the following addressed as the parameter array $\underline{P}_k$, were identified separately for each channel and each contraction segment, of variable length N samples, by minimization of the mean channel error ε_k,

$$\varepsilon_k(\tau_k, \underline{P}_k) = \frac{1}{N}\sum_{n=1}^{N}(\text{IUP}(n) - \widehat{\text{IUP}}_k(n+\tau_k))^2, \qquad (3.8)$$

between the invasively recorded IUPC signal and the IUP estimated in the channel k, $\widehat{\text{IUP}}_k(n+\tau_k)$. The Nelder-Mead Simplex search method [35] was used for the minimization of ε_k.

To this end, contiguous time segments of the IUPC signal, each containing one contraction, were previously automatically selected using an adaptive threshold [12]. Each contraction segment included one contraction and part of the baseline tone preceding and following the contraction itself. For each channel and model, an estimate of the IUP was eventually derived by using a single set of coefficients, which was obtained by the median value of all the coefficients identified separately for each contraction. The median value rather than the average value was chosen to ensure robustness with respect to possible outliers.

The delay between the unnormalized first moment and the IUP signals was initially calculated by maximization of their cross-correlation function for each recording. For each channel k, the average delay τ_k across all the subjects was then considered for the entire data-set.

3.3   Evaluation of the estimate quality

Previous studies for estimating the uterine mechanical activity by EHG processing mainly comprised the calculation of the root mean squared value (RMS) of the EHG signal and, more recently, the employment of optimal linear filtering [13, 36]. These two algorithms were tested on each channel of our data-set to evaluate the performance of the proposed method. The comparison aimed at the evaluation of the methods in the prospective of noninvasive measurements in a clinical setting.

According to the method proposed by [10, 36], for each bipolar down-sampled signal we calculated the RMS values in 60-s sliding Hamming windows. Then, prior to comparison with the results obtained by the other methods, the model defined in (3.5) was applied to the calculated RMS series according to the procedure previously described.

For the implementation of the Wiener filter [13], further preprocessing was needed to normalize, down-sample, and rectify the preprocessed signal $x(n)$. The performance of the algorithm described in [13] was further improved by removing the mean value from both the rectified EHG signal and the IUPC signal prior to training the filter coefficients. For each channel and patient, the weights were calculated on the basis of the entire recording employing linear regression. For each channel a set of weights was then obtained by averaging the values across the examined subjects. The final results were eventually derived by filtering the rectified EHG signals from all the subjects employing the calculated average weights.

The results obtained by the proposed methods for IUP estimation were compared to those provided by optimal filtering and RMS analysis in terms of correlation coefficient R and root mean squared error (RMSE) between the IUP estimate and the IUP

measured by the catheter.

$$\text{RMSE} = \sqrt{E(\text{IUP}(n) - \widehat{\text{IUP}}_k(n))^2}, \tag{3.9}$$

where $E[\cdot]$ is the expected value operator, with the IUPC signal, $\text{IUP}(n)$.

For a clinical feasibility assessment, the peak pressure amplitude of each contraction, $\widehat{\text{IUP}}_P$, measured on the IUP estimate was compared to the peak pressure amplitude, IUP_P, derived from the IUPC signal. The peak pressure amplitude is, in fact, one of the parameters commonly employed in clinical practice for the evaluation of uterine contractility by IUPC recordings [37, 38].

The correlation coefficient R and the RMSE are important figures of merit for the characterization of the estimate. As the correlation coefficient is a measure of similarity in shape between two waveforms, a high value of R between the real IUP and its estimate can be directly related to a high probability of detecting the correct number of contractions. The RMSE, on the other hand, is influenced by scaling

Table 3.1: *Average Results*

Method	R ($p < 0.01$)	RMSE (mmHg)
Optimal Linear Filtering	0.5 ± 0.16	11.4 ± 3.12
RMS	0.36 ± 0.16	13.17 ± 4.62
Proposed (polynomial model)	0.73 ± 0.11	13.47 ± 6.67
Proposed (logarithmic model)	0.74 ± 0.11	5.13 ± 4.74
Proposed (exponential model)	0.74 ± 0.10	6.36 ± 5.63

factors and DC offset. Therefore, for a fair comparison with optimal linear filtering, the RMSE of the estimate provided by RMS analysis and by the proposed method was calculated after removal of the average value from both the IUPC signal and the estimate. Notice that the RMSE retains the same units of pressure of the desired signal (mmHg).

3.4 Results

The results provided by the proposed method, RMS analysis, and optimal linear filtering are shown in Table 3.1, where the average values of R and RMSE across all channels and patients are reported together with their inter-patient variability. The proposed method in combination with a polynomial model already provided estimates that are highly correlated with the invasively recorded IUP. However, as from table 3.1, the logarithmic and the exponential model provided a significant estimation improvement with respect to all the other methods, especially in terms of RMSE.

Therefore, for testing clinical feasibility, only the methods using the logarithmic and the exponential model were further analyzed.
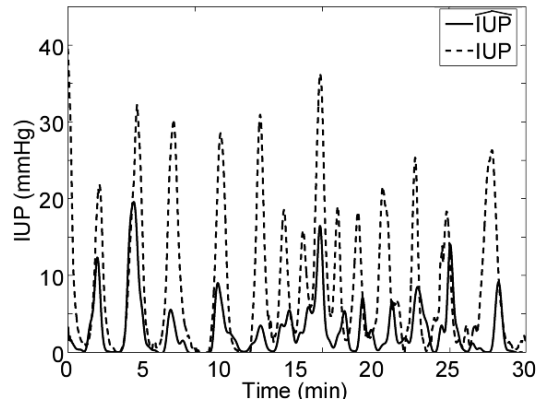
Figure 3.3: *Example of IUP estimated by the RMS analysis method. For the entire waveform R = 0.70 and RMSE = 16.5 mmHg.*
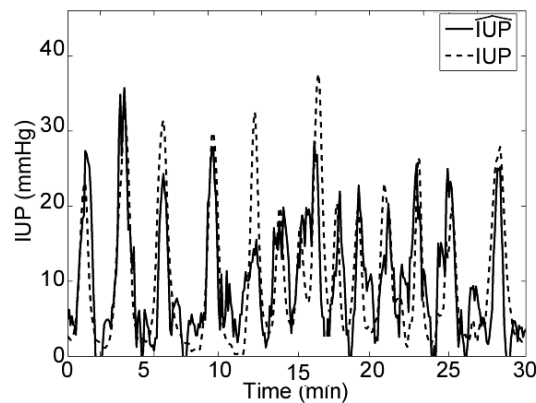
Figure 3.4: *Example of IUP estimated by optimal linear filtering. For the entire waveform R = 0.71 and RMSE = 6.65 mmHg. The removed mean value was restored for both waveforms on the basis of the mean value of the invasively recorded IUPC.*

In Figs. 3.3, 3.4, 3.5, 3.6, and 3.7 an example of IUPC recording (IUP) and corresponding IUP estimate ($\widehat{\text{IUP}}$) is presented for each method applied to the same channel and subject.

By employment of the polynomial model, the estimate accuracy improved for both the RMS analysis and the unnormalized first statistical moment. Especially for the proposed method, the average correlation coefficient with the invasively recorded
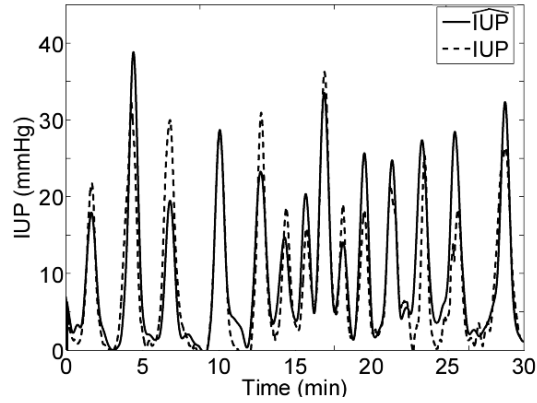
Figure 3.5: *Example of IUP estimated by the polynomial model. For the entire waveform R = 0.87 and RMSE = 6.5 mmHg.*
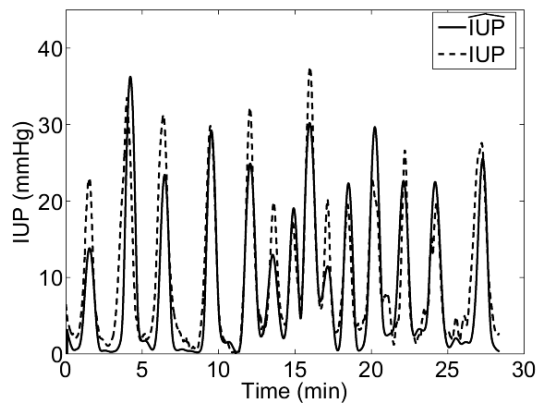
Figure 3.6: *Example of IUP estimated by the logarithmic model. For the entire waveform R = 0.86 and RMSE = 4.5 mmHg.*

IUP improved from $R = 0.59$ to $R = 0.73$; the root mean squared error improved from RMSE = 17.20 mmHg to RMSE = 13.47 mmHg. The average time delay τ_k between the estimated IUP and the IUPC was 9.96 ± 0.99 s.

3.5 Clinical feasibility

The mean peak pressure of the IUP estimated by exponential and logarithmic modeling was, respectively, 11.21 ± 5.82 mmHg and 10.4 ± 12.9 mmHg lower than the peak pressure recorded by the catheter. The average IUPC signal peak pressure value was 41.6 mmHg. A more detailed overview of the peak pressure difference between
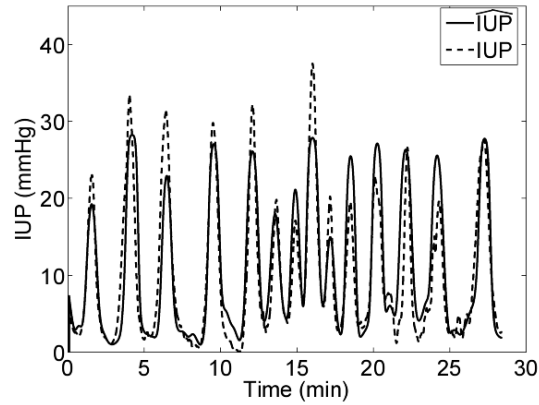
Figure 3.7: Example of IUP estimated by the exponential model. For the entire waveform $R = 0.87$ and $\mathrm{RMSE} = 4.8$ mmHg.

the IUPC signal and the estimates is provided by the Bland-Altman plots in Fig. 3.8 and Fig. 3.9, for the logarithmic and for the exponential model, respectively. The IUP peak amplitude difference is shown as percentage of the mean of IUP_P and $\widehat{\mathrm{IUP}}_P$.
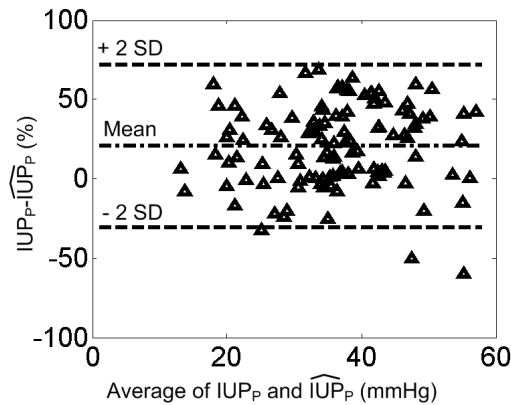
Figure 3.8: Bland-Altman plot of the peak pressure, IUP_P, of the IUPC signal and the peak pressure, $\widehat{\mathrm{IUP}}_P$, of the IUP estimated by logarithmic modeling.

In Fig. 3.8 and Fig. 3.9, all contractions and channels of all subjects were equally considered. If the average value of peak pressure difference was calculated separately for each patient, the mean peak pressure difference resulted in $-9\% \pm 5\%$ and $-18 \pm 9\%$ of the average between IUP_P and $\widehat{\mathrm{IUP}}_P$ for the logarithmic and for the exponential model, respectively.
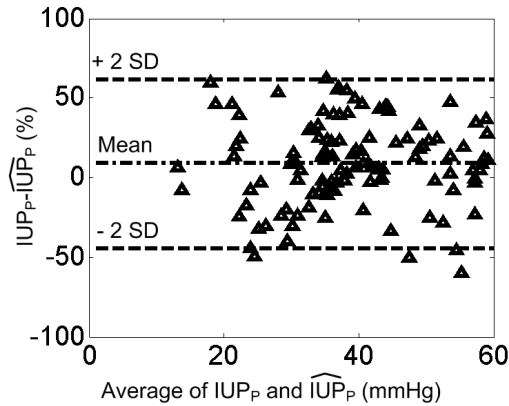
Figure 3.9: *Bland-Altman plot of the peak pressure,* IUP_P*, of the IUPC signal and the peak pressure,* $\widehat{\text{IUP}}_P$*, of the IUP estimated by exponential modeling.*

3.6 Discussion and conclusions

In this chapter a noninvasive method to estimate the IUP is proposed that is based on the joint analysis of amplitude and time-frequency features of the EHG signal. The method was tested on a set of measurements from nine women during delivery. The results were compared to those provided by other two methods proposed in the literature for quantitative estimation of the uterine mechanical activity, namely optimal linear filtering and an improved version of RMS analysis. The comparison aimed at the evaluation of the methods in the perspective of noninvasive clinical measurements. By simultaneously recording a four-channel EHG signal and the IUPC output, we could reliably assess the IUP estimates provided by the methods.

In terms of correlation coefficient with the invasively recoded IUP, the proposed method with a polynomial model already resulted in a significantly increased correlation with respect to the RMS analysis and the optimal linear filtering. Nevertheless the logarithmic and the exponential model provided a significant improvement with respect of all the other methods, especially when the RMSE between the estimate IUP and the invasively recorded IUPC signal was considered. On average, the logarithmic model, which does not account for an asymptotic behavior of the IUP, provides more accurate estimates than the exponential model.

With reference to the methodology, the RMS analysis has the great advantage of being simple and suitable for real-time applications. The optimal linear filtering suggests a technical approach aimed at the identification of a linear transfer function between the rectified EHG signal and the IUP. The physiological assumptions of these two methods can be summarized in the use of the EHG amplitude, either in terms of

EHG signal envelop or in terms of rectified EHG signal, as indicative of the tension produced by the contracting myometrium. On the other hand, the proposed method was fundamentally conceived on the basis of the physiologic phenomena underling the generation of the recorded signals and their relationship.

In this work, IUPC signals were used for validation because IUPC recordings are currently the most reliable technique for uterine contraction monitoring [39]. Nevertheless, in [40], from the IUP measured by three fluid-filled catheters simultaneously inserted in the same uterus, the authors found a measurement uncertainty up to 25%. In [38], where, like in the present study, transducer-tipped catheters were used, a lower measure uncertainty was found; for catheters inserted independently in the same uterus, the mean peak pressure difference (bias) for each patient was about $9.96\% \pm 9.7\%$ of the average value recorded by the two catheters.

In the present study, when comparing peak pressure measurements derived from the estimate of all patients and channels to the invasively recorded IUP, both the exponential and the logarithmic model resulted in a biased estimate with a standard deviation of about 25%. However, by comparing the invasive catheter recording and the noninvasive IUP estimated by EHG signal analysis in terms of average peak difference per patient, as it was done in [38], we obtained an average peak pressure difference for the logarithmic model of $-9\% \pm 5\%$, which can be comparable to the measurement uncertainty ratios reported for transducer-tipped IUP catheter recordings in [38].

The good results of the estimation suggest that the model coefficients did not show significant variations across the considered subjects. However, in the perspective of introducing the proposed method in everyday clinical practice, the proposed approach could support dedicated studies aimed at the identification of more complex models, possibly including additional parameters for a specific characterization of patient differences.

In general, the proposed method, due to the adopted physiology-based approach, may offer additional insight for a better understanding of uterine muscle activity. As the EHG signal is associated with the primary cause of the uterine contraction, we believe that the EHG signal analysis has great potential beyond the estimation or prediction of the uterine mechanical activity. Nevertheless, many aspects related to the uterine muscle contraction process still need to be clarified. Future research will therefore include the propagation properties of the EHG signal with the ultimate goal of providing a reliable and noninvasive technique for preterm labor prediction.

Bibliography

[1] G.S. Berkowitz and E. Papiernik, "Epidemiology of preterm birth," *Epid. Rev.*, vol. 15, pp. 414–443, 1993.

[2] N.S. Padhye, Z. Duan, and M.T. Verklan, "Response of fetal heart rate to uterine contractions," in *IEEE EMBS Proc. Int. Conference*, 2004, pp. 3953–3955.

[3] A.C. Guyton and J.E. Hall, *Textbook of medical physiology*, Elsavier Saunders, Philadelphia, 2006.

[4] H. Eswaran, J.D. Wilson, P. Murphy an H. Preissl, and C.L. Lowery, "Application of Wavelet tranform to uterine electromyographic signals recorded using abdominal surface electrodes," *J. Matern.-Fetal Neonatal Med.*, vol. 11, pp. 158–166, 2002.

[5] R.E. Garfield, G. Saade, C. Buhimschi, I. Buhimschi, L. Shi, S.Q. Shi, and K. Chwalisz, "Control and assessment of the uterus and cervix during pregnancy and labor," *Hum. Reprod. Update*, vol. 4, pp. 673–695, 1998.

[6] A.M. Miles, M. Monga, and K.S. Richeson, "Correlation of external and internal monitoring of uterine activity in a cohort of term patients," *Am. J. Perinatol.*, vol. 18, pp. 137–140, 2001.

[7] R.E. Garfield, H. Maul, W. Maner, C. Fittkow, G. Olson, L. Shi, and G. R. Saade, "Uterine electromyography and light-induced fluorescence in the management of term and preterm labor," *J. Soc. Gynecol. Invest.*, vol. 9, pp. 265–275, 2002.

[8] H. Maul, W.L. Maner, G. Olson, G.R. Saade, and R.E. Garfield, "Noninvasive transabdominal uterine electromyography correlates with the strength of intrauterine pressure and is predictive of labor and delivery," *J. Matern. Fetal. Med.*, vol. 15, pp. 297–301, 2004.

[9] C. Buhimschi and R.E. Garfield, "Uterine contractility as assessed by abdominal surface recording of electromyographic activity in rats during pregancy," *Am. J. Obstet. Gynecol.*, vol. 174, pp. 744–753, 1996.

[10] K. Horoba, J. Jezewski, J. Wrobel, and S. Graczyk, "Algorithm for detection of uterine contractions from electrohysterogram," in *IEEE EMBS Proc. Int. Conference*, 2001, pp. 2161–2164.

[11] C. Buhimschi, M.B. Boyle, and R.E. Garfield, "Electrical activity of the human uterus during pregnancy as recorded from the abdominal surface," *Obstet. Gynecol.*, vol. 90, pp. 102–111, 1997.

[12] J. Jezewski, K. Horoba, A.Matonia, and J. Wrobel, "Quantitative analysis of contraction patterns in electrical activity signal of pregnant uterus as an alternative to mechanical approach," *Physiol. Meas.*, vol. 26, pp. 753–767, 2005.

[13] M.D. Skowronski, J.G. Harris, D.E. Marossero, R.K. Edwards, and T.Y. Euliano, "Prediction of intrauterine pressure from electrohysterography using optimal linear filtering," *IEEE Trans. Biomed. Eng.*, vol. 53, pp. 1983–1989, 2006.

[14] J. Duchêne, D. Devedeux, S. Mansour, and C. Marque, "Analyzing uterine EMG: Tracking instantaneous burst frequency," *IEEE Eng. Med. Biol. Mag.*, vol. 14, pp. 125–132, 1995.

[15] C. K. Marque, J. Terrien, S. Rihana, and G. Germain, "Preterm labour detection by use of a biophysical marker: the uterine electrical activity," *BMC Pregnancy Childbirth*, vol. 7 Suppl 1:S5, pp. 2393–7, 2007.

[16] D. Devedeux, C. Marque, S. Mansour, G. Germain, and J. Duchêne, "Uterine electromyography: a critical review," *Am. J. Obstet. Gynecol.*, vol. 169, pp. 1636–1653, 1993.

[17] A.C. Metting van Rijn, A. Peper, and C.A. Grimbergen, "High-quality recording of bioelectric events. part 1 interference reduction, theory and practice," *Med. Biol. Eng. Comput.*, vol. 28, pp. 389–397, 1990.

[18] S. Graczyk, J. Jezewski, J. Wrobel, and A. Gacek, "Abdominal electrohysterogram data acquisition problem and their source of origin," in *IEEE EMBS Proc. Int. Conference*, 1995, pp. 13–14.

[19] P. Carré, H. Leman, C. Fernandez, and C. Marque, "Denoising of the uterine EHG by an undecimated Wavelet transform," *IEEE Trans. Biomed. Eng.*, vol. 45, pp. 1010–1017, 1998.

[20] C. Marque, J. Duchêne, S. Leclercq, G. Panczer, and J. Chaumont, "Uterine EHG processing for obstetrical monitoring," *IEEE Trans. Biomed. Eng.*, vol. BME-33, pp. 1182–1187, 1986.

[21] H. Leman, C. Marque, and J. Gondry, "Use of the electrohysterogram signal for characterization of contractions during pregnancy," *IEEE Trans. Biomed. Eng.*, vol. 46, pp. 1222–1229, 1999.

[22] J.C. Andrieux, M.R. Feix, G. Mourgues, P. Bertrand, B. Izrar, and V.T. Nguyen, "Optimum smoothing of the Wigner-Ville distribution," *IEEE Trans. Acoust. Speech Signal Process.*, vol. 35, pp. 764–769, 1987.

[23] I. Daubechies, "The Wavelet transform, time-frequency localization and signal analysis," *IEEE trans. Inform. Theory*, vol. 36, pp. 961–1004, 1990.

[24] O. Rioul and P. Flandrin, "Time-scale energy distribution: a general class extending Wavelet transforms," *IEEE Trans. Signal Process.*, vol. 40, pp. 1746–1757, 1992.

[25] P. Flandrin, *Time-frequency/Time-Scale Analysis*, Academic Press, San Diego, 1999.

[26] O. Rioul and M. Vetterli, "Wavelets and signal processing," *IEEE Signal Process. Mag.*, vol. 8, pp. 14–38, 1991.

[27] C. Torrence and G.P. Compo, "A practical guide to Wavelet analysis," *Bull. Amer. Meteorol. Soc.*, vol. 79, no. 1, pp. 61–78, 1998.

[28] B. Boashas, *Time Frequency Signal Analysis and Processing. A Comprehensive Reference*, Elsevier, Oxford, 2003.

[29] L. Sörnmo and P. Laguna, *Bioelectrical signal processing in cardiac and neurological applications*, Elsavier, New York, 2005.

[30] J.G. Proakis and D.G. Manolakis, *Digital signal processing*, Prentice Hall International, London, third edition, 1996.

[31] C. Rabotti, M. Mischi, J.O.E.H. van Laar, S.G. Oei, and J.W.M. Bergmans, "Relationship between electrohysterogram and internal uterine pressure: a preliminary study," in *IEEE EMBS Proc. Int. Conference*, 2006, vol. 1, pp. 1661–4.

[32] W.L. Maner, R.E. Garfield, H. Maul, G. Olson, and G. Saade, "Predicting term and preterm delivery with transabdominal uterine electromyography," *Obstet. Gynecol.*, vol. 101, pp. 1254–1260, 2003.

[33] A. Csapo, "Dependence of isometric tension and isotonic shortening of uterine muscle on temperature and on strength of stimulation," *Am. J. Physiol.*, vol. 177, pp. 348–354, 1954.

[34] P.J. Steer, "Non-invasive transabdominal uterine electromyography correlates with the strength of intrauterine pressure and is predictive of labor and delivery," *J. Matern. Fetal. Med.*, vol. 15, pp. 297–301, 2004.

[35] J.C. Lagarias, J.A. Reeds, M.H. Wright, and P.E. Wright, "Convergence properties of the Nelder-Mead simplex method in low dimensions," *SIAM J. Optim.*, vol. 9, pp. 112–147, 1998.

[36] K. Horoba, S. Graczyk, J. Jezewski, A. Gacek, and J. Wrobel, "Statistical approach to analysis of electrohysterographic signal," in *IEEE EMBS Proc. Int. Conference*, Atlanta, GA, USA, 1999, p. 887.

[37] G.F. Phillips and A.A. Calder, "Units for the evaluation of uterine contractility," *BJOG*, vol. 94, pp. 236–241, 1987.

[38] S. Chua, S. Arulkumaran, M. Yang, S.S. Ratnam, and P.J. Steer, "The accuracy of catheter-tip pressure transducers for the measurement of intrauterine pressure in labour," *BJOG*, vol. 99, pp. 186–189, 1992.

[39] R.E. Garfield, H. Maul, L. Shi, W. Maner, C. Fittkow, G. Olsen, and G.R. Saade, "Methods and devices for the management of term and preterm labor," *Ann. NY Acad.Sci.*, vol. 943, pp. 203–224, 2001.

[40] J.D. Knoke, L.L. Tsao, M.R. Neuman, and J.F. Roux, "The accuracy of measurements of intrauterine pressure during labor: a statistical analysis," *Comput. Biomed. Res.*, vol. 9, pp. 177–186, 1976.

Chapter 4

Large-scale electrohysterographic propagation analysis

In medio stat virtus [1]

4.1   Introduction

Preterm birth accounts for 75% and 50% of perinatal mortality and long-term morbidity, respectively [1]. Pregnant women with symptoms of preterm delivery, i.e., preterm uterine activity in the form of painful uterine contractions, are commonly treated with tocolytic agents for suppressing the contractions. Although an early treatment improves the effectiveness of tocolytics [2], their indiscriminate use at the first signs of preterm delivery can be risky for mother and fetus [3]. Therefore, timely recognition of the process leading to labor is of prime importance.

The contractile element of the uterus is the myometrium. The myometrial tissue is composed of depolarizing and repolarizing smooth muscle cells, which are spontaneously active [4]. Early in pregnancy, the poor electrical coupling among the cells is responsible for the quiescent status of the uterus. As delivery approaches, the formation of low resistance electrical paths allows the propagation of electrical activity from cell to cell in the form of action potentials [5, 6]. The electrical activity can originate at any region of the myometrium (pacemaker area) and then propagate to the neighboring cells. Up until now, there is no recognized conduction pathway for the electrical transmission in this muscle. The propagation of action potentials through an adequate number of cells results in a coordinated contraction of the myometrium. Effective contractions are capable of inducing progressive cervical dilatation and produce an increase of the internal uterine pressure (IUP) acting towards the expulsion of the fetus at the end of delivery.

---

[1]Literally 'Virtue stands in the middle'. Even if this concept was already used by Aristotle in the 'Ethica Nicomachea' as 'méson te kai áriston' ('the best thing is in the middle') and then by Horatius in the 'Satira' as 'est modus in rebus' ('there is a measure in things'), this Latin motto is famous due to the medieval Scholastic philosophy.

There are no means for an early discrimination between effective premature contractions, which need to be promptly suppressed with tocolytics, and unproductive premature uterine activity, which does not lead to delivery and hence does not require treatments.

In the presence of uterine activity, the contraction rate can be reliably measured by an external tocodynamometer. However, due to the weak relation between contraction rate and preterm delivery [7], an early prediction of labor cannot be provided by a tocodynamometer. Evaluation of the cervical changes caused by uterine activity using digital or ultrasound examination have demonstrated poor sensitivity and low positive predictive values [7]. Some biomarkers, such as the fetal fibronectin in symptomatic women, seem promising predictors of preterm delivery [8, 9], but their clinical utility and applicability needs still to be clarified.

The electrohysterogram EHG is the signal associated to the electrical activity propagating through the myometrium cells during a contraction [10, 11].

In the literature, several studies investigated the use of the electrohysterographic (EHG) signal for predicting labor and discriminating contractions leading to preterm delivery. Overall, many parameters derived from the EHG signal have been considered, both in time [4, 12, 13] and in frequency domain [4, 12–16]. The shift of the EHG burst frequency components from low frequencies, during pregnancy, to higher frequencies, during labor, seems the most significant and one of the earliest observable characteristics. However, such EHG spectral changes were observed as delivery approaches in both term and preterm deliveries [17].

The prediction of preterm labor on the basis of the EHG signal frequency content can therefore be hampered by the possibility that the spectral changes observed for preterm contractions are simply the result to an earlier evolution of the same process leading to a delivery at term. Instead, as the spreading of electrical activity in the myometrium is the first trigger of a coordinated and effective contraction, a multichannel analysis of direction and speed of the propagating EHG signal could provide a fundamental contribution for predicting delivery. Extensive research has been carried out on EHG frequency analysis, but only few preliminary studies have been reported on the investigation of the EHG signal propagation [18, 19].

The challenging objective of predicting premature birth necessitates, in the first place, the development of dedicated signal processing techniques to permit the required clinical studies.

In this chapter, a dedicated method is proposed for calculating the interelectrode time-delay of EHG signals, which is based on the adaptive estimation of the interelectrode transfer function and the relative detection delay. The problem is simplified by calculating the delay between couples of electrode signals. This choice permits choosing the electrode with the best signal-to-noise ratio (SNR) as common reference for the delay calculation and exploiting the interelectrode transfer function for
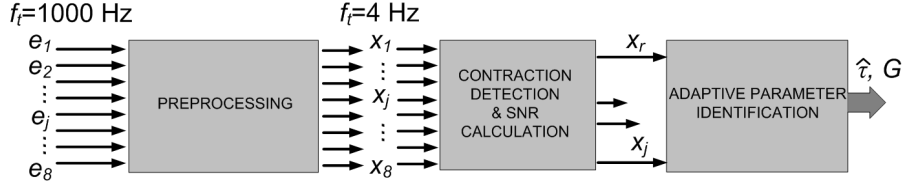
Figure 4.1: *Block scheme of the proposed approach.*

improving the estimate accuracy. A simple maximization of the cross-correlation function (CCF) between the channels was first considered and compared to a high-resolution estimator based on spectral matching [20]. The temporal resolution provided by the CCF method is limited by the employed sampling period. However, the resolution can be improved by interpolating around the maximum of the CCF [21] or, if the computational time is not relevant, by using higher sampling frequencies. Methods based on spectral matching and phase-difference (PD) are equivalent alternatives for providing the time-lag between two signals without any temporal resolution limitation [20, 22, 23].

The performances of these estimators, however, are highly dependent on the similarity of the input signals, i.e., the methods perform best when they are applied to the delayed versions of the same signal [24]. We propose an improvement of the performance of the spectral matching method by increasing the interchannel similarity prior to delay calculation. Such an improvement is achieved by prior adaptive estimation of the interelectrode transfer function. This transfer function is modeled by a zero-phase, finite impulse response (FIR) filter, whose design is based on accurate physiological observations and modeling.

The estimators are implemented, evaluated, and compared on simulated and real data. Furthermore, a feasibility study is performed by analyzing the propagation properties of EHG signals recorded in a multielectrode configuration on seven women in labor.

4.2 Methodology

For the assessment of the interelectrode delay, we implemented the following methods: two standard delay estimators, namely spectral matching and maximization of the CCF, and a dedicated method.

The main steps of the dedicated method are schematically described in Fig. 4.1 and explained in detail in the following sections. The unipolar EHG signals, $(e_1, ..., e_8)$ were recorded at different locations spatially distributed on the entire maternal abdomen and digitized at 1000 Hz, i.e., a sufficiently high sampling frequency (f_t) to avoid aliasing of the components deriving from the subject's electrocardiogram (ECG) and skeletal electromyogram (EMG). The recorded signals were then prepro-

cessed to improve the SNR and reduce f_t to 4 Hz. The second block comprises the detection of contractions and the calculation of the SNR at each electrode. The outputs of this block are the contraction segments and the signal with the best SNR, x_r. The last block operates an adaptive estimation of two parameters: the transfer function G and the delay $\widehat{\tau}$ between each electrode signal x_j and the reference electrode signal x_r. In order to improve the similarity between each x_j and x_r, the transfer function G is estimated during calculation of $\widehat{\tau}$, which is the actual output of the scheme and the parameter of interest.

Spectral matching required the same processing steps as the dedicated approach with the exception of the estimation of the adaptive filter G.

The CCF maximization method did not include downsampling in order to obtain a temporal resolution that was comparable to the other implemented estimators; the CCF was in fact calculated at 1000 Hz.

4.2.1   Data acquisition

The experimental data were collected at the Máxima Medical Center in Veldhoven (the Netherlands). The study was approved by the ethical committee of the hospital. Seven women during labor underwent multichannel electrical EHG recordings after signing an informed consent. All women were at term with the exception of two, who were post-term. Prior to EHG recording, four women had labor induction.

After accurate skin preparation with an abrasive paste for skin impedance reduction, eight disposable contact Ag-AgCl electrodes were placed on the abdomen as shown in Fig. 4.2(a). The electrode position was chosen to cover as much of the uterus as possible, but the number of sensors was limited to 8 to avoid patient's discomfort and make the experiments feasible in a clinical environment. The common reference (REF) for the recording electrodes was placed on the right hip. In order to obtain an efficient rejection of the electromagnetic interference, we employed a driven-right-leg (DRL) ground electrode and actively shielded cables [25]. The IUP was simultaneously measured by a Koala M1333A (Philips Medical Systems, Best, the Netherlands) intrauterine pressure catheter inserted in the uterine cavity due to medical prescription. The EHG signals were recorded at 1000 Hz and digitized at 20-bit resolution by an M-PAQ amplifier (Maastricht Instruments Ltd., the Netherlands), a 16-channel system for physiological measurements with programmable gain and sampling frequency. The length of data recorded from each subject ranged from 25 to 73 minutes (from 9 to 23 contractions). In total, we analyzed approximately 5 hours of recordings containing 93 uterine contractions.

(a) (b)
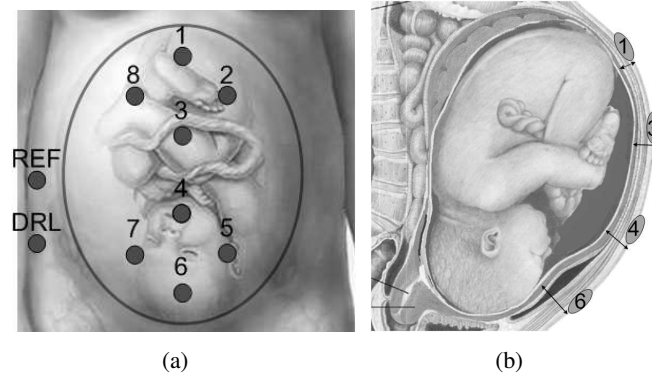
Figure 4.2: *Electrode configuration: front view (a), side view (b). On the abdominal profile it is possible to infer the different properties of the tissues interposed between the EHG source and the recording electrodes.*

4.2.2 Preprocessing

The uterine EHG signal can be affected by several noise sources, e.g., the mother's ECG (MECG), the EMG generated by the contraction of abdominal skeletal muscles, respiration, and different motion artifacts.

Previous work demonstrated that the frequency content of EHG signals non invasively recorded during delivery is concentrated below 1 Hz [14, 15, 26]. On the other hand, the minimum frequency content of the ECG corresponds to the minimum value of the instantaneous heart rate [27]. For example, a minimum ECG frequency content of 1 Hz corresponds to a heart rate of of 60 beat per minute, which can be considered a lower-bound value for women during delivery. The MECG was therefore suppressed by low-pass filtering. The stop band lower frequency of the filter was set at the minimum value of the instantaneous mother's HR calculated during each recording by the method described in [28]. In order to obtain a steep transitional band, we used a Chebyshev Type II filter with the minimum order required to meet the following specifications: 0.4 Hz transition bandwidth, 3 dB maximum pass-band ripple, and 60 dB stop-band attenuation.

Another source of noise is the abdominal EMG. It was demonstrated that the electrical signal associated to voluntary contraction of the abdominal muscle has a dominant frequency component of about 30 Hz [29]. After low-pass filtering, the noise due to EMG activity is therefore negligible.

The baseline oscillations due to slow electrical waves [13] such as respiration were then removed by a four-order Butterworth high-pass filter with cut-off frequency set at 0.34 Hz [14].

After band pass filtering, the EHG signal is confined in a narrow band that is

upper bounded by the minimum value of HR, which is usually lower than 2 Hz (in our recordings it was in the range 1.1-1.83 Hz). The sampling frequency could then be decreased to 4 Hz without introducing aliasing effects. A decrease of the sampling frequency, which is made possible by the low frequency characteristics of the EHG signal [14, 29, 30], decreases significantly the computational time of the following steps of the algorithm.

4.2.3 Standard delay estimators

The EHG signal originates from the action potentials propagating in the myometrium. Therefore, the EHG time sequence $x_j(m)$, $m = 1, \cdots, M$ recorded by electrode j during a contraction could theoretically be represented as the delayed version of the signal $x_r(m)$ recorded during the same contraction at a different location, r, with the addition of noise $w(m)$. Therefore, $x_j(m)$ is given as

$$x_j(m) = x_r(m - \tau) + w(m), \tag{4.1}$$

where $\tau \in \mathbb{R}$ is the continuous detection delay of the signals with respect to the channel j.

In the narrow frequency band of interest, the noise $w(m)$ can be considered white and Gaussian, as confirmed by the analysis of the signal when no contraction is present. The delay corresponding to the maximum of the CCF between the signals $x_j(m)$ and $x_r(m)$ corresponds to a least squares estimation of the delay and, under the assumption of white-Gaussian noise, this is also equivalent to a maximum likelihood estimate.

However, in practice, the temporal resolution of the delay estimated by signal CCF maximization is limited by the employed sampling period. Increasing the sampling frequency or interpolating around the maximum of the CCF partly overcomes this limit [21]. An elegant alternative is the PD method, which relies on the difference between the phases of the two signals in the frequency domain for the time-delay estimation [22]. A procedure that is analogous to the PD method consists of estimating the time-delay in the frequency domain by minimization of the mean squared error (MSE) between the DFT of the two signals. This method was referred to as spectral matching [20].

Nevertheless, the assumption of pure temporal translation in (4.1) is not completely fulfilled and, even during the same contraction, the EHG signals have different shapes at different electrodes. As the accuracy of the mentioned delay estimators can be seriously hampered by poor interchannel similarity, significant improvements can be obtained by compensating for the poor interchannel similarity prior to assessing their relative delay. To this end, we suggest the adaptive identification of a filter G (Fig.4.3), which represents the volume conductor transfer function between the sensors, during estimation of the interelectrode delay by spectral matching.

4.2.4   Shape variation modeling

In order to properly design the adaptive filter G, we need to identify the main cause of the shape changes, which can be due to
1) the propagation of the signal at the myometrium level and
2) the biological tissues interposed between the source on the muscle and the recording site on the skin (volume conductor).

The signal recorded by each surface electrode is the weighted average of the electrical activity of all the underlying excited cells [31, 32]. Due to possible different cell-to-cell propagation properties of the action potentials, it is plausible that the electrical activity of the group of cells excited underneath one electrode does not mirror exactly the electrical patterns of the cells underneath the other electrodes.

However, the thickness and the properties of the tissue layers between the myometrium and the skin surface may also vary considerably from location to location as suggested by Fig. 4.2(b). This effect can be prevailing when, as in our measurements, the interelectrode distance is large.

Unfortunately, not much is known on these two phenomena, and a combination of the two seems the most plausible explanation for the interchannel shape changes. However, during labor, the electrical activity of the myometrium is well propagated and all the cells underneath each electrode can be considered simultaneously excited. Additionally, our aim is studying the global propagation of the electrical burst rather than detecting the distribution of the cell-to-cell transmission of the electrical activity. For the design of the adaptive filter G, we will therefore assume that the interelectrode signal shape changes are exclusively due to the effect of the volume conductor, which can be characterized by a low-pass filter in the spatial frequency domain [33]. The characteristics of this filter are determined by the electrical and geometrical properties of the tissue layers.

As shown in Fig. 4.3(a), the tissue interposed between the source location on the myometrium and the recording site on the abdomen is mainly composed by a skin layer, a fat layer, and a skeletal muscle layer. Each physical layer can be viewed as equivalent to a low-pass spatial filter. These spatial filters have been previously analytically formalized in the spatial frequency domain, rather than in the space domain, for mathematical convenience [34]. The spatial frequency domain formulation is adopted also in this work, because it allows the estimation of the parameter of interest, $\hat{\tau}$ in Fig. 4.1, without any resolution limit due to the finite sampling frequency.

In Fig. 4.3(a), $H_{0j}(k)$, $H_{1j}(k)$, and $H_{2j}(k)$ represent the transfer functions of the filter associated to the skeletal muscle, to the fat, and to the skin layer, respectively, with k being the spatial angular frequency. In the spatial frequency domain, the signals $X_r(k)$ and $X_j(k)$ recorded by two electrodes, r and j, can be represented as the underlying electrical signals $\Phi_r(k)$ and $\Phi_j(k)$ multiplied by the transfer functions, $G_r(k)$ and $G_j(k)$, which are the series of low-pass filters representing each underlying

(a)   (b)
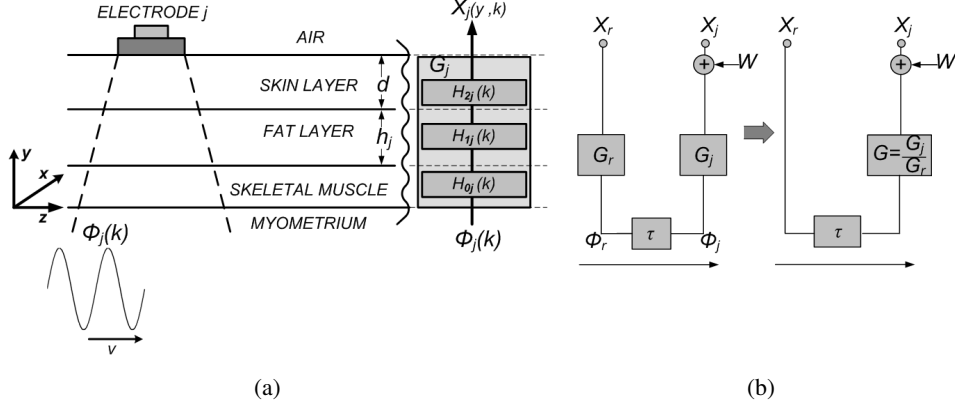
Figure 4.3: *Volume conductor spatial filtering effect: schematic description of the layers interposed between the myometrium and the skin surface for one electrode (a), simplified two-electrode scheme (b).*

tissue layer (Fig. 4.3(b)).

Given a traveling wave, the spatial frequency domain is related to the temporal frequency domain by the component of the propagation velocity in the considered direction [35]. In particular, considering the direction parallel to the line connecting two electrodes and the velocity component in that direction, v, to be constant and known, the spatial sampling frequency f_s can be derived from the temporal sampling frequency f_t by

$$f_s = \frac{1}{v} f_t. \tag{4.2}$$

Based on the equivalence in Fig. 4.3(b), our assumptions can then be formalized by considering the EHG signal $X_j(k)$ as the filtered and translated version of the signal $X_r(k)$, recorded during the same contraction in a different location, with the addition of noise $W(k)$, i.e.,

$$X_j(k) = G(k)X_r(k)e^{-jz_t k/M} + W(k), \tag{4.3}$$

where

$$G(k) = \frac{G_j(k)}{G_r(k)} = \frac{H_{0j}(k)H_{1j}(k)H_{2j}(k)}{H_{0r}(k)H_{1r}(k)H_{2r}(k)}, \tag{4.4}$$

M is the number of considered samples, and z_t is a dimensionless factor, expressed in the continuous domain, which determines the wave translation from one electrode to the other. The physical translation z_0, which equals the distance between two electrodes r and j, is then given as $z_0 = \frac{z_t}{f_s}$.

The parameter provided by the standard delay estimators described in Section 4.2.3 is the temporal detection delay τ in (4.1), while in (4.3) a spatial translation factor is

considered. For a wave traveling at velocity v, the temporal detection delay τ between two electrodes placed at a reciprocal distance z_0 can be obtained from the translation factor z_t by

$$\tau = \frac{z_0}{v} = \frac{z_t/f_s}{v} = \frac{z_t}{f_t}, \tag{4.5}$$

where the last equality is obtained by using (4.2).

Among the abdominal tissues, the thickness of the fat layer shows considerable local differences from location to location. Conversely, the thickness of the skin and the skeletal muscle layers is more homogeneous. Therefore, by assuming $H_{0r}(k) \approx H_{0j}(k)$ and $H_{2r}(k) \approx H_{2j}(k)$, we obtain $G(k) \approx \frac{H_{1j}(k)}{H_{1r}(k)}$, i.e., the transfer function in space domain between the signals recorded by two electrodes is equivalent to the ratio between the transfer function of the fat layer in the considered locations. From the model developed in [34], we can analytically derive the expression of the transfer function associated to the fat layer and compute $G(k)$ (see Appendix I), which depends on the following parameters:

-h_j, h_r, thickness of the fat layer under the electrode j and r, respectively;
-d, thickness of the skin layer, which is assumed to be the same at both electrode locations;
-R_c, conductivity ratio between skin and fat layer.

4.2.5 Adaptive parameter estimation

In order to improve the calculation efficiency for the estimation of the transfer function $G(k)$ in (4.11), we represented it by a centered zero-phase FIR filter with N symmetric coefficients a_n, with frequency response

$$G(k) = \sum_{n=\frac{-N+1}{2}}^{n=\frac{N-1}{2}} a_n e^{jnk}, \tag{4.6}$$

and with magnitude

$$|G(k)| = |1 + 2 \sum_{n=1}^{n=\frac{N-1}{2}} a_n cos(nk)|. \tag{4.7}$$

In order to assess the required filter order N, the value of $G(k)$ was calculated by its analytical expression (Appendix I) for the following range of parameters:
-R_c from 10 to 260, with steps of 10 units;
-h_j and h_r from 2 mm to 4 cm, with steps of 1 mm;
-propagation velocity v from 2 cm/s to 8 cm/s, with steps of 5 mm/s [10].
The analytical response was then fitted by different order N zero-phase FIR filters with the amplitude response in (4.7).
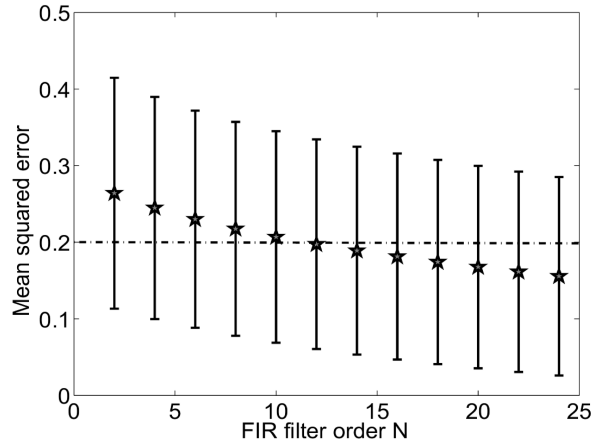
Figure 4.4: *Average mean squared error between the normalized analytical transfer function G(k) and its approximation by a zero-phase FIR filter of different order N.*

The mean squared error (MSE) between the transfer function of the analytical filter and the fitted digital FIR was then calculated for different values of N. The MSE was measured as the ratio between the mean fit squared error and the mean energy of the analytical transfer function in the frequency band of interest. Fig.4.4 shows the average value and standard deviation (SD) of the MSE over all the combinations of the considered physiological parameters.

For $N > 12$, the average approximation error is below 20% and the improvement obtained by increasing N is lower than 10^{-2}. We chose therefore $N = 12$, which implies, for the symmetry properties of the filter, the identification of 6 coefficients, a_1, a_2, a_3, a_4, a_5, and a_6.

For each single active contraction segment and electrode signal $x_j(m)$, the filter coefficients and the translation factor $\hat{z}_t$ were adaptively estimated employing as reference the electrode signal $x_r(m)$ with the best SNR. A single reference was used for the entire set of translation estimates during one recording. We defined the SNR as the ratio between the power of the signal during a contraction and the power during the quiescent period [36]. The contractions were detected and separated on the basis of the IUP estimated from the EHG signal using the method described in [26]. The accuracy of the detected contractions was supported by the simultaneously recorded IUP.

The interelectrode translation and the coefficients of the filter $G(k)$ were identified by an MSE-based algorithm according to the scheme in Fig. 4.5. For a contraction segment of length M samples, the error array $\underline{e} = e(m), m = \{1, \cdots, M\}$, was
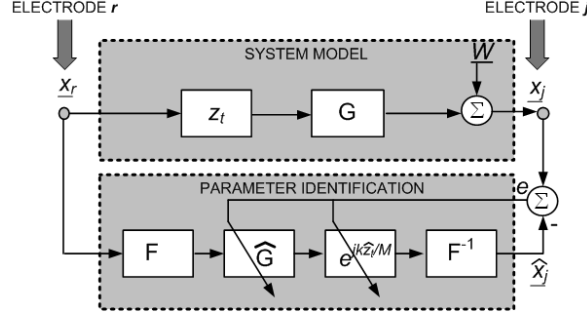
Figure 4.5: *System model and scheme employed for the identification of the translation factor $\widehat{z}_t$ and for the coefficients of the transfer function $\widehat{G}(k)$.*

defined as

$$\underline{e} = \underline{x}_j - \widehat{\underline{x}}_j, \tag{4.8}$$

where $\widehat{\underline{x}}_j = \widehat{x}_j(m)$ is the array representing the time sequence estimate of the signal $x_j(m)$, in the following addressed, in vector notation, as $\underline{x}_j$. The FIR filter coefficients representing the transfer function $\widehat{G}(k)$ and the translation factor $\widehat{z}_t$ were identified in the frequency domain, i. e.,

$$\widehat{\underline{x}_j} = \mathbf{F}\underline{x}_r e^{-jk\widehat{z}_t/M}\widehat{G}(k)\mathbf{F^{-1}}, \tag{4.9}$$

where $\mathbf{F}$ is the $M \times M$ DFT matrix and $\widehat{z}_t$ is an estimate of the spatial translation.

The coefficients of $\widehat{G}(k)$ were calculated by a simple matrix inversion (see Appendix II), while the translation $\widehat{z}_t$ was adaptively estimated by the Nelder-Mead Simplex search method [37]. For comparison with the other methods, the time delay $\widehat{\tau}$ was obtained from the estimated translation $\widehat{z}_t$ by (4.5). The initial value of the translation was set to the shift corresponding to the maximum of the CCF previously calculated on the preprocessed signals down-sampled at 4 Hz. By performing the adaptive estimation in the frequency domain, a delay $\widehat{\tau}$ with unlimited temporal resolution was then obtained.

4.3 Results

4.3.1 CCF maximization and spectral matching methods

In order to assess the equivalence of the two methods on noisy EHG signals, we employed the CCF delay estimator at a sampling frequency of 1000 Hz and the spectral matching method at 4 Hz on couples of simulated signals $\underline{x}_r$ and $\underline{x}_j$. For the simulation, the model in (4.1) was used where $\underline{x}_r$ was a real EHG signal recorded in the
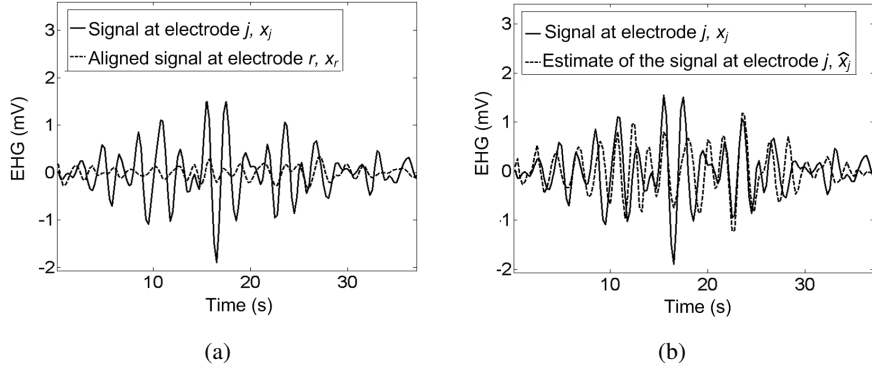
Figure 4.6: *Aligned preprocessed signals recorded in two different elec-
trodes (a). Shape similarity improvement after employing the
adaptive filter (b).*

channel with the best SNR. The two methods were compared for different values of
the delay τ, ranging from 0 to 25 ms with steps of 5 ms. To simulate $w(m)$, white
Gaussian noise was added with SNR = 3 dB, which is the average value of SNR
calculated on the available data-set. The delays estimated by the two methods were
compared using 20 sequences of random Gaussian noise for each value of delay.
Overall, the mean and the standard deviation of the difference between the estimates
by the two methods was lower than the sampling period for the CCF method, i.e.,
$SD < 10^{-3}$, proving the equivalence of these two methods. Therefore, for compari-
son with the dedicated approach, only the delay $\widehat{\tau}_{SM}$ estimated by spectral matching
at 4 Hz is used.

4.3.2   Signal similarity improvement

The proposed method includes an adaptation step for increasing the shape similarity
between the inputs of the delay estimator in order to improve the estimation accuracy.
The shape similarity between two waveforms can be measured by their correlation
coefficient R. The improvement provided by the adaptive filter was assessed by com-
paring the average correlation coefficients:
-R_0 between the preprocessed signals x_j and x_r;
-R_1 between the preprocessed signals aligned according to the delay $\widehat{\tau}_{SM}$ estimated
by spectral matching;
-R_2 between the signals $\widehat{x}_j$ and x_j.
The average correlation coefficients were calculated over all the channels of the seven
analyzed women during 93 recorded contractions.

The average correlation coefficient increased from $R_0 = 0.49$ for the prepro-
cessed signals to $R_1 = 0.56$ after alignment with the delay provided by spectral
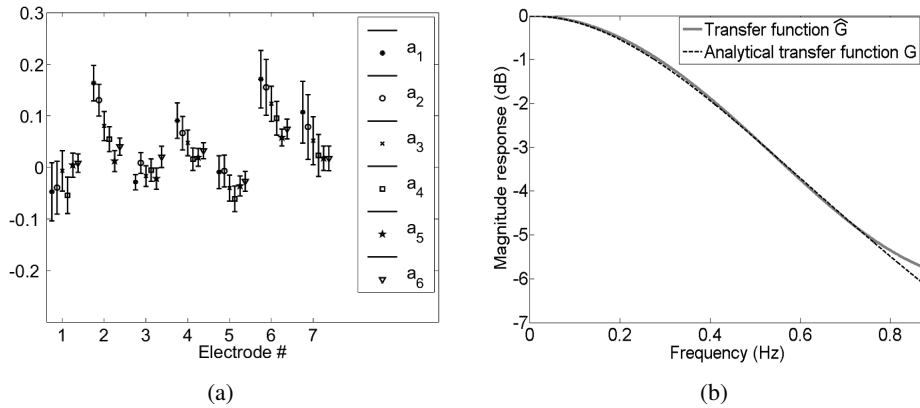
Figure 4.7: *Example of the estimated volume conductor transfer function. The average and standard deviation of the coefficients in each electrode is shown (a) together with the FIR filter magnitude response (b) obtained from the estimated coefficients of electrode 2. For comparison, the analytical filter G magnitude response was fitted on the estimated one.*

matching, and to $R_2 = 0.60$ after filtering and translating with the values of coefficients and delay adaptively estimated. We can conclude that the relative correlation improvement due to the alignment is 14% and that a further 8% is due to the shape similarity improvement. For those contraction signals with initial high correlation coefficients the improvement was negligible, while for poorly correlated signals the use of the FIR filter increased R significantly. An example of the improvement from the pre-aligned signals is shown in Fig. 4.3.2, where the correlation coefficient improved from $R_1 = 0.24$ to $R_2 = 0.50$.

We assumed that the filter $G(k)$ was representative of the biological tissues and the recording materials interposed between the electrodes and the myometrium. In order to test this hypothesis, we estimated the filter coefficients separately for each contraction and we analyzed their variability in two situations: when the properties of tissue layers underlying the electrodes are constant, i.e., during each patient recording, and when they are expected to be highly different, i.e., in different subject recordings. In agreement with our assumptions, the average SD of the coefficients per channel for each subject was 30% of their mean values, while the average interpatient variability was 300%.

The intrapatient stability of the filter coefficients is also confirmed by the example reported in Fig. 4.7(a), which refers to the average and the standard deviation of the coefficients identified in the recording containing the highest number of contractions (23 contractions).

An example of the FIR filter magnitude response is shown in Fig. 4.7(b) for the

(a)   (b)
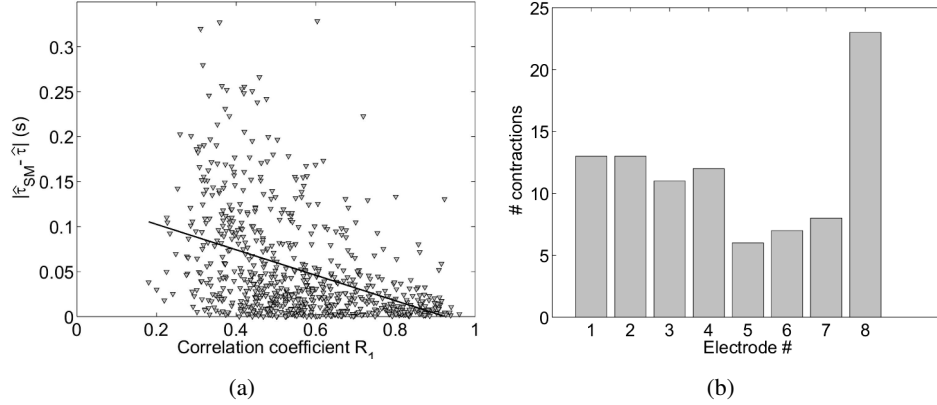
Figure 4.8: *Absolute difference between the delays obtained by spectral matching and the dedicated approach versus the correlation coefficient R_1 between the aligned preprocessed signals (a). Total number of contractions during which each electrode was the pacemaker sensor (b).*

estimated coefficients of electrode 2 in Fig. 4.7(a). For comparison, the analytical transfer function G was fitted on the estimated one, $\widehat{G}$, between 0.34 and 0.87 Hz, i.e., the stop band frequencies of the HP and LP filters employed for this subject.

4.3.3 Feasibility of the estimators on real data

The two methods were applied to the available dataset for calculating the interelectrode delay for each contraction. The average absolute difference between the delay provided by spectral matching, $\widehat{\tau}_{SM}$, and the delay calculated by the proposed approach, $\widehat{\tau}$, was 0.05 s over all the analyzed contractions and channels. The difference between the two estimates for the analyzed data is reported in Fig. 4.8(a) as a function of the interchannel correlation coefficients R_1 of the aligned signals. The correlation ($R_v = -0.45$, $p < 0.001$) between R_1 and the estimated delay difference (Fig. 4.8(a)) suggests that for lower values of interchannel correlation the estimates produced by the two methods show larger differences.

The estimated relative delays of all the electrodes during the same contraction permitted the assessment of the direction of propagation of the EHG signal. In particular, the area where the EHG signal originates (pacemaker area) was located, for each contraction, as corresponding to the pacemaker sensor, i.e., the electrode providing the first detection of the burst.

In Fig. 4.8(b), the histogram of the pacemaker sensors is reported based on the 93 contractions recorded from the seven subjects. Electrode 8, the uppermost left electrode, provided the first detection in 25% of the cases. By summing the occur-
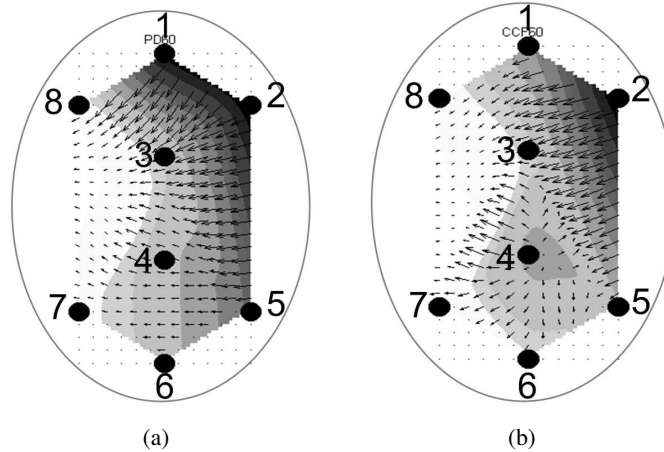
Figure 4.9: *Example of visual analysis of EHG signal propagation during a contraction obtained by the dedicated (a) and the spectral matching method (b). The values for the local delays are proportional to the color intensity of the map.*

rences of the uppermost electrodes (1, 2, 3, and 8) as pacemaker sensors, we deduce that 65% of the contraction started in the upper part of the myometrium. The average propagation time, i.e., from the first to the last electrode detecting the burst, was 9.52 ± 11.4 s according to both the spectral matching and the dedicated method. By analyzing and comparing the delay detected in each channel during a contraction, a study of the global propagation of the EHG signal could be conducted. In Fig. 4.9(a) and Fig. 4.9(b), an example of propagation analysis is shown. By interpolating the values of the electrode delays, a spatial grid representing the uterus surface was obtained, where the intensity is proportional to the local delay with respect to the pacemaker sensor. The uterine activation map in Fig. 4.9(a) was obtained by the dedicated approach. Here, the electrical signal clearly propagates from the upper left region towards the central-right part of the uterus. From the propagation map we can also derive an indication of the propagation path on the rear of the uterus. The uterine activation map in Fig. 4.9(b) was obtained, for the same contraction in Fig. 4.9(a), employing the delays obtained by spectral matching. In this case, the propagation path is more chaotic, probably due to an inaccurate estimate of the delay at sensor 4.

4.4 Discussion and conclusions

The purpose of this study is the definition of a method for analyzing the propagation of EHG signals. The final goal is supporting further clinical studies for assessing the capability of EHG propagation-related parameters in predicting premature birth.

We implemented the time-lag estimators based on the CCF maximization and spectral matching and we developed a dedicated interelectrode time delay estimator. The electrode configuration employed in our experiments was chosen to maximize the coverage of the uterine surface to test the robustness and the feasibility of the estimators on real data. For more specific information on the propagation properties of EHG signals, a larger number of sensors and lower iterelectrode distance should be employed in the future.

The main novelty of the dedicated approach is the employment of an adaptive filter for improving the signal similarity between the inputs of the delay estimator. To this end, on the basis of physiological observations, we propose a simple model, which is representative of the propagation mechanism of the EHG signal in labor. The algorithm is suitable for sampling frequencies as low as 4 Hz, as the method resolution is not limited by the sampling period.

By comparing the average correlation coefficient of the signals before and after the employment of the adaptive filter, we experienced an overall improvement of the waveform shape similarity. This result provides a preliminary validation of the adopted model. Shorter distances between the electrodes could however be used in the future to strengthen the validity of our assumptions on the signal transmission through the myometrium, decreasing the effect of the volume conductor and, therefore, of the designed filter, on the signal similarity. For example, considering a myometrium-skin distance of about 1 cm, 1 cm interelectrode spacing could already provide some improvement. If we assume the EHG signal to be modeled by a planar wave propagating at constant velocity, the future use of shorter electrode distance could also permit to estimate the EHG signal propagation direction and velocity by analysis of larger sets of electrodes, therefore improving the estimations robustness and accuracy.

For the adaptive filter design, we assumed that the shape variations between the signals recorded by different electrodes are mainly due to the inhomogeneous structure and properties of the biological tissues interposed between the signal source and the recording site.

When applied to real signals, the employed estimators provided delays with larger scattering for poor similarity among the preprocessed signals. This result is in agreement with the conclusion that poor values of interchannel correlation might affect the accuracy of time-delay estimators based on spectral matching and on the maximization of the CCF.

Finally, we demonstrated the feasibility of the proposed approach for the analysis of EHG signal propagation by testing it on the available dataset. The evaluation of the number of occurrences of each electrode as the pacemaker sensor highlighted the upper region of the uterus as the most probable pacemaker area. About 65% of the contractions were first detected by the uppermost electrodes, suggesting a preferred

top-down propagation of the myometrial electrical burst. Since the mechanical contraction of the uterine muscle acts towards the expulsion of the fetus, during labor this propagation pattern could be expected and might be associated to the effectiveness of the contractile activity. However, these are preliminary results for a circumscribed stage of pregnancy and a limited number of patients. Further clinical investigations on a more extended database including more patients with different abdominal fat content and at different gestational ages are needed to relate the propagation properties of the EHG signal to the effectiveness of uterine contractions and to the prediction of preterm labor.

It is important to notice that the EHG signal can also originate and propagate in the rear of the uterus, which cannot be directly monitored. Identification of the pacemaker sensor can then provide only partial information on the propagation pattern. To overcome these limitations, visual tools for the clinical and statistical analysis of EHG propagation, like the uterine activation maps in Fig. 4.9, can be provided based on the calculation of the interelectrode delay. The global view of the map suggests the presence of a propagation path on the rear of the uterus, which gives a fundamental contribution to the mechanical efficiency of a contraction. Note that, even if a single pacemaker sensor is generally assumed, the presence of multiple pacemaker regions is not excluded and can be possibly detected. Both the employed time-lag estimators resulted in an average propagation time from the first to the last sensor of about 9 s. Although the assessment of the conduction velocity was not in the aim of the present study, considering an average uterine length of about 40-50 cm, the detected values are in the velocity range reported in the literature [10].

By neglecting the pattern of the action potentials spreading though the myometrium cells, we achieved a significant problem simplification, which is suitable for the specific aim of this study but does not represent entirely the real underlying process. Our future work will therefore focus on specific models and experiments for assessing the propagation distribution action potentials in order to obtain more insight on the unknown processes leading to the onset of effective uterine contractions and to preterm delivery.

Appendix I

From the model developed in [34], we can analytically derive the expression of the transfer function $H_{1j}(k, h_j, d)$ in the location j of a fat layer of thickness h_j

$$H_{1j}(k, h_j, d) = \frac{cosh(kd)}{cosh(kh_j)cosh(kd) + R_c sinh(kh_j)sinh(kd)}, \qquad (4.10)$$

where R_c is the conductivity ratio between skin and fat, d is the thickness of the skin layer, and k is the angular frequency in the y direction (Fig. 4.3(a)). By assuming the

spatial variations of the properties of skin and skeletal muscle layers to be negligible, the transfer function between two electrode locations j and r is an isotropic filter given by the ratio of the transfer functions representing the fat layer, i.e.,

$$G(k) \approx \frac{cosh(kh_j)cosh(kd)) + R_c sinh(kh_j)sinh(kd)}{cosh(kh_r)cosh(kd)) + R_c sinh(kh_r)sinh(kd)}, \qquad (4.11)$$

where h_r is the thickness of the fat layer in the position r. This function provides a zero-phase spatial filter with a global low-pass characteristics if $h_j > h_r$, while it has a high-pass characteristics otherwise.

Appendix II

By $X_j(k)$ we indicate the frequency transformed signal recorded by the electrode j, i.e., $X_j(k) = \mathbf{F}x_j$, and by $X_r(k)$ the FFT of the signal at the reference electrode r, i.e., $X_r(k) = \mathbf{F}x_r$, where $\mathbf{F}$ is the $M \times M$ DFT matrix. The error vector $\underline{e}(\widehat{z_t}, \widehat{w})$ can be expressed as a function of the translation factor $\widehat{z_t}$ and coefficient array $\underline{\widehat{P}} = (a_1, \cdots, a_6)^T$ by

$$\underline{e}(\widehat{z_t}, \underline{\widehat{P}}) = (X_r(k) - \Omega(\widehat{z_t})\underline{\widehat{P}})\mathbf{F}^{-1}, \qquad (4.12)$$

where, for the frequency samples $k_1, k_2 \cdots, k_M$, it follows from the magnitude response of the zero-phase FIR filter that

$$\Omega(\widehat{z_t}) = e^{\frac{-jk\widehat{z_t}}{M}} \begin{bmatrix} X_j(k_1) & 2X_j(k_1)cos(k_1) & \cdots & 2X_j(k_1)cos(Nk_1) \\ X_j(k_2) & 2X_j(k_2)cos(k_2) & \cdots & 2X_j(k_2)cos(Nk_2) \\ \vdots & \vdots & \vdots & \vdots \\ X_j(k_M) & 2X_j(k_M)cos(k_M) & \cdots & 2X_j(k_M)cos(Nk_M) \end{bmatrix}.$$

The optimal coefficient vector, $\underline{\widehat{P}}_o(\widehat{z_t}) = (a_{o1}, \cdots, a_{o6})^T$, can be obtained by minimization of the squared error $\underline{e}^T(\widehat{z_t}, \underline{\widehat{P}})\underline{e}(\widehat{z_t}, \underline{\widehat{P}})$ as a function of the translation $\widehat{z_t}$ as

$$\underline{\widehat{P}}_o(\widehat{z_t}) = (\Omega(\widehat{z_t})^T\Omega(\widehat{z_t}))^{-1}\Omega(\widehat{z_t})^T X_r(k). \qquad (4.13)$$

The error can therefore be expressed as a function of a single parameter $\widehat{z_t}$, i.e.,

$$\underline{e}(\widehat{z_t}) = X_r(k) - \Omega(\widehat{z_t})\underline{\widehat{P}}_o(\widehat{z_t})\mathbf{F}^{-1}. \qquad (4.14)$$

Bibliography

[1] R.L. Goldenberg, J.F. Culhane, J.D. Jams, and R. Romero, "Epidemiology and causes of preterm birth," *Lancet*, vol. 371, pp. 75–84, 2008.

[2] M. Mclean, A. Walters, and R. Smith, "Prediction and early diagnosis of preterm labour: a critical review," *Obstet. Gynecol. Surv.*, vol. 48, pp. 209–225, 1993.

[3] N. M. Fisk and J. Chan, "The case for tocolysis in threatened preterm labour," *BJOG*, vol. 110, no. s20, pp. 98–102, 2003.

[4] C. Buhimschi and R.E. Garfield, "Uterine activity during pregnancy and labor assessed by simultaneous recordings from the myometrium and abdominal surface in the rat," *Am. J. Obstet. Gynecol.*, vol. 178, pp. 811–822, 1998.

[5] R. E. Garfield and R. H. Hayashi, "Appearance of gap junctions in the myometrium of women during labor," *Am. J. Obstet. Gynecol.*, vol. 140, pp. 254–260, 1981.

[6] C. Buhimschi and R.E. Garfield, "Uterine contractility as assessed by abdominal surface recording of electromyographic activity in rats during pregancy," *Am. J. Obstet. Gynecol.*, vol. 174, pp. 744–753, 1996.

[7] J.D. Iams et al., "Frequency of uterine contractions and the risk of spontaneous preterm delivery," *New. Engl. J. Med.*, vol. 346, no. 4, pp. 250–256, 2002.

[8] A.M. Peaceman et al., "Fetal fibronectin as a predictor of preterm birth in patients with symptoms: a multicenter trail," *Am. J. Obstet. Gynecol.*, vol. 177, pp. 13–18, 1997.

[9] H Leitich and A. Kaider, "Fetal fibronectin - how useful is it in the prediction of preterm birth?," *BJOG*, vol. 110, no. 20, pp. 66–70, 2003.

[10] D. Devedeux, C. Marque, S. Mansour, G. Germain, and J. Duchêne, "Uterine electromyography: a critical review," *Am. J. Obstet. Gynecol.*, vol. 169, pp. 1636–1653, 1993.

[11] R.E. Garfield, H. Maul, L. Shi, W. Maner, C. Fittkow, G. Olsen, and G.R. Saade, "Methods and devices for the management of term and preterm labor," *Ann. NY Acad.Sci.*, vol. 943, pp. 203–224, 2001.

[12] I. Verdenik, M. Pajntar, and B. Leskošek, "Uterine electrical activity as predictor of preterm birth in women with preterm contractions," *Eur. J. Obstet. Gynecol. Reprod. Biol.*, vol. 95, pp. 149–153, 2001.

[13] C. Marque, J. Duchêne, S. Leclercq, G. Panczer, and J. Chaumont, "Uterine EHG processing for obstetrical monitoring," *IEEE Trans. Biomed. Eng.*, vol. BME-33, pp. 1182–1187, 1986.

[14] W.L. Maner, R.E. Garfield, H. Maul, G. Olson, and G. Saade, "Predicting term and preterm delivery with transabdominal uterine electromyography," *Obstet. Gynecol.*, vol. 101, pp. 1254–1260, 2003.

[15] R.E. Garfield, W.L. Maner, L.B. MacKay, D. Schlembach, and G.R. Saade, "Comparing uterine electromyography activity of antepartum patients versus term labor patients," *Am. J. Obstet. Gynecol.*, vol. 193, pp. 23–29, 2005.

[16] M. Doret, R. Bukowski, M. Longo, H. Maul, W.L. Maner, R.E. Garfield, and G.R. Saade, "Uterine electromyography characteristics for early diagnosis of mifepristone-induced preterm labor," *Obstet. Gynecol.*, vol. 105, pp. 822–830, 2005.

[17] M.P.G.C. Vinken, C. Rabotti, S.G. Oei, and M. Mischi, "Accuracy of frequency-related parameters of the electrohysterogram for predicting preterm delivery: a review of the literature," *Ob. Gyn. Survey*, vol. 64, pp. 529–541, 2009.

[18] J. Planes, J. Morucci, H. Grandjean, and R. Favretto, "External recording and processing of fast electrical activity of the uterus in human parturition," *Med. Biol. Eng. Comput.*, vol. 22, pp. 585–591, 1984.

[19] T.Y. Euliano, D. Marossero, M.T. Nguyen, N.R. Euliano, J. Principe, and R.K. Edwards, "Spatiotemporal electrohysterography patterns in normal and arrested labor," *Am. J. Obstet. Gynecol.*, pp. 54.e1–54.e7, 2009.

[20] K.C. McGill and L.J. Dorfman, "High resolution alignment of sampled waveform," *IEEE Trans. Biomed. Eng.*, vol. 31, pp. 462–468, 1984.

[21] B. Wheeler, S. Smith, and S. High, "High resolution alignment of action potential waveforms using cubic spline interpolation," *J. Biomed. Eng.*, vol. 10, pp. 47–53, 1988.

[22] C.J. Houtman, D.F. Stegeman, J.P. Van Dijk, and M.J. Zwartz, "Changes in muscle fiber conduction velocity indicate recruitment of distinct motor unit populations," *J. Appl. Physiol.*, vol. 95, pp. 1045–1054, 2003.

[23] W.H.J.P. Linssen, D.F. Stegeman, E.M. Joosten, M.A. van't Hof, R.A. Binkhorst, and S.L. Notermans, "Variability and interrelationships of surface EMG parameters during local muscle fatigue.," *Muscle Nerve*, vol. 16, pp. 849–856, 1993.

[24] D. Farina, W. Muhammad, E. Fortunato, O. Meste, R. Merletti, and H. Rix, "Estimation of single motor unit conduction velocity from surface electromyogram signals detected with linear electrode arrays," *Med. Biol. Eng. Comput.*, vol. 39, pp. 225–236, 2001.

[25] A.C. Metting van Rijn, A. Peper, and C.A. Grimbergen, "High-quality recording of bioelectric events. part 1 interference reduction, theory and practice," *Med. Biol. Eng. Comput.*, vol. 28, pp. 389–397, 1990.

[26] C. Rabotti, M. Mischi, J.O.E.H. van Laar, S.G. Oei, and J.W.M. Bergmans, "Estimation of internal uterine pressure by joint amplitude and frequency analysis of electrohysterographic signals," *Physiol. Meas.*, vol. 29, pp. 829–41, 2008.

[27] J.J. Bailey, "The triangular wave test for electrocardiographic devices: a historical perspective," *J. Electrocardiol.*, vol. 37, pp. 71–73, 2004.

[28] R. Vullings, C.H.L. Peters, R.J. Sluijter, M. Mischi, S.G. Oei, and J.W.M. Bergmans, "Dynamical segmentation and linear prediction for maternal ECG removal in antenatal abdominal recordings," *Physiol. Meas.*, vol. 30, pp. 291–307, 2009.

[29] C. Buhimschi, M.B. Boyle, and R.E. Garfield, "Electrical activity of the human uterus during pregnancy as recorded from the abdominal surface," *Obstet. Gynecol.*, vol. 90, pp. 102–111, 1997.

[30] H. Leman, C. Marque, and J. Gondry, "Use of the electrohysterogram signal for characterization of contractions during pregnancy," *IEEE Trans. Biomed. Eng.*, vol. 46, pp. 1222–1229, 1999.

[31] M.J. Zwarts and D.F. Stegeman, "Multichannel surface EMG: basic aspects and clinical utility," *Muscle Nerve*, vol. 28, pp. 1–17, 2003.

[32] J.P. van Dijk, D.F. Stegeman, and M.J. Lapatki, B.G.and Zwarts, "Evidence of potential averaging over the finite surface of a bioelectric electrode using high-density EMG," in *XVI Congr. of the ISEK*, 2006, p. 62.

[33] D.F. Stegeman, J.H. Blok, H. J. Hermens, and K. Roeleveld, "Surface EMG models: properties and applications," *J. Electromyogr. Kines.*, vol. 10, pp. 313–326, 2000.

[34] D. Farina and A. Rainoldi, "Compensation of the effect of sub-cutaneous tissue layers on surface EMG: a simulation study," *Med. Eng. Phys.*, vol. 21, pp. 487–496, 1999.

[35] D. Farina and F. Negro, "Estimation of muscle fiber conduction velocity with a spectral multidip approach," *IEEE Trans. Biom. Eng.*, vol. 54, pp. 1583–1589, 2007.

[36] W.L. Maner and R.E. Garfield, "Identification of human term and preterm labor using artificial neural networks on uterine electromyography data," *Ann. NY Acad. Sci.*, vol. 35, pp. 465–473, 2007.

[37] J.C. Lagarias, J.A. Reeds, M.H. Wright, and P.E. Wright, "Convergence properties of the Nelder-Mead simplex method in low dimensions," *SIAM J. Optim.*, vol. 9, pp. 112–147, 1998.

Chapter 5

Electrohysterographic volume conductor modeling

C. Rabotti, M. Mischi et al., IEEE Trans. Biomed. Eng., vol.57 , pp. 519-527, 2010.

> *Everything should be made as simple as possible, but no simpler (A. Einstein)* [1]

5.1   Introduction

The sequence of contraction and relaxation of the uterine muscle (myometrium) results from the cyclic depolarization and repolarization of the muscle-cell membranes [2]. The spontaneous electrical activity of the myometrium, which can initiate in any cell (pacemaker) and then excites surrounding regions, consists of bursts of action potentials that can be measured at the abdominal surface by electrohysterography (EHG) [3, 4]. Uterine contractions are often the first sign of labor; therefore, when occurring preterm, they need to be promptly suppressed by tocolytics. During labor, instead, a coordinated and strong uterine activity is required for the effective expulsion of the fetus at the end of delivery. Accurate monitoring of the uterine activity is therefore essential. The methods currently employed in clinical practice for uterine activity monitoring, such as internal and external tocography, cervical change evaluation by digital or ultrasound examination, and the measurements of biomarkers (e.g., fibronectine) in symptomatic women, could support the selection of patients at higher risk of preterm delivery within few days, but they are either invasive or not sufficiently accurate for effective prognosis and, therefore, prompt treatment of premature birth [5–7].

During a contraction, the EHG signal can be recorded noninvasively by standard Ag-AgCl contact electrodes placed on the abdomen. Many studies demonstrated that the analysis of the EHG signal may play a key role for accurate monitoring of the

---

[1]This is the better known variant of 'It can scarcely be denied that the supreme goal of all theory is to make the irreducible basic elements as simple and as few as possible without having to surrender the adequate representation of a single datum of experience', from 'On the Method of Theoretical Physics', The Herbert Spencer Lecture, delivered at Oxford (10 June 1933), also published as [1].

uterine contractions, prediction of labor, and improvement of perinatal outcome [8–12]. However, many issues related to the conduction pattern of electrical activation are still unsolved [13].

An important contribution for studying noninvasively the conduction properties of EHG signals and for the development of novel monitoring technology can be provided by modeling techniques. At the myometrium level, the cellular action potential generation and the excitation-contraction coupling have been recently accurately modeled as a function of a large number of electrophysiological parameters related to ionic concentrations [14, 15]. The myometrium-skin volume conductor, instead, has been only partially investigated, and it is typically considered as a homogeneous infinite layer [14, 16]. As a result, the myometrium-skin conduction properties are assumed only dependent on the distance between source and recording site. Nevertheless, a complete understanding of the volume conductor effect on the measured signals is fundamental to support the development of accurate prognostic and diagnostic tools based on the EHG signal analysis.

In this study, a myometrium-skin conduction model is developed that consists of a four-layer model obtained by extension of simulation studies reported in the literature for the skeletal electromyogram [17]. The volume conductor effect is formalized in the spatial frequency domain by a transfer function that accounts for the physical and geometrical properties of the biological tissues interposed between the source of electrical current in the myometrium and the recording site on the skin. The intracellular action potential is mathematically modeled by a Gamma probability density function [18]. After model reduction, the potential recorded on the skin surface depends on five parameters, of which three are related to the source signal shape and two are given by the thickness of the fat and the abdominal muscle. The model parameters are estimated from EHG measurements performed by a grid of 64 high-density (HD) electrodes on five pregnant women at term with uterine contractions. For comparison, the values of fat and abdominal muscle thickness were also measured by echography.

5.2 Methodology

5.2.1 Background

The contractile element of the uterus is the myometrium, which is composed of billions of smooth muscle cells. The sequence of contraction and relaxation results from a cyclic depolarization and repolarization of the muscle cells in the form of action potentials (AP). The intracellular AP results from time-dependent changes in the membrane ionic permeability caused by hormonal changes or by cell-to-cell excitation. Due to changes in the permeability, ions diffuse across the membrane according to their electrochemical gradients and a transmembrane ionic current is established.

APs occur in bursts; they arise in cells that act as pacemakers and propagate from cell to cell through gap junctions, which are low-resistance electrical connections [3]. It has been shown that gap junctions are present between myometrial cells in pregnant animals only during parturition [19]. Due to a lack of evidence [20], many authors concluded that no classical linear propagation of single action potentials, similar to the myocardium, could be assumed for the myometrium, and that only a global propagation of the whole burst envelop could be measured [20, 21]. However, more recently, extensive measurements of the electrical activity of the guinea pig uterus using a grid of extracellular electrodes clearly demonstrated that also for the myometrium, similarly to the myocardium, a linear propagation of single electrical spikes occurs and can be measured [13, 22, 23].

In this study, the potential recorded on the skin surface is formalized as a function of the transmembrane ionic current and the properties of the volume conductor between the myometrium and the skin. For identifying the model parameters, single surface APs are visually selected from the bursts recorded during contractions. We assume that, below the recording electrodes, the current source can be approximated by a planar wave that propagates, as hypothesized in [14], either along the longitudinal or the circumferential axis of the uterus.

5.2.2 System modeling

Volume conductor modeling

The biological tissues interposed between the electrical source at the myometrium and the recording site at the skin act as a volume conductor producing a spatial low-pass filtering effect. Similarly to the study reported in [17] for skeletal muscles, the volume conductor between the myometrium and the skin is considered as made of parallel interfaces separating the tissue layers. As the abdominal curvature is negligible in a limited region, the interfaces can locally be approximated by infinite parallel planes. The biological tissues involved in the conduction of EHG signals are represented in Fig. 5.1 and consist of myometrial tissue (a), where the source is placed at a depth $y = y_0$, a Δh_b thick abdominal muscle layer (b), a Δh_c thick fat layer (c), and a Δh_d thick skin layer (d).

The general relation between the potential and the current density source in a non-homogeneous and anisotropic layer is expressed by the Poisson equation [24],

$$-\frac{\partial}{\partial x}\left(\sigma_x \frac{\partial \phi(x,y,z)}{\partial x}\right) - \frac{\partial}{\partial y}\left(\sigma_y \frac{\partial \phi(x,y,z)}{\partial y}\right) - \frac{\partial}{\partial z}\left(\sigma_z \frac{\partial \phi(x,y,z)}{\partial z}\right) = I_V(x,y,z) \quad (5.1)$$

where $I_V(x,y,z)$ is the volume current source $[\text{A}\cdot\text{m}^{-3}]$, $\phi(x,y,z)$ is the potential [V], and σ_x, σ_y, and σ_z $[\text{S}\cdot\text{m}^{-1}]$ are the conductivities of the medium in the x, y, and z direction, respectively.
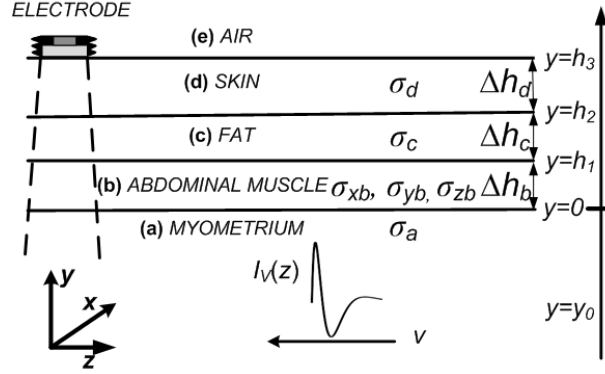
Figure 5.1: *Schematic description of the biological tissue layers involved in the volume conductor of EHG signals.*

Skin, fat, and myometrial tissue can be considered isotropic, i.e., the value of conductivity does not depend on the direction of propagation and $\sigma_x = \sigma_y = \sigma_z = \sigma$, while the abdominal muscle is anisotropic, i.e., $\sigma_x = \sigma_{xb} \neq \sigma_z = \sigma_{zb}$ [17]. In the y direction, $\sigma_y = \sigma_{yb} = \sigma_{xb}$ if the muscle fiber orientation is parallel to the z axis, $\sigma_{yb} = \sigma_{zb}$ if it is parallel to the x axis. All the tissues can be regarded as homogeneous. In the myometrium, the relation in (5.1) becomes

$$-\sigma_a \left(\frac{\partial^2}{\partial x^2} + \frac{\partial^2}{\partial y^2} + \frac{\partial^2}{\partial z^2} \right) \phi_a(x,y,z) = I_V(x,y_0,z)\delta(y-y_0), \qquad (5.2)$$

with $\phi_a(x,y,z)$ and σ_a being the potential and the conductivity, and $I_V(x,y,z)$ the current source at depth y_0.

All the other layers contain no current source. In the anisotropic muscle layer b,

$$\left(\sigma_{xb} \frac{\partial^2}{\partial x^2} + \sigma_{yb} \frac{\partial^2}{\partial y^2} + \sigma_{zb} \frac{\partial^2}{\partial z^2} \right) \phi_b(x,y,z) = 0, \qquad (5.3)$$

where $\phi_b(x,y,z)$ is the potential in this layer. In the isotropic fat layer c, with potential $\phi_c(x,y,z)$, and similarly in the layers d, and e, with potentials $\phi_d(x,y,z)$ and $\phi_e(x,y,z)$, respectively, relations of the form

$$\left(\frac{\partial^2}{\partial x^2} + \frac{\partial^2}{\partial y^2} + \frac{\partial^2}{\partial z^2} \right) \phi_c(x,y,z) = 0 \qquad (5.4)$$

hold. The solution of (5.2), (5.3), and (5.4) can be obtained in the spatial frequency domain by calculating the two-dimensional Fourier transform in the x and z directions. Indicating by k_x and k_z the spatial angular frequencies in the x and z direction, due to the Fourier transform properties, the second derivatives in the x and in the z directions become, in the spatial frequency domain, multiplications by $-k_x^2$ and $-k_z^2$,

respectively. Furthermore, we define $k_y = \sqrt{k_x^2 + k_z^2}$ and $k_{yb} = \sqrt{\frac{\sigma_{yb}}{\sigma_{xb}}k_x^2 + \frac{\sigma_{zb}}{\sigma_{xb}}k_z^2}$. Therefore, indicating by Φ_a, Φ_b, and Φ_c the Fourier transform of the potentials ϕ_a, ϕ_b, and ϕ_c, in the spatial frequency domain, (5.2), (5.3), and (5.4) become

$$\left(\frac{\partial^2}{\partial y^2} - k_y^2\right)\Phi_a(k_x, y, k_z) = \frac{I_V(k_x, y, k_z)}{\sigma_a}\delta(y - y_0),\tag{5.5}$$

$$\left(\frac{\partial^2}{\partial y^2} - k_{yb}^2\right)\Phi_b(k_x, y, k_z) = 0,\tag{5.6}$$

and

$$\left(\frac{\partial^2}{\partial y^2} - k_y^2\right)\Phi_c(k_x, y, k_z) = 0,\tag{5.7}$$

respectively. Equations of the same form as (5.7), which refers to layer c, hold also for the skin layer, d, and the air, e. In order to obtain the expression of the potential at the skin surface, all the obtained partial differential equations can be solved by adding the boundary conditions at the four interfaces, namely the continuity of the current in the y direction, the continuity of the electrical field in the z and x directions, and the decay to zero of the potential for $y \to \pm\infty$.

The expression of the potential $\Phi_e(k_x, y, k_z)$ in the spatial frequency domain on the skin surface $(y = h_3)$ as a function of the current source $I_V = I_V(k_x, y_0, k_z)$ and of the volume conductor properties can then be derived as given in (8) using the following conventions:
- $R_a = \sigma_a/\sigma_{xb}$,
- $R_b = \sigma_{zb}/\sigma_{xb}$,
- $R_c = \sigma_c/\sigma_{xb}$,
- $R_d = \sigma_d/\sigma_c$,
- $\alpha_1(k_x, k_z) = k_y\cosh(\Delta h_b k_{yb})R_a + k_{yb}\sinh(\Delta h_b k_{yb})$,
- $\alpha_2(k_x, k_z) = k_y\sinh(\Delta h_b k_{yb})R_a + k_{yb}\cosh(\Delta h_b k_{yb})$.

$$\Phi_e(k_x, h_3, k_z) =$$
$$\left(\frac{(1-R_d)\left\{k_{yb}\alpha_1(k_x,k_z)\cosh[(\Delta h_c-\Delta h_d)k_y]-R_c k_y\alpha_2(k_x,k_z)\sinh[(\Delta h_c-\Delta h_d)k_y]\right\}}{2e^{k_y y_0}I_V(k_x,y_0,k_z)k_{yb}/\sigma_{xb}}\right.$$
$$\left.+\frac{(1+R_d)\left\{k_{yb}\alpha_1(k_x,k_z)\cosh[(\Delta h_c+\Delta h_d)k_y]+R_c k_y\alpha_2(k_x,k_z)\sinh[(\Delta h_c+\Delta h_d)k_y]\right\}}{2e^{k_y y_0}I_V(k_x,y_0,k_z)k_{yb}/\sigma_{xb}}\right)^{-1}\tag{5.8}$$

In the following, the expression of the surface potential, which has been formalized in two dimensions for completeness, is simplified and addressed as a one-dimension problem. Due to the planar wave assumption, the use of a two-dimension

model is not expected to provide additional relevant information. The z axis is considered the main component (horizontal or vertical) of the electrical activity propagation velocity. The spatial angular frequency in the x direction, k_x, is set to zero and a single line (row or column) of the electrode grid is employed to identify the model parameters. In this respect, the use of a two-dimension grid for the acquisition is exploited to single out, on the basis of the signal quality and the direction of the electrical activity propagation, the line that is used as reference for the model identification.

Source modeling

Microelectrode recordings of uterine electrical activity showed that the uterine intracellular AP, similarly to skeletal muscles, is characterized, in time, by a fast depolarization followed by a reversal of membrane polarity and a slower repolarization [25]. In the considered direction, z, the intracellular AP appearance in the time domain, t, is converted to the space domain by assuming a constant intracellular AP propagation velocity component in the z direction, v_z, using the relation

$$z = -v_z t. \tag{5.9}$$

As also suggested for skeletal muscles [18], the intracellular AP at the myometrium, IAP(z), can be suitably described in the space domain by a function that has the shape of a Gamma probability density function

$$\text{IAP}(z) = \begin{cases} \dfrac{z^{\alpha-1}e^{-z/\beta}}{\beta^{\alpha}\Gamma(\alpha)} & z \geq 0 \\ 0 & z < 0 \end{cases}, \tag{5.10}$$

where Γ is the Gamma operator, $\alpha \in \mathbb{R}^+$ is a dimensionless shape parameter, and $\beta \in \mathbb{R}^+$ is a spatial scale parameter.

The example of the function IAP(z) modeled by (5.10) in Fig. 5.2(a) refers to a propagation velocity v_z parallel and opposite to the z axis. Considered the relation in (5.9) between the spatial and temporal properties of a waveform, when compared to the intracellular APs depicted in the literature [25, 26], the shape of the modeled intracellular AP in Fig. 5.2(a) is representative of microelectrode recordings of uterine activity.

As from (5.1), the source of our model, I_V, is a volume current source density; being a measure of the current outflow per unit volume, I_V can then be obtained by the divergence of the current density $\underline{J}(x,y,z)$, $[\text{A}\cdot\text{m}^{-2}]$, i.e.,

$$I_V = \nabla \cdot \underline{J}(x,y,z) = \frac{\partial}{\partial z}(\underline{J}(z)), \tag{5.11}$$

where the last equality results from the hypothesis of a single propagation direction along z. Assuming the core-conductor model [24], the transmembrane ionic current

density $\underline{J}(z)$ is proportional to the second spatial derivative of the intracellular AP profile [24]. In the spatial frequency domain, the volume current source $I_V(k_z)$ of the model in (5.8) is therefore given as

$$I_V(k_z) = \mathfrak{F}\left\{A\frac{\partial^3 \text{IAP}(z)}{\partial z^3}\right\} = \frac{Aik_z^3\left(-ik_z + \frac{1}{\beta}\right)^{-\alpha}\beta^{-\alpha}}{\sqrt{2\pi}}, \quad (5.12)$$

where $\mathfrak{F}$ indicates the Fourier transform, A is an amplitude scaling factor that accounts for the number of cells simultaneously active during the contraction, and $i = \sqrt{-1}$.
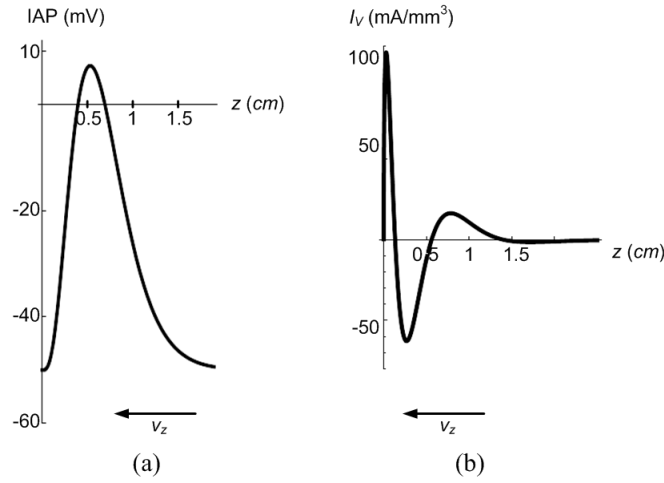
Figure 5.2: *Example of intracellular action potential, (a), and volume current source, (b), modeled in the space domain by a Gamma probability density function and its third derivative, respectively. The IAP propagation direction is parallel and opposite to the z axis. Assuming a propagation velocity of about 10 cm/s, the depicted example corresponds to an action potential duration of 150 ms.*

Model reduction

The surface potential $\phi_e(k_x, h_3, k_z)$ in (5.8) depends on the tissue thicknesses and conductivities, on the source depth, y_0, and on the parameters α, β, and A in 5.12. The tissue conductivities are however relatively invariant and the values reported in the literature are used [27–29]. For APs propagating in the direction parallel to the abdominal muscle fiber orientation, i.e., z parallel to the vertical line of the abdomen, by assuming a uterine conductivity $\sigma_a = 0.2 \text{ S}\cdot\text{m}^{-1}$ [27], and a transversal muscle conductivity $\sigma_{xb} = 0.09 \text{ S}\cdot\text{m}^{-1}$ [28], we obtain $R_a = 2.2$, $R_b = 5$, $R_c = 0.5$, and $R_d = 20$ [29]. For APs propagating horizontally, σ_{xb} is the longitudinal abdominal

Figure 5.3: *Schematic description of the sensor placement.*

muscle conductivity; therefore, $\sigma_{xb} = 0.4$ S·m^{-1} [28], $R_a = 0.5$, $R_b = 0.2$, and $R_c = 0.225$.

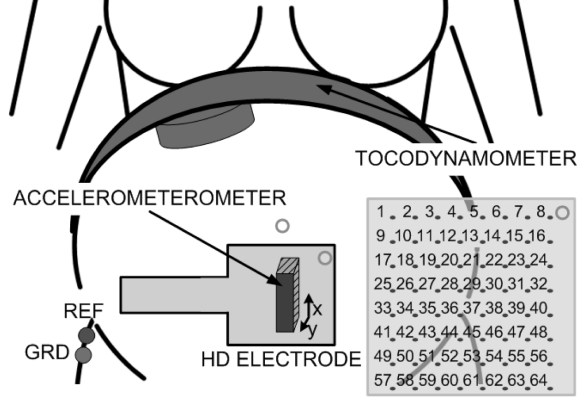A further reduction of the model parameter number is obtained by setting the skin tissue thickness, Δh_d, to a constant value. A low intersubject variability of the skin thickness, demonstrated already in previous studies [30], is also suggested by 15 echographic measurements performed at the Máxima Medical Center in Veldhoven (the Netherlands) from 12 pregnant and 3 nonpregnant women. In agreement with the values employed in other modeling approaches [29] and those measured for dermatological investigations on the abdomen [30], we measured a skin thickness equal to 2 mm in 87% of the cases. Therefore, the model is identified assuming a constant skin thickness $\Delta h_d = 2$ mm.

An additional model reduction concerns also the source depth y_0. Assuming the source to be close to the myometrium-abdominal muscle interface, $y_0 \to 0$ and, therefore, the exponential term in (5.8) can be approximated by a McLaurin expansion $e^{k_y y_0} \to 1$.

5.2.3   Experimental data recording and preprocessing

The measurements were performed at the Máxima Medical Center in Veldhoven (the Netherlands) after approval by the ethical committee of the hospital. Five women in labor, admitted to the hospital with contractions, were enrolled in the study after signing an informed consent. The sensors were placed as described in Fig. 5.3 after skin preparation for contact impedance reduction. The EHG was recorded using a Refa system (TMS International, Enschede, the Netherlands), comprising a multichannel amplifier for electrophysiological signals and a grid of 64 (8x8) HD electrodes (1 mm diameter, 4 mm interelectrode distance). The sampling frequency was 1024 Hz. The electrodes have a flexible support, which can be fixed to the skin by a double-sided adhesive tape mask that covers the interelectrode space and leaves the sensing sur-

face recessed in a cavity. The cavity can be filled by electrolyte gel. The combined use of flexible and recessed electrodes contributes to the reduction of movement artifacts [31].

The HD electrode grid was placed on the mid line of the lower abdomen immediately below the umbilicus. By analyzing a set of previous measurement performed with electrodes distributed on the abdomen, the signals recorded by electrodes placed in this region resulted less affected by movement artifacts, such as respiration, than the signals recorded by electrodes placed in other locations [32]. The common reference for the monopolar EHG signals recorded by the HD electrode was placed on the right hip, close to the ground (GRD) electrode. The external tocogram, simultaneously recorded due to medical prescription, was employed to support the assessment of the contraction period. An accelerometer was fixed on the HD electrodes to detect movements and exclude from the analysis signal segments affected by motion artifacts. An Aloka ultrasound scanner was employed to measure the thickness of the fat and the abdominal muscle layers underneath the HD electrode. Two echographic images were recorded: one during the quiescent period and one at the contraction peak. The values of thickness were then measured on the echographic image by two independent observers.

The uterine EHG signal can be affected by various noise sources, e.g., electrocardiographic (ECG) signals, electromyographic (EMG) interference generated by the contraction of abdominal muscles, and different motion artifacts. It has been extensively reported that the EHG signal does not have significant frequency components outsides the frequency band 0.1- 5 Hz [21]. The interference due to the EMG signal has a dominant frequency component of about 30 Hz [9], the main frequency of respiration is up to 0.34 Hz, and the lower frequency of the ECG signal is given by the heart rate, which can be as low as 1 Hz [33]. In the literature, either narrow band-pass filtering (i.e., between 0.34 and 1 Hz) [11], or maternal ECG subtraction combined with band-pass filtering between 0.1 and 3 Hz were proposed to improve the EHG SNR [12]. In this work, a sixth-order Butterworth band-pass filter with cut-off frequencies at 0.1 and 0.8 Hz is used. The example of action potential in Fig. 5.4, filtered between 0.1 and 5 Hz and between 0.1 and 0.8 Hz, suggests, in fact, that low-pass filtering below 0.8 Hz does not affect the signal shape while removing the ECG interference at the heart-rate. Due to the electrode typology and position, low-frequency oscillations due to the respiration are not visible in the recorded signals.

5.2.4 Model parameter identification

For each woman, two different signal time segments, each containing a propagating (i.e., it shows a delay between consecutive channels) surface AP, were visually selected on the preprocessed signal and used as reference for validation by mean square estimation of the model parameters.
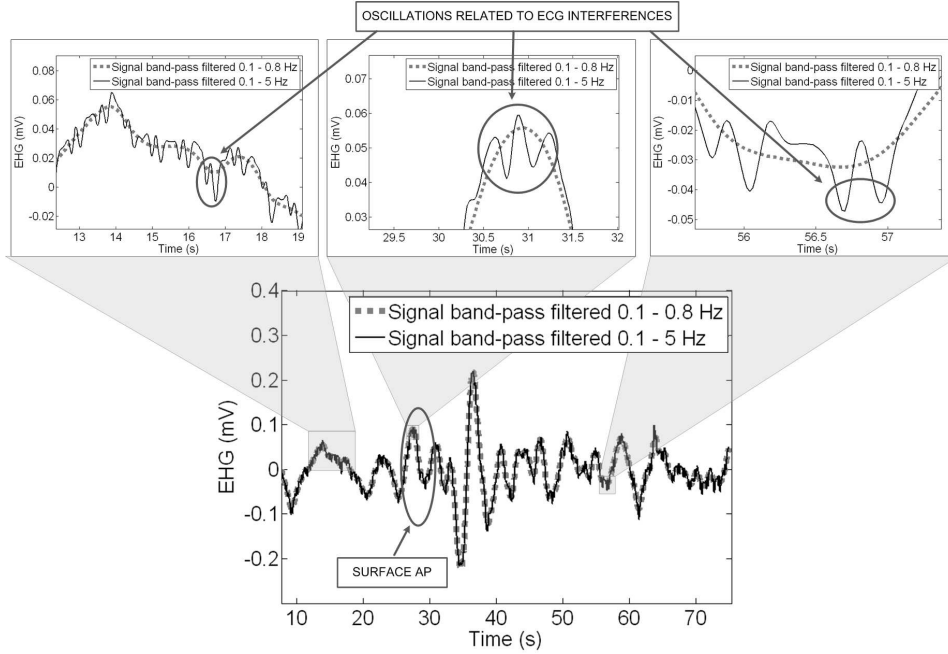
Figure 5.4: *Example of preprocessed EHG signal recorded during labor (39 week of gestation) and effect of filtering in two different frequency bands.*

Since possible artifacts, such as those due to ECG and movements, do not propagate along the electrode grid, the surface APs in the different channels represent the same AP propagating below the electrodes. We assume that the conduction wave can be approximated by a planar wave. Due to the planar wave assumption, the spatio-temporal information of the surface AP recorded by one column and one row of the electrode grid is representative of the AP propagation. The best row and column are then selected using the similarity among the recorded signals as quality index. A high interchannel signal similarity provides, in fact, a first evidence that the selected electrodes are recording APs originating from a single source. Furthermore, as we assume that the AP propagates either vertically or horizontally [14], we single out the line (either the column or the raw) that is parallel to the AP direction of propagation, estimated by analysis of the AP conduction velocity. In fact, no spatial information could be derived from electrodes that are aligned orthogonally to the AP propagation direction. Note that, due to the preliminary line selection based on the interchannel signal similarity, the conduction velocity estimates in the selected line is more reliable [34].

Possible indexes of the shape similarity between two signals are the correlation coefficient and the coherence spectrum [35]. Differently from the correlation coef-

ficient, the similarity index provided by the coherence spectrum, which is the frequency equivalent of the correlation coefficient, is independent of the signal phase and, therefore, does not require preliminary signal alignment. The coherence spectrum is therefore calculated for all the couples of signals in a line and the median value considered as line signal-quality index.

For assessing the surface AP conduction velocity between two electrodes, the phase-difference method is employed [36]. The conduction velocity is calculated between all the possible couples of channels in the considered lines. A more robust estimation of the delay can then be obtained by exploiting the redundancy of this information and taking the median value of the delay estimates.

Once a channel line is identified on the basis of coherence and propagation, the 8-channel-surface APs in the time domain are used for identification of the model parameters in the space domain. However, due to the wavelength of the uterine AP and the spatial low-pass filtering effect of the biological tissues interposed between the myometrium and the skin, the signal simultaneously recorded by the eight electrodes may not provide enough spatial information for reconstructing a complete surface AP in the space domain. After calculation of the surface AP conduction velocity, assumed to be constant, time information is used to recover the missing spatial information. Eventually, the surface AP, $SAP(z)$, is represented by 16 spatial samples (Fig. 5.8).

The parameters of the model in (5.8) and (5.11) are identified on simulated and real signals by minimization of the mean error e,

$$e = \sqrt{\sum_{z=1}^{N} \frac{(SAP(z) - SAP_M(z))^2}{N}}, \tag{5.13}$$

between the measured (simulated) reference signal, $SAP(z)$, and the modeled potential $SAP_M(z) = \mathfrak{F}^{-1}\{\phi_e(k_z)\}$. The Nelder-Mead Simplex search method is used for the minimization of e, which is given for $SAP_M = \widehat{SAP}_M$ [37]. For the minimization of e, the values of the abdominal fat and muscle thickness are initialized at 19 mm and 12 mm, respectively; for the considered abdominal tissues, these are the mean values reported in the literature for young women [38].

5.3   Results

5.3.1   Simulation results

Simulated surface APs were obtained for all the possible combinations of realistic values of Δh_b and Δh_c, and for a fixed set of source parameters. Ten values of abdominal muscle thickness, Δh_b, and fat tissue thickness, Δh_c, between 1 and 16 mm and

SD$_c$(mm), SNR=12 dB   SD$_b$ (mm), SNR=12 dB

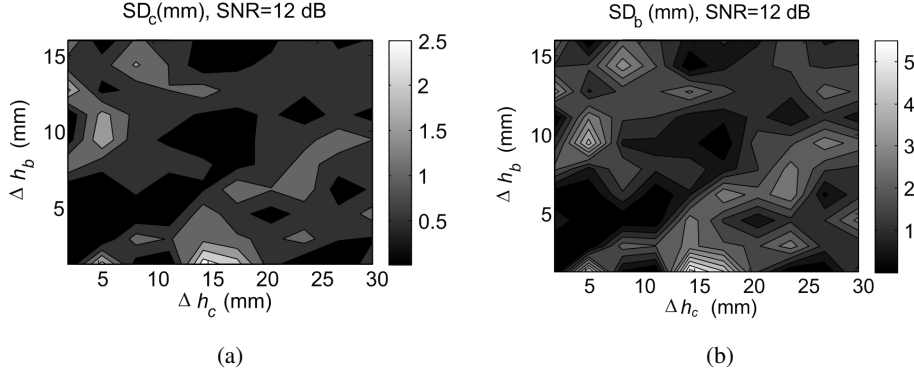(a)   (b)

Figure 5.5: *Standard deviation of the fat thickness estimates,* SD$_c$, *a), and standard deviation of the abdominal muscle thickness estimates,* SD$_b$, *b), over 50 simulated surface APs with SNR = 12dB. The plots show the results (grey level) as a function of the tissue-thickness values adopted for the surface AP simulation.*

between 1 and 30 mm, respectively, were considered for the simulations [38]. Gaussian white noise was added to each of the simulated surface AP. The noise power was estimated as the mean squared error between SAP and $\widehat{SAP}_M$ obtained by the model identification on the real signals. Each noisy simulated surface AP was used as reference to obtain an estimate of the fat thickness, $\widehat{\Delta h_c}$, and of the abdominal muscle thickness, $\widehat{\Delta h_b}$, as described in Section 5.2.4.

The standard deviation, SD$_b$, of the abdominal muscle thickness estimates and the standard deviation, SD$_c$, of the fat tissue thickness estimates were calculated over 50 noise sequences. The standard deviation of the fat and abdominal muscle thickness estimates in Fig. 5.5(a) and Fig. 5.5(b) refer to the worst case SNR, i.e., SNR = 12 dB. In these simulations, vertical propagation was assumed, i.e., the abdominal muscle conductivity in the z direction, σ_{zb}, is the longitudinal conductivity and σ_{xb} is the transversal one.

The estimates are unbiased. Furthermore, Fig. 5.5(a) shows that for $\Delta h_b > 1$ mm, SD$_c < 1.5$ mm. As for the standard deviation of the abdominal muscle estimates, Fig. 5.5(b), for $\Delta h_b > 1$ mm, SD$_b < 4$ mm. In the simulations reported in Fig. 5.5(a) and Fig. 5.5(b), the standard deviation of the abdominal muscle thickness estimates is, in general, higher than the fat thickness. For a simulated vertical propagation, this tendency is present also when higher values of SNR are considered, and it is due to the convexity of the error function, which is slightly higher in the direction of Δh_c than in the direction of Δh_b. When horizontal propagation is simulated, the surface AP is more sensitive to variations of the abdominal muscle thickness and the estimation of Δh_b becomes more accurate than Δh_c.
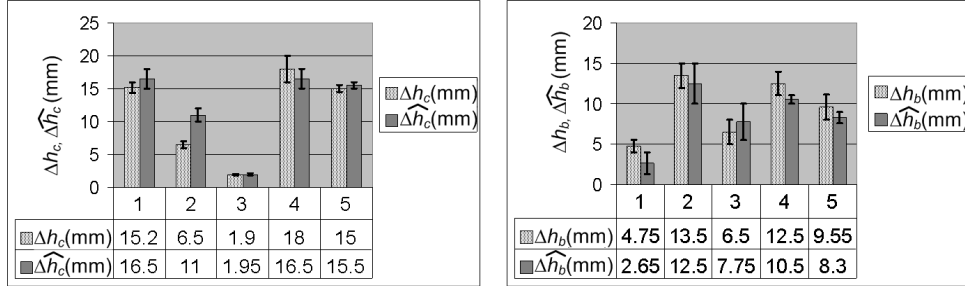
Figure 5.6: *Measured and estimated values of fat tissue thickness, (a), and abdominal muscle thickness, (b).*
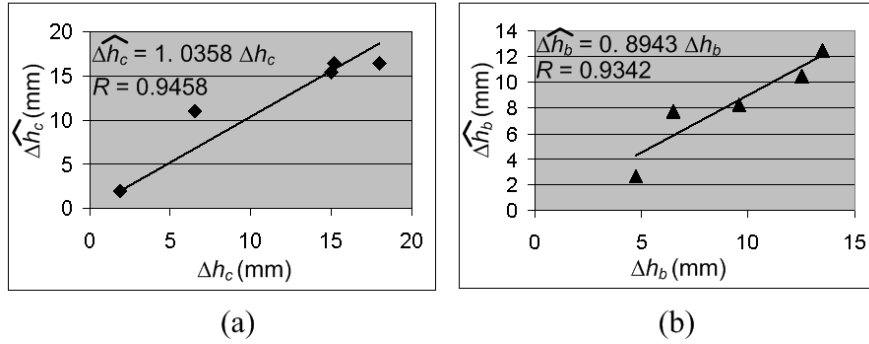
Figure 5.7: *Mean estimated values of fat, (a), and abdominal muscle thickness, (b), and zero-intercept trend-line as a function of the mean values measured on the echographic image.*

5.3.2 Measurement results

For each patient, the abdominal muscle and the fat layer thickness were measured by echography by two independent observers and the model parameters identified on two different time segments of the EHG signal. The values of tissue thickness recorded by echography and those estimated from the EHG signal using the volume conductor model are shown in Fig. 5.6 for each analyzed patient. In Fig. 5.6, the echographic measurements refer to the contraction period and are reported in terms of inter-observer mean and standard deviation. The difference between the values of tissue thickness recorded by echography during the quiescent period and during contraction (not reported in the figure) was 0.11 ± 0.67 mm for the fat tissue and -0.23 ± 0.34 mm for the abdominal muscle. For comparison, Fig. 5.6 shows also the mean and standard deviation of the parameters estimated from the surface APs. As from the table in Fig. 5.6, the mean values of thickness measured echographically by the two observers were $\Delta h_c = 11.32 \pm 6.17$ mm and $\Delta h_b = 9.36 \pm 3.63$ mm. The
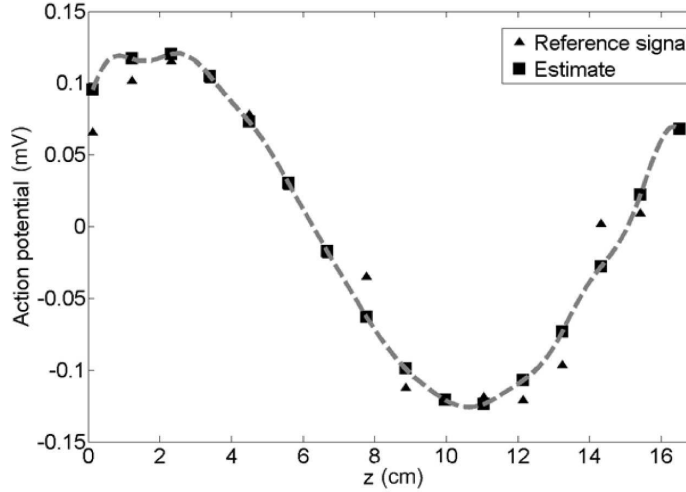
Figure 5.8: *Example of recorded and modeled surface AP.*

mean difference between the echographic and the electrophysiological estimates was $\Delta_c = 0.97 \pm 1.99$ mm for the fat and $\Delta_b = -1.02 \pm 1.21$ mm for the abdominal muscle. The mean total difference between the echographic and the EHG estimates, i.e., with no distinction between the two different tissues, was 0.02 ± 1.9 mm.

The variability between the two types of measurements was comparable, with a mean interobserver variability of 1.1 mm by echography and a mean difference between the tissue thickness estimated by the two surface APs of 1.2 mm.

In Fig. 5.7, the estimated values of tissue thicknesses are plotted against the values measured by echography. By operating a linear regression of the data with the hypothesis of zero intercept, we obtained correlation coefficients $R = 0.9458(p < 0.05)$ and $R = 0.9342(p < 0.05)$, for the fat and the abdominal muscle tissue, respectively. The angular coefficient of the regression lines is 1.03 and 0.89 for the fat tissue and the abdominal muscle, respectively.

On average, we obtained values of the error, $e = 4.8 \cdot 10^{-3} \pm 3.4 \cdot 10^{-3}$ mV. Fig. 5.8 shows an average example of model fit ($e = 4.19 \cdot 10^{-3}$ mV).

5.4   Discussion and conclusions

In this chapter, we propose a four-layer mathematical model of the conduction of EHG signals from the myometrium to the skin surface. The cellular action potential is modeled by a Gamma probability density function. Based on physiological and experimental observations, the number of model parameters can be reduced. The model is then identified from the EHG signal recorded on women in labor by surface

electrodes. Of the five estimated parameters, two can also be measured by ecography. The model can therefore be reliably validated by comparison with the echographic measurements [39].

The model was tested on ten segments of EHG signals recorded on five women in labor. On average, the parameters estimated using the model differed from the ones measured by echography by less than 1 mm for the fat tissue and by 1.2 mm for the abdominal muscle tissue. The good agreement between the measured and estimated parameters was also confirmed by their high correlation ($R = 0.9458$ and $R = 0.9342$).

On the experimental data, the estimation accuracy of the fat thickness was comparable to that of the abdominal muscle thickness. On simulated signals, the error between the measured and estimated surface AP resulted more sensitive to the abdominal muscle or to the fat tissue thickness error depending on the considered direction of propagation (vertical or horizontal). This dependency between the estimate accuracy and the AP direction of propagation is likely to be related to the anisotropy of the abdominal muscle. The comparable parameter errors obtained on real data for the two different biological tissues can therefore be explained by the comparable number of selected surface AP propagating horizontally (four) with respect to those propagating vertically (six).

For each woman, the tissue thickness was echographically measured by two observers and estimated on two different segments of the EHG signal. The interobserver variability of the echographic measurements was comparable to the variability between the tissue values estimated by analysis of two surface APs; both variabilities resulted to be slightly higher than the mean difference between the two methods. In general, our simulations show that even considering the worst realistic value of SNR, the standard deviation of the parameter estimates is modest for any realistic value of tissue thickness.

The tissue thickness was measured twice in the same location: during contraction and during the quiescent period. For the validation of the model, the reference values were those obtained during contraction, since APs are present only during the contraction period. According to our echographic measurements, a decrease in the fat and an increase in the abdominal muscle tissue thickness is observed when a contraction occurs. However, the small mean difference measured in our experiments, (0.11 mm for the fat and 0.23 mm for the abdominal muscle) is not statistically significant ($p > 0.5$), leading to the conclusion that the thickness of these tissues is approximately constant independently on the contraction of the uterine muscle.

In general, the values of fat and abdominal muscle thickness of our experiments are lower than those reported in the literature for nonpregnant women in the same age range. During pregnancy, in fact, due to the expansion of the uterus, the subcutaneous tissues tend to stretch especially in the region surrounding the umbilicus.

In conclusion, our results show that the proposed mathematical model of the vol-

ume conductor is in agreement with human anatomy and can provide an accurate description of the EHG action potential and volume conductor. Furthermore, even if the main focus of the present work is volume conductor modeling, the proposed mathematical description of the cellular action potential, derived from striated muscle electromyography, resulted suitable for the scope. Further investigation might be dedicated to the advantages of integrating our volume conductor model with more complex descriptions of the myometrial cell AP generation [14, 15]. In view of the recent investigations on the guinea pig myometrium [13], possible limitations of the proposed model are the assumption that the myometrial tissue is isotropic and the hypothesis that action potentials propagate exclusively along either the longitudinal or the circumferential axis of the uterus. Therefore, in the future, the role played by the complex three-dimensional geometrical and anatomical structure of the myometrium in the conduction of electrical activity needs to be understood and possibly integrated in the source model. Nevertheless, on the basis of our results, the proposed mathematical model for the potential source leads to an accurate description of the data with a limited number of parameters. Therefore, it is suitable to support future studies on the mechanism of action potential propagation in humans and, ultimately, to sustain the development of accurate noninvasive techniques for uterine contraction monitoring and preterm labor prediction.

Bibliography

[1] A. Einstein, "On the method of theoretical physics," vol. 1, pp. 163–169, 1934.

[2] H. Maul, W.L. Maner, G.R. Saade, and R.E. Garfield, "The physiology of uterine contractions," *Clin. Perinatol.*, vol. 30, pp. 665–676, 2003.

[3] T. Chard and J. Grudzinskas, *The uterus*, Cambridge University Press, 1994.

[4] R.E. Garfield, H. Maul, L. Shi, W. Maner, C. Fittkow, G. Olsen, and G.R. Saade, "Methods and devices for the management of term and preterm labor," *Ann. NY Acad.Sci.*, vol. 943, pp. 203–224, 2001.

[5] J.D. Iams et al., "Frequency of uterine contractions and the risk of spontaneous preterm delivery," *New. Engl. J. Med.*, vol. 346, no. 4, pp. 250–256, 2002.

[6] A.M. Peaceman et al., "Fetal fibronectin as a predictor of preterm birth in patients with symptoms: a multicenter trail," *Am. J. Obstet. Gynecol.*, vol. 177, pp. 13–18, 1997.

[7] S. Arulkumaran, M. Yang, C. Y. Tien, and S. S. Ratnam, "Reliability of intrauterine pressure measurements," *Obstet. Gynecol.*, vol. 78, no. 5, pp. 800–802, 1991.

[8] C. Marque, J. Duchêne, S. Leclercq, G. Panczer, and J. Chaumont, "Uterine EHG processing for obstetrical monitoring," *IEEE Trans. Biomed. Eng.*, vol. BME-33, pp. 1182–1187, 1986.

[9] C. Buhimschi, M.B. Boyle, and R.E. Garfield, "Electrical activity of the human uterus during pregnancy as recorded from the abdominal surface," *Obstet. Gynecol.*, vol. 90, pp. 102–111, 1997.

[10] M.P.G.C. Vinken, C. Rabotti, S.G. Oei, and M. Mischi, "Accuracy of frequency-related parameters of the electrohysterogram for predicting preterm delivery: a review of the literature," *Ob. Gyn. Survey*, vol. 64, pp. 529–541, 2009.

[11] W.L. Maner, R.E. Garfield, H. Maul, G. Olson, and G. Saade, "Predicting term and preterm delivery with transabdominal uterine electromyography," *Obstet. Gynecol.*, vol. 101, pp. 1254–1260, 2003.

[12] H. Leman, C. Marque, and J. Gondry, "Use of the electrohysterogram signal for characterization of contractions during pregnancy," *IEEE Trans. Biomed. Eng.*, vol. 46, pp. 1222–1229, 1999.

[13] W.J.E.P. Lammers, H. Mirghani, B. Stephen, S. Dhanasekaran, A. Wahab, and M.A.H. Al Sultan, "Patterns of electrical propagation in the intact guinea pig uterus," *Am. J. Physiol. Regul. Integr. Comp. Physiol.*, vol. 294, pp. R919–R928, 2008.

[14] S. Rihana and C. Marque, "Preterm labor-modeling the uterine electrical activity from cellular level to surface recording," in *IEEE EMBS Proc. Int. Conference*, 2008, pp. 3726–3729.

[15] L. Bursztyn, O. Eytan, A. J. Jaffa, and D. Elad, "Mathematical model of excitation-contraction in a uterine smooth muscle cell," *Am. J. Physiol. cell. Physiol.*, vol. 292, pp. C1816–C1829, 2007.

[16] C. K. Marque, J. Terrien, S. Rihana, and G. Germain, "Preterm labour detection by use of a biophysical marker: the uterine electrical activity," *BMC Pregnancy Childbirth*, vol. 7 Suppl 1:S5, pp. 2393–7, 2007.

[17] D. Farina and A. Rainoldi, "Compensation of the effect of sub-cutaneous tissue layers on surface EMG: a simulation study," *Med. Eng. Phys.*, vol. 21, pp. 487–496, 1999.

[18] D.F. Stegeman, J.H. Blok, H. J. Hermens, and K. Roeleveld, "Surface EMG models: properties and applications," *J. Electromyogr. Kines.*, vol. 10, pp. 313–326, 2000.

[19] R.E. Garfield, S. Sims, E.E. Daniel, et al., "Gap junctions: their presence and necessity in myometrium during parturition," *Science*, vol. 198, pp. 958–960, 1977.

[20] J. Duchêne, C. Marque, and S. Planque, "Uterine EMG signal: propagation analysis," in *IEEE EMBS Proc. Int. Conference*, 1990, pp. 831–832.

[21] D. Devedeux, C. Marque, S. Mansour, G. Germain, and J. Duchêne, "Uterine electromyography: a critical review," *Am. J. Obstet. Gynecol.*, vol. 169, pp. 1636–1653, 1993.

[22] W.J.E.P. Lammers, K. Arafat, A. El-Kays, and T.Y. El-Sharkawy, "Spatial and temporal variation in local spike propagation in the myometrium of the 17-day pregnant rat," *Am. J. Physiol. Cell. Physiol.*, vol. 267, pp. C1210–C1223, 1994.

[23] R.E. Garfield, "Is knowledge of electrical activity in the pregnant uterus helpful to our understanding of uterine function? focus on 'patterns of elecrical propagation in the intact guinea pig uterus' by Lammers et al.," *Am. J. Physiol. Regul. Integr. Comp. Physiol.*, vol. 294, pp. R917–R918, 2008.

[24] R. Plonsey, "Action potential sources and their volume conductor fields," *Proc. IEEE*, vol. 65, pp. 601–611, 1977.

[25] J.M. Marshall, "Regulation of activity in uterine smooth muscle," *Physiol. Rev. Suppl.*, vol. 5, pp. 213–227, 1962.

[26] A.C. Guyton and J.E. Hall, *Textbook of medical physiology*, Elsavier Saunders, Philadelphia, 2006.

[27] S. Gabriel, R.W. Lau, and C. Gabriel, "The dielectric properties of biological tissues: II. mesurements in the frequency range 10 Hz to 20 GHz," *Phys. Med. Biol.*, vol. 41, pp. 2251–2269, 1996.

[28] L. Mesin and R. Merletti, "Distribution of electrical stimulation current in a planar multilayer anisotropic tissue," *IEEE Trans. Biomed. Eng.*, vol. 2, pp. 660–670, 2008.

[29] D. Farina, C. Cescon, and R. Merletti, "Influence of anatomical, physical, and detection-system parameters on surface EMG," *Biol. Cybern.*, vol. 86, pp. 445–456, 2002.

[30] C.Y. Tan, B. Statham, R. Marks, and P.A. Payne, "Skin thickness measurement by pulsed ultrasound: its reproducibility, validation and variability," *Brit. J. Dermatol.*, vol. 106, pp. 657–667, 1982.

[31] John G. Webster, *Medical Instrumentation*, John Wiley & Sons Inc, New York, 1998.

[32] C. Rabotti, M. Mischi, J.O.E.H. van Laar, S.G. Oei, and J.W.M. Bergmans, "Estimation of internal uterine pressure by joint amplitude and frequency analysis of electrohysterographic signals," *Physiol. Meas.*, vol. 29, pp. 829–41, 2008.

[33] J.J. Bailey, "The triangular wave test for electrocardiographic devices: a historical perspective," *J. Electrocardiol.*, vol. 37, pp. 71–73, 2004.

[34] D. Farina, W. Muhammad, E. Fortunato, O. Meste, R. Merletti, and H. Rix, "Estimation of single motor unit conduction velocity from surface electromyogram signals detected with linear electrode arrays," *Med. Biol. Eng. Comput.*, vol. 39, pp. 225–236, 2001.

[35] R.M. Ranayyan, *Biomedical Signal Analysis*, Wiley-IEEE press, New York, 2002.

[36] C.J. Houtman, D.F. Stegeman, J.P. Van Dijk, and M.J. Zwartz, "Changes in muscle fiber conduction velocity indicate recruitment of distinct motor unit populations," *J. Appl. Physiol.*, vol. 95, pp. 1045–1054, 2003.

[37] J.C. Lagarias, J.A. Reeds, M.H. Wright, and P.E. Wright, "Convergence properties of the Nelder-Mead simplex method in low dimensions," *SIAM J. Optim.*, vol. 9, pp. 112–147, 1998.

[38] H. Kanehisan, M. Miyatani, K. Azuma, S. Kuno, and T. Fukunaga, "Influences of age and sex on abdominal muscle and subcutaneous fat thickness," *Eur. J. App. Physiol.*, vol. 91, pp. 534–537, 2004.

[39] R.P. Stolk, O. Wink, P.M. Zelissen, R. Meijer, A. P. van Gils, and D.E. Grobbee, "Validity and reproducibility of ultrasonography for the measurement of intra-abdominal adipose tissue," *Int. J. Obes. Relat. Metab. Disord.*, vol. 25, pp. 1346–1351, 2001.

Chapter 6

Small-scale conduction velocity estimation

C. Rabotti, M. Mischi et al., "Noninvasive estimation of the electrohysterographic action-potential conduction velocity," IEEE Trans. Biomed. Eng., conditional acceptance

Panta rei os potamòs [1]

6.1 Introduction

The understanding of risk factors and mechanisms related to preterm labor has been advancing and many public health and medical interventions to reduce the incidence of preterm birth have been introduced. The preterm birth rate has however risen in most industrialized countries and it still accounts for 75% of perinatal mortality and more than 50% of long term morbidity [2], with an associated annual societal economic cost that, in the United States alone, was estimated to amount to 26.2 billion in 2005 [3]. It is well established that pregnancy monitoring techniques are essential to assess the key risk factors and permit timely medical intervention; however, accurate prediction of the delivery time, which can be the key parameter for timely treatment of premature labor, still remains a major challenge [4].

Next to fetal heart rate monitoring, detection and evaluation of the uterine contractions is of major importance. Typical techniques adopted in clinical practice involve the use of either an external tocodynamometer, which provides a noninvasive indication of contraction onset timing based on external strain gauges, or an internal catheter, which measures the intrauterine amniotic pressure [4]. Only the latter technique provides quantitative information, but it is invasive and applicable only during labor [4].

In the past few years, a noninvasive alternative technique has been proposed that promises reliable assessment of the uterine activity without the use of intrauterine catheterization. Quantitative information on the myometrium (uterine muscle) is in

---

[1]Literally, 'Everything flows like a river'; this aphorism was used by Simplicius to characterize Heraclitus' philosophy [1]

fact derived from the analysis of its electrical activity, referred to as electrohystero-gram. Several techniques have been proposed for the analysis of the electrohysterographic (EHG) signal. Some authors have developed methods for the noninvasive estimation of the intrauterine pressure [5–7], while other authors could distinguish between two different EHG frequency components [8] or observe a shift in the frequency content of the EHG signal as delivery approaches [9, 10], possibly being able to predict the course of pregnancy. The ultimate goal and main challenge remains the prediction of preterm delivery. While the reported techniques are mostly based on single channel measurements [10], we believe that important information for monitoring and predicting the progress of pregnancy resides in the EHG signal propagation characteristics as also suggested in [11, 12].

Differently from skeletal muscles, which are striated and present an anatomical direction of propagation parallel to the fiber orientation, the myometrium is a smooth muscle; as a result, the direction of propagation of the myometrium intracellular action potential (AP), i.e., the electrical activation of the myometrial cells, is *a priori* unknown [8]. The propagation of electrical activity in the myometrium mainly depends, in fact, on the specific pattern of gap-junction connections which are dynamically formed between cells during each contraction [13, 14]. Possible additional parameters that may influence the propagation of uterine action potentials are calcium waves [15] and the possible bundle arrangement of the myometrium fibers [16].

APs usually occur in bursts. Each burst usually corresponds to a contraction event [17]. The burst frequency and duration as well as the AP frequency within a burst are highly dependent of the subject and the parturition stage. In human, the bursts duration can be more than one minute [17], with a burst frequency around 0.1 Hz [8]. The AP frequency within a burst has been reported to range between 0.1 and 10 Hz [8], with the majority of studies focusing on the frequency range 0.1-3 Hz [18, 19] and 0.3-1 Hz [9, 12, 17, 20]. Most of the previous literature was dedicated to the analysis of the entire burst and only few studies were dedicated to the analysis of single surface APs [14, 20, 21]. However, *in-vitro* studies have demonstrated that, in association with the increase of the gap-junction number, individual APs propagate for longer distance and with higher conduction velocity (CV) at parturition than at preterm [14].

In this paper we focus, for the first time, on a method for the estimation of the CV of single surface APs, which are extracted from EHG signals recorded noninvasively on women in labor. By surface AP we refer to a spike extracted from a single channel EHG burst that, being recorded noninvasively, is the weighted average of the electrical activity of all the underlying excited cells [22, 23]. An additional novelty of this study resides in the EHG signal recording methodology, which comprises the use of a high-density (HD) electrode grid. The grid, in fact, integrates a larger number of electrodes (64) with a reduced surface and smaller interelectrode distance

with respect to the previous literature [6, 7, 11, 19, 24]. Furthermore, due to the *a priori* unknown AP direction of propagation, the bi-dimensional arrangement of the electrodes on the grid (8x8) permits to estimate all the possible CV directions along the abdominal plane parallel to the abdominal surface.

Several methods are available from the electromyography literature for the measurement of the surface AP CV. Due to the signal source (skeletal muscles), these methods use monodimensional information, as the direction of propagation can be derived from the muscle fiber orientation. These methods can be divided in four major categories [25]: cross-correlation function maximization [26], phase difference [27], maximum likelihood (ML) [28], and the detection of spectral dips [29]. A four electrode implementation of this method (multidip), leading to an analytical solution, has been presented in [30], where the authors mention the possibility of further increase of the number of electrodes. One of the main issues related to the use of spectral dips is the large variance in their detection, which is due to the variance of the estimated power spectrum [25]. Furthermore, more extensive validation is required before adapting the method to our EHG measurement. In particular, due to the varying direction of propagation of the AP, the extension of the spectral multidip method to two dimensions is neither trivial nor practical.

Among the remaining three methods, the phase difference and the ML method, unlike the cross-correlation method, are both implemented in the frequency domain and permit CV measurements that are not limited by the time sampling rate [25]. Given the EHG frequency content, usually lower than 1 Hz [5], this characteristic is highly desirable, permitting low sampling rates and, therefore, reducing the complexity of the signal analysis. The ML method [31], compared to the phase difference method, permits a complete exploitation of our multichannel measurements because it allows using all the available acquisition channels, leading to an increased robustness to a low signal-to-noise ratio (SNR). Furthermore, differently from the spectral multidip, the ML method can be easily extended to two dimensions.

The ML method has been therefore chosen for the EHG analysis. Due to the models assumed for the AP propagation and for the noise, the ML estimation is equivalent to a mean square error minimization. We improved the ML method described in [31] by weighting the derived cost function. A set of weights is automatically determined based on SNR estimates at each channel. Two different weighting approaches are here presented and compared. The method in [31] has been further extended to two dimensions, permitting to estimate amplitude and direction of the CV.

6.2 Methodology

In this Section, more detailed information is provided on the proposed CV-estimation methods. These methods are based on the characteristics of the measured signals,
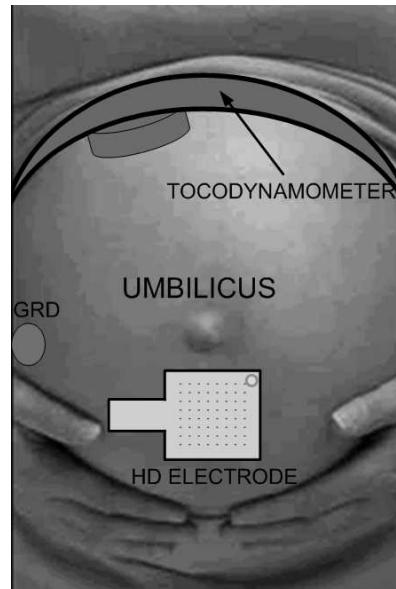
Figure 6.1: *Scheme of the measurement setup.*

depending on the measurement system, presented in Section 6.2.1, as well as on the implemented preprocessing steps, presented in Section 6.2.2. The implemented ML method and the proposed improvements are then presented in Sections 6.2.3 and 6.2.4, respectively.

6.2.1   Measurement

After approval of the medical committee of the hospital, ten measurements were performed at the Máxima Medical Center in Veldhoven (the Netherlands) on ten women in labor who signed an informed written consent. The sensors were placed as described in Fig. 6.1 after skin preparation with an abrasive paste for contact impedance reduction. The EHG was recorded by a Refa system (TMS International, Enschede, the Netherlands) comprising a multichannel amplifier for electrophysiological signals and a grid of 64 (8x8) HD electrodes (1 mm diameter, 4 mm interelectrode distance). The HD electrode grid, whose characteristics are more extensively described in [20], was placed on the mid-line of the abdomen below the umbilicus; the ground (GRD) electrode was positioned on the right hip. In order to obtain an efficient rejection of electromagnetic interference, an active GRD electrode was used and all cables were actively shielded [32]. An external tocogram was employed to support the assessment of the contraction period.
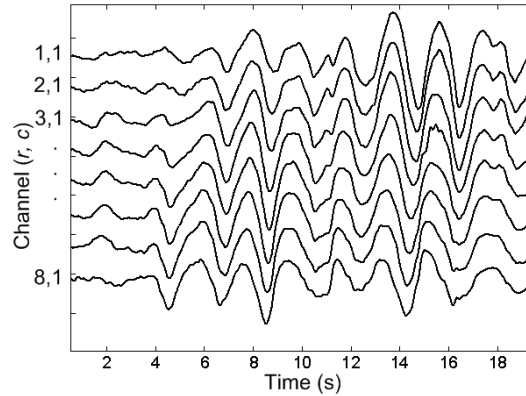
Figure 6.2: Example of EHG surface APs recorded by one column of the acquisition matrix after filtering and downsampling.

6.2.2 Data preprocessing

Given the narrow-band nature of the EHG signal, similarly to previous studies [9, 12, 17, 20], the acquired signals were band-pass filtered by a sixth order Butterworth filter with low and high cut-off frequencies at 0.1 and 0.8 Hz, respectively. This permitted to suppress most of the noise introduced by the respiration, the maternal electro-cardiogram (ECG), and the abdominal electromyogram [20, 33]. The filtered signals could therefore be downsampled from 1024 to 16 Hz without introducing aliasing and reducing significantly the computational complexity of the following analysis. This is particularly convenient when dealing with 64 parallel channels. Fig. 6.2 shows an EHG surface AP sequence registered by one column (8 channels) of the acquisition matrix after filtering and downsampling. Similarly as it has been shown in [21], the example indicates that within the same burst the direction and speed of propagation can vary from one surface AP to the next. This peculiarity of the single surface AP suggests that the analysis of APs, relative to the whole EHG burst analysis, provides additional and different information that may be of clinical relevance. The expected shape of the EHG surface AP can be derived by the previous studies on the EHG surface AP, where propagating action potentials were directly recorded from the uterus surface [21], and where the EHG surface AP has been measured and modeled [20].

6.2.3 Maximum likelihood method

Following the schematic representation of Fig. 6.3, we assume the EHG to propagate with velocity v and with incidence angle θ ($\theta \in [-\pi, \pi]$) with respect to the vertical axis of the electrode grid. Due to size of the electrode grid, which is of the order of the signal wavelength [20], we can assume the EHG surface AP to be a planar
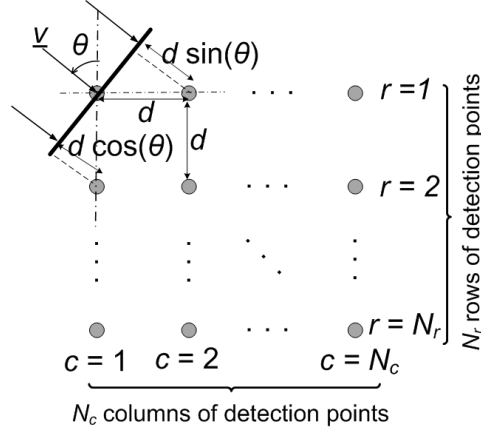
Figure 6.3: *Schematic description of the system model.*

wave. The signal is detected by N_r rows and N_c columns of electrodes. Assuming that the same signal shape $s(n)$ is measured at each channel, the adopted ML method is developed under the hypothesis that the signal x_{rc} measured at the channel (r,c) in the rth row ($r \in [1,2,...,N_r]$) and c^{th} column ($c \in [1,2,...,N_c]$) of the electrode grid can be modeled as

$$x_{rc}(n) = s(n - (r-1)\tau_r - (c-1)\tau_c) + w_{rc}(n), \qquad (6.1)$$

where n indicates the time sample ($n \in [1,2,...,N]$) and $w_{rc}(n)$ is white Gaussian noise with variance σ_{rc}^2 that is present at channel (r,c). The choice of the noise model is supported by the narrow band nature of the signal of interest. As from (6.1), in each channel (r,c) the reference signal shape $s(n)$ is delayed by τ_r and τ_c time samples with respect to the previous row and column, respectively.

The CV calculation requires the estimation of (τ_r, τ_c), which can be obtained by the maximization of $p((\tau_r,\tau_c)|x_{rc}(n),s(n))$. Using Bayesian inference and assuming $p(\tau_r,\tau_c)$ uniform, the maximization of $p((\tau_r,\tau_c)|x_{rc}(n),s(n))$ corresponds to the maximization of the probability $p(x_{rc}(n)|(\tau_r,\tau_c),s(n))$ of the samples of the signal $x_{rc}(n)$, given the row and column sample delays τ_r and τ_c and the reference shape $s(n)$, i.e.,

$$p(x_{rc}(n)|(\tau_r,\tau_c),s(n)) = \frac{1}{(2\pi)^{\frac{N}{2}}\sigma_{rc}^N} \cdot$$
$$\cdot e^{-\frac{\sum_{n=1}^{N}[x_{rc}(n) - s(n-(r-1)\tau_r - (c-1)\tau_c)]^2}{2\sigma_{rc}^2}}. \qquad (6.2)$$

Furthermore, the ML estimation of (τ_r, τ_c) corresponds to the maximization of

$\ln(p(x_{rc}(n)|(\tau_r, \tau_c), s(n)))$ [34], where

$$\ln(p(x_{rc}(n)|(\tau_r, \tau_c), s(n))) = \ln\left(\frac{1}{(2\pi)^{\frac{N}{2}}\sigma_{rc}^N}\right) +$$

$$-\frac{\sum_{n=1}^N [x_{rc}(n) - s(n - (r-1)\tau_r - (c-1)\tau_c)]^2}{2\sigma_{rc}^2}. \tag{6.3}$$

The expression in (6.3) can be extended to the entire matrix including all rows r and columns c. The estimation of (τ_r, τ_c) reduces therefore to the minimization of the cost function

$$\varepsilon^2(\tau_r, \tau_c) = \sum_{r=1}^{N_r}\sum_{c=1}^{N_c}\sum_{n=1}^{N}[x_{rc}(n) +$$

$$-s(n - (r-1)\tau_r - (c-1)\tau_c)]^2. \tag{6.4}$$

Since the signals $x_{rc}(n)$ are only available for discrete values of τ_r and τ_c, minimization of (6.4) results in a discrete estimate of the optimum (τ_r, τ_c), which depends on the sampling rate. By using Parseval's equality, (6.4) can be transformed in the frequency domain, where τ_r and τ_c become continuous multiplicative factors of the phase and can be estimated without resolution limits. Indicating by $X_{rc}(f)$ and $S(f)$ the Fourier transform of the signal recorded at the channel (r, c) and of the reference shape, respectively, the resulting cost function is

$$E^2(\tau_r, \tau_c) = \frac{2}{N}\sum_{r=1}^{N_r}\sum_{c=1}^{N_c}\sum_{f=1}^{N/2}\left[X_{rc}(f) +\right.$$

$$\left. -S(f)e^{-j2\pi f[(r-1)\tau_r + (c-1)\tau_c]}\right]^2. \tag{6.5}$$

From the description in Fig. 6.3, for an interelectrode distance equal to d and a temporal sampling frequency f_s, it follows that τ_r and τ_c are related to the conduction velocity v and to the incidence angle θ by

$$\tau_r = f_s \cdot \frac{d \cdot cos(\theta)}{v}$$

$$\tau_c = f_s \cdot \frac{d \cdot sin(\theta)}{v}. \tag{6.6}$$

The shape function $S(f)$ can be estimated as the average of all the channels $X_{rc}(f)$ after alignment, i.e., in the temporal frequency domain

$$\widehat{S}(f) = \frac{1}{N_c N_r}\sum_{r=1}^{N_r}\sum_{c=1}^{N_c}X_{rc}e^{j2\pi f[(r-1)\tau_r + (c-1)\tau_c]}. \tag{6.7}$$

The resulting estimated cost function $\widehat{E}^2(\tau_r, \tau_c)$ is then

$$\widehat{E}^2(\tau_r, \tau_c) = \frac{2}{N} \sum_{r=1}^{N_r} \sum_{c=1}^{N_c} \sum_{f=1}^{N/2} \left[X_{rc}(f) + \right.$$

$$\left. - \frac{1}{N_r N_c} \sum_{m=1}^{N_r} \sum_{p=1}^{N_c} X_{mp}(f) e^{j2\pi f[(m-r)\tau_r + (p-c)\tau_c]} \right]^2. \tag{6.8}$$

6.2.4 Channel weighting

The model in (6.1) is based on the assumption, that the signals recorded at different channels are delayed versions of the same reference shape $s(n)$. This assumption, already weak for skeletal muscles [28], is even weaker for the myometrium, where differences in the volume conductor and cell-to-cell conduction path underneath the electrodes may cause shape variations of the propagating APs [8]. In (6.1) such shape variations are accounted for by the noise term $w_{rc}(n)$. In order to increase the robustness of the CV estimation to surface AP shape variations due to the presence of noise, the method is improved by introducing proper weights, $a_{rc} \in \mathbb{R}^+$, in the cost function. The resulting weighted cost function $\widehat{E}^2_a(\tau_r, \tau_c)$ is defined as

$$\widehat{E}^2_a(\tau_r, \tau_c) = \frac{2}{N} \sum_{r=1}^{N_r} \sum_{c=1}^{N_c} \sum_{f=1}^{N/2} \left[a_{rc} \Big(X_{rc}(f) + \right.$$

$$\left. - \widehat{S}(f) e^{-j2\pi f[(r-1)\tau_r + (c-1)\tau_c]} \Big) \right]^2. \tag{6.9}$$

The weights are chosen to be inversely proportional to the standard deviation of the channel noise σ_{rc} [35], i.e,

$$a_{rc} = \frac{A}{\sigma_{rc}} = \frac{A}{\frac{2}{N} \sqrt{\sum_{f=1}^{N/2} |W_{rc}(f)|^2}}, \tag{6.10}$$

were A indicates a proper scaling factor to normalize the weight sum to 1. For the expression of a_{rc} in the frequency domain, last term of (6.10), Parseval's equality is used, where $|W_{rc}(f)|^2$ is the noise power spectrum in the considered channel (r, c).

In order to obtain an estimate of the noise power for the generic channel (r, c), the model in (6.1) is expressed in the temporal frequency domain f as

$$X_{rc}(f) = S(f) e^{-j2\pi f[(r-1)\tau_r + (c-1)\tau_c]} + W_{rc}(f) \tag{6.11}$$

By assuming the reference shape $S(f)$ and the noise $W_{rc}(f)$ to be uncorrelated, the noise can be estimated from

$$\sum_{f=1}^{N/2} X_{rc}(f) \cdot X_{rc}^*(f) = \sum_{f=1}^{N/2} S(f) \cdot S^*(f) + \sum_{f=1}^{N/2} |W_{rc}(f)|^2, \tag{6.12}$$

Table 6.1: Cost functions and weighting strategies.

Cost function	Weights	Reference shape
$\widehat{E}^2(\tau_r, \tau_c) = \frac{2}{N}\sum_{r=1}^{N_r}\sum_{c=1}^{N_c}\sum_{f=1}^{N/2}\left(X_{rc}(f) - \widehat{S}(f)e^{-j2\pi f[(r-1)\tau_r+(c-1)\tau_c]}\right)^2$	N/A	$\widehat{S}(f) = \frac{1}{N_r N_c}\sum_{r=1}^{N_r}\sum_{c=1}^{N_c}X_{rc}e^{j2\pi f[(r-1)\tau_r+(c-1)\tau_c]}$
$\widehat{E}_a^2(\tau_r, \tau_c) = \frac{2}{N}\sum_{r=1}^{N_r}\sum_{c=1}^{N_c}\sum_{f=1}^{N/2}\left[a_{rc}\left(X_{rc}(f) - \widehat{S}(f)e^{-j2\pi f[(r-1)\tau_r+(c-1)\tau_c]}\right)\right]^2$	$a_{rc} = \dfrac{A}{\frac{2}{N}\sqrt{\sum_{f=1}^{N/2}\left(X_{rc}(f)\cdot X_{rc}^*(f) - \widehat{S}(f)\cdot \widehat{S}^*(f)\right)}}$	$\widehat{S}(f) = \frac{1}{N_r N_c}\sum_{r=1}^{N_r}\sum_{c=1}^{N_c}X_{rc}e^{j2\pi f[(r-1)\tau_r+(c-1)\tau_c]}$
$\widehat{E}_{a^w}^2(\tau_r, \tau_c) = \frac{2}{N}\sum_{r=1}^{N_r}\sum_{c=1}^{N_c}\sum_{f=1}^{N/2}\left[a_{rc}^w\left(X_{rc}(f) - \widehat{S}_w(f)e^{-j2\pi f[(r-1)\tau_r+(c-1)\tau_c]}\right)\right]^2$	$a_{rc}^w = \dfrac{A}{\frac{2}{N}\sqrt{\sum_{f=1}^{N/2}\left(X_{rc}(f)\cdot X_{rc}^*(f) - \widehat{S}_w(f)\cdot \widehat{S}_w^*(f)\right)}}$	$\widehat{S}_w(f) = \sum_{r=1}^{N_r}\sum_{c=1}^{N_c}a_{rc}^w X_{rc}e^{j2\pi f[(r-1)\tau_r+(c-1)\tau_c]}$

where $(\cdot)^*$ is the conjugate operator. The noise power derived by (6.12) can then be substituted in (6.10) to provide the weights

$$a_{rc} = \frac{A}{\frac{2}{N}\sqrt{\sum_{f=1}^{N/2}\left(X_{rc}\left(f\right)\cdot X_{rc}^*\left(f\right)-S(f)\cdot S^*(f)\right)}}. \tag{6.13}$$

The shape $\widehat{S}(f)$ defined in (6.7) as the average of the aligned signals X_{cr}, which is used as estimate of the reference signal $\widehat{S}(f)$ in (6.9), can be employed in (6.13).

Alternatively, the estimate $\widehat{S}_w(f)$ of the reference shape $S(f)$ in (6.13) can be calculated as the weighted average of the signals $X_{rc}(f)$, i.e,

$$\widehat{S}_w(f) = \sum_{r=1}^{N_r}\sum_{c=1}^{N_c} a_{rc}^w \cdot X_{rc} e^{j2\pi f[(r-1)\tau_r+(c-1)\tau_c]}. \tag{6.14}$$

Using $\widehat{S}_w(f)$ as estimate of $S(f)$ in (6.13), the alternative channel weights a_{rc}^w are defined as

$$a_{rc}^w = \frac{A}{\frac{2}{N}\sqrt{\sum_{f=1}^{N/2} X_{rc}\left(f\right)\cdot X_{rc}^*\left(f\right)-\widehat{S}_w(f)\widehat{S}_w^*(f)}}. \tag{6.15}$$

and using (6.14) for $\widehat{S}_w(f)$ and $\widehat{S}_w^*(f)$, (6.15) can be expressed as

$$a_{rc}^w = \frac{A}{\frac{2}{N}\sqrt{\sum_{f=1}^{N/2} X_{rc}\left(f\right)\cdot X_{rc}^*\left(f\right)-\sum_{r=1}^{N_r}\sum_{c=1}^{N_c}(a_{rc}^w)^2\cdot X_{rc}(f)X_{rc}^*(f)}}. \tag{6.16}$$

The $N_r\cdot N_c$ equations of the same form as (6.16), which holds for each channel (r,c), and the condition on the weight sum

$$\sum_{r=1}^{N_r}\sum_{c=1}^{N_c} a_{rc}^w = 1 \tag{6.17}$$

lead to a system of $N_r\cdot N_c+1$ linearly independent equations, where the $N_r\cdot N_c$ unknown weights and the scaling factor A can be univocally derived. Using the same weights a_{rc}^w for the cost function and the reference shape in (6.13) leads to the following expression of the estimated alternative cost function $\widehat{E}_{a^w}^2(\tau_r,\tau_c)$,

$$\widehat{E}_{a^w}^2(\tau_r,\tau_c) = \frac{2}{N}\sum_{r=1}^{N_r}\sum_{c=1}^{N_c}\sum_{f=1}^{N/2}\left[a_{rc}^w\Big(X_{rc}(f)+\right.$$
$$\left.-\widehat{S}_w(f)e^{-j2\pi f[(r-1)\tau_r+(c-1)\tau_c]}\Big)\right]^2, \tag{6.18}$$
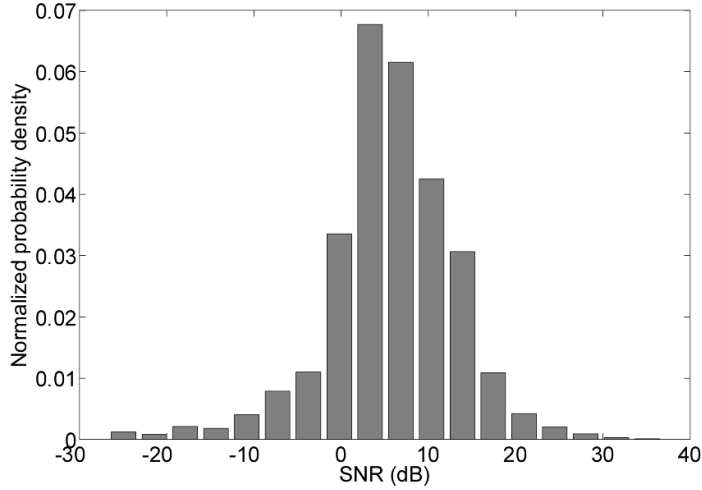
Figure 6.4: SNR distribution of 40 APs randomly selected from ten patients.

where, differently from the cost function $E^2(\tau_r, \tau_c)$ in (6.9), the weights a_{rc}^w are calculated using the weighted average $\widehat{S}_w(f)$ of the signals $X_{rc}(f)$ as estimate of the reference shape $S(f)$.

For validation, the three cost functions $E^2(\tau_r, \tau_c)$, $E_a^2(\tau_r, \tau_c)$, and $\widehat{E}_{a^w}^2(\tau_r, \tau_c)$, whose definitions are summarized in Table 6.1, were compared on simulated and real signals. In our previous study [36], the use of clustering in combination with weighting was successfully proposed, for the first time, to select a subset of electrodes for the CV estimation in one direction and to improve the estimate accuracy. In the present study, we tested the combined use of clustering and weighting by defining the cluster distance as the reciprocal of the weights a_{rc}^w.

For the minimization of the cost functions, the Nelder-Mead Simplex search method was used [37]. The values of τ_r and τ_c are initialized according to the average values reported in the literature for the uterine AP CV in the circumferential direction (2.8 cm/s) and in the longitudinal direction (6.8 cm/s), respectively [21]. The proposed methods were implemented in Matlab (Mathworks). For each surface AP, with the algorithm running on an Intel Core2 Duo Processor with 1.97 GB RAM, the CV estimate was obtained in about 1 minute.

6.3 Results

6.3.1 Simulated signals

The presented CV-estimation methods are evaluated by means of simulations based on real signals. A time interval of 10 s including a complete EHG surface AP was

Table 6.2: *Standard deviation of the delay estimates for different velocities and angles of incidence.*

Cost Function	v= 4cm/s							
	$\theta = 0$		$\theta = \pi/12$		$\theta = \pi/6$		$\theta = \pi/4$	
	SD$_r$	SD$_c$	SD$_r$	SD$_c$	SD$_r$	SD$_c$	SD$_r$	SD$_c$
$\widehat{E}^2(\tau_r, \tau_c)$	7.0 ms	5.5 ms	6.2 ms	5.4 ms	6.2 ms	5.9 ms	6.4 ms	5.6 ms
$\widehat{E}_a^2(\tau_r, \tau_c)$	3.2 ms	2.5 ms	3.0 ms	2.8 ms	2.9 ms	3.0 ms	3.0 ms	3.1 ms
$\widehat{E}_{a^w}^2(\tau_r, \tau_c)$	2.7 ms	2.3 ms	2.5 ms	2.4 ms	2.5 ms	2.5 ms	2.7 ms	2.6 ms

Cost Function	v= 10cm/s							
	$\theta = 0$		$\theta = \pi/12$		$\theta = \pi/6$		$\theta = \pi/4$	
	SD$_r$	SD$_c$	SD$_r$	SD$_c$	SD$_r$	SD$_c$	SD$_r$	SD$_c$
$\widehat{E}^2(\tau_r, \tau_c)$	4.5 ms	4.2 ms	4.1 ms	3.7 ms	3.8 ms	3.5 ms	3.7 ms	3.5 ms
$\widehat{E}_a^2(\tau_r, \tau_c)$	2.9 ms	2.3 ms	2.7 ms	2.1 ms	2.6 ms	2.2 ms	2.4 ms	2.3 ms
$\widehat{E}_{a^w}^2(\tau_r, \tau_c)$	2.0 ms	1.9 ms	1.8 ms	1.7 ms	1.6 ms	1.6 ms	1.6 ms	1.6 ms

extracted from real EHG recording to obtain the reference shape $s(n)$. This signal was then artificially delayed to simulate the measurement of the same surface AP by the other electrodes on the grid. Two arbitrary velocities of 4 cm/s and 10 cm/s and four different angles of incidence, equal to 0, $\pi/12$, $\pi/6$, and $\pi/4$, were considered. After downsampling at 16 Hz, the delays corresponded to a fraction of the sampling frequency.

White Gaussian noise was then added to the reference shape signal to simulate the remaining 63 channels. In order to determine a realistic SNR, 40 APs (four per subject) were selected from the available recorded signals. The SNR was estimated by (6.12) in each channel. The distribution of the SNR expressed in dBs over the 40 64-channel recordings, (fig. 6.4), resulted well represented by a Gaussian probability density function (correlation coefficient $R = 0.97$ with the Gaussian fit), with mean and standard deviation equal to 5.88 dB and 7.41 dB, respectively. Therefore, for each simulated velocity and angle of incidence, 1000 different noise sequences were generated and added to each channel; the SNR was randomly distributed among the channels according to a Gaussian probability density function with the same mean and standard deviation estimated from the real signals.

The 64-channel simulations were then used to evaluate the different methods for the CV estimation. The CV-estimates were calculated by the ML method alone, and after the use of the two different weighting strategies in Table 6.1. The standard deviations of the error for the row delay τ_r (SD$_r$) and the column delay τ_c (SD$_c$) are reported in Table 6.2 for each simulated angle of incidence and for the different used cost functions. The maximum mean error was lower than 5% of the reference value of delay. On average, weighting the cost function reduced the standard deviation of the error by 44.06% ± 8.03%. Weighting both the cost function and the reference shape provided an average improvement of 56.70% ± 2.25%.

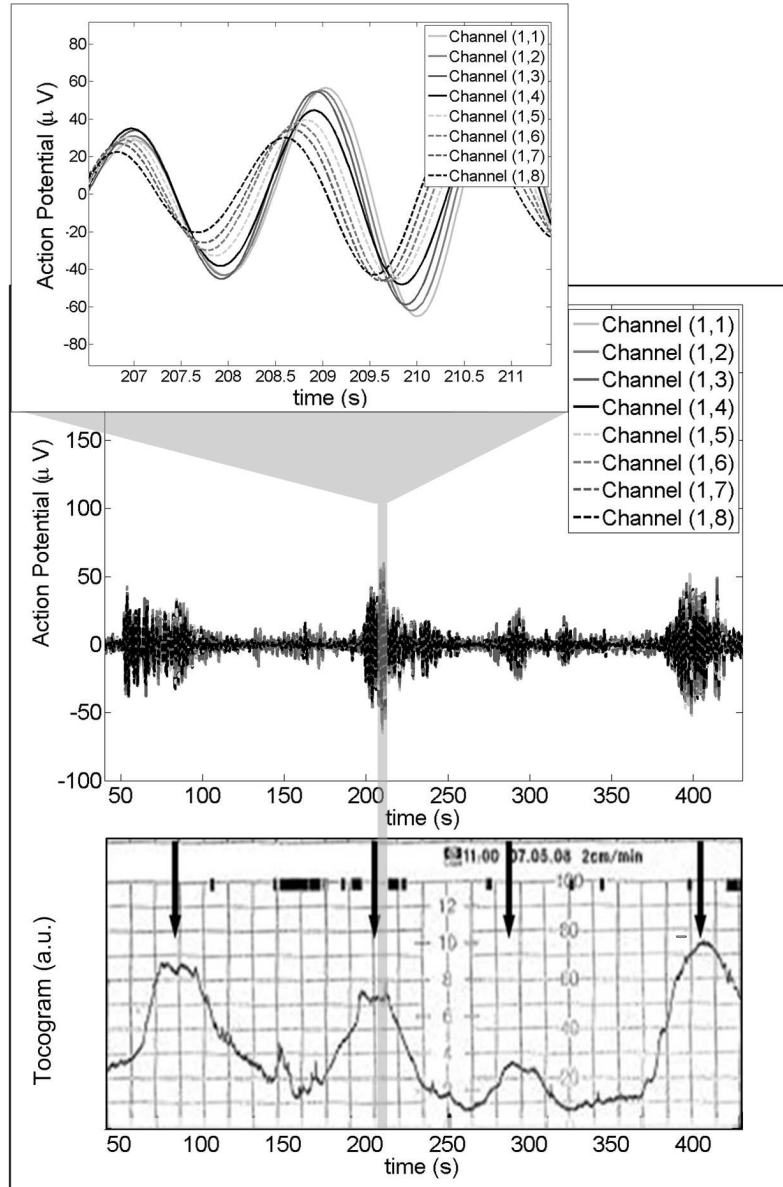***Figure 6.5:*** *Example of EHG bursts and corresponding tocogram. An example of selected surface AP is also shown in the top of the figure by magnifying a time segment of the burst at the contraction peak.*

6.3.2 Real signals

The measurement feasibility was also tested on ten women between the 38th and the 41st week of gestation with uterine contractions. Nine women were classified to be
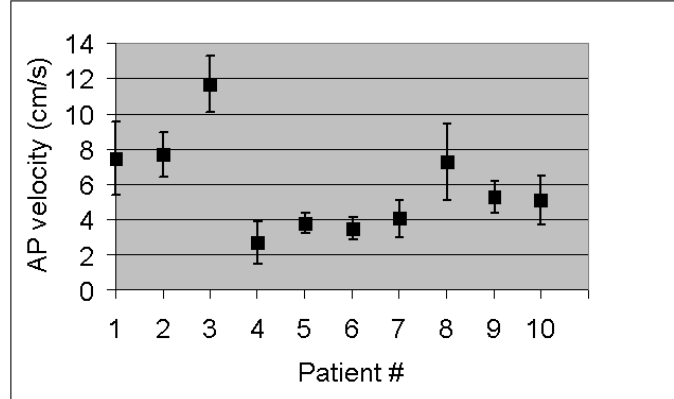
Figure 6.6: *Mean and standard deviation of the CV amplitude for all patients.*

in labor (dilatation > 3 cm) and delivered within 13 hours from the EHG recording. During contractions, time segments were visually inspected and two surface APs were determined per each woman around the contraction peak. In Fig. 6.5 an example recording of EHG bursts after preprocessing and the associated tocographic signal are shown. The figure shows that the amplitude during the quiescent period is significantly lower than during the activity burst. The magnified time segment in Fig. 6.5 shows that the surface AP propagates along the recording electrodes with a velocity of few cm/s. This suggests that the selected waveform originates from uterine activity and not from artifacts due to motion, which typically do not propagate, or to the ECG, which is not expected to show propagation along electrodes placed on the abdomen. The longer duration of surface APs relative to the internal measurements reported in the literature [21] can be explained by the effect of the volume conductor [20] and by the fact that the signal recorded by each surface electrode is the weighted average of the electrical activity of all the underlying excited cells [22, 23].

The surface AP visual selection aimed at excluding possible circulating excitations and re-entries [38]. Surface APs originating in the middle of the electrode grid and then propagating in two different directions or not propagating through the entire electrode were also excluded. Only those surface APs originating outside or on the border of the electrode grid and then propagating through the entire electrode grid were selected.

The method comprising the minimization of the cost function $\widehat{E}_{a^w}^2(\tau_r, \tau_c)$ was applied on the entire 8x8 electrode matrix. The average and standard deviation of the velocity amplitude are reported in Fig. 6.6 for all patients. On average, we found vertical and horizontal components of the velocity amplitude equal to 3.68±3.24 cm/s and 3.76±3.21 cm/s, respectively. These estimates are within the expected physiological range [8]. Concerning the wave incidence angle, as was previously demonstrated
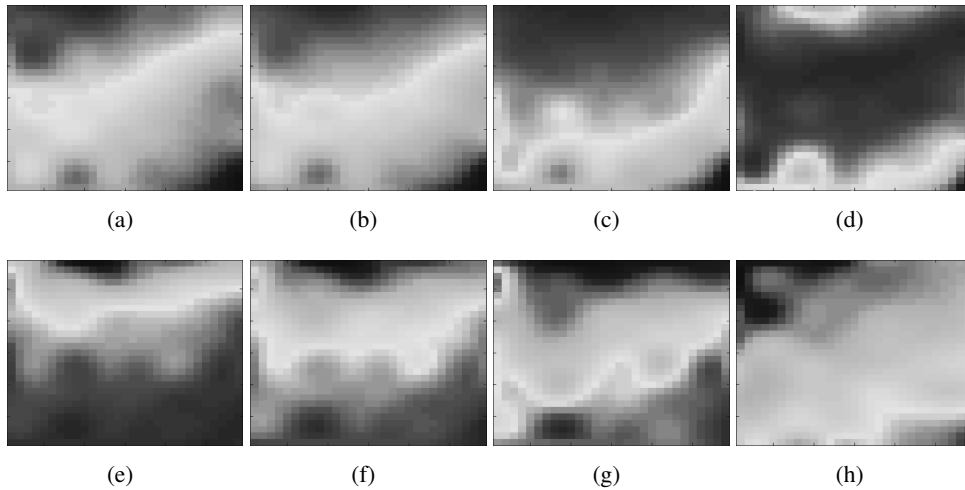
Figure 6.7: *Temporal sequence of surface AP propagation maps as recorded by the whole 64-channel electrode grid after spatial interpolation. The local amplitude of the surface AP is proportional to the grey level of the map. The reported maps, from (a) to (b), were recorded every 100 ms.*

by *in-vitro* studies, a preferred direction of propagation of single APs could not be highlighted and, even within the same contraction, different incidence angles were detected for different APs.

An example of surface AP propagation is shown in Fig. 6.7 by means of a temporal sequence of spatial maps representing the electrode grid; the local amplitude of the recorded surface AP is proportional to the grey level of the map. Therefore, the dark region represents the depolarization phase of the surface AP. In the first four maps the repolarization phase of the preceding surface AP (light region) is also visible. The reported maps refer to 8 different instants, one every 100 ms, of the surface AP propagation. In the presented example, the surface AP propagates with an incidence angle of about 6 degrees and a velocity of 4 cm/s, as detected by the proposed method.

6.4 Discussion and conclusion

Only few studies dedicated to the EHG signal propagation properties by multichannel recordings [11, 12]. These studies investigated the propagation on a large scale by analyzing the EHG bursts on the whole uterine muscle. A similar approach has also been attempted by multichannel tocography [39]. On the contrary, this paper focuses on the CV estimation of single APs. The surface AP CV is an additional parameter of

potential clinical relevance. As on a large scale this parameter cannot be accurately derived [12], the propagation analysis is here carried out on a small scale using a HD electrode grid. This small-scale analysis provides local propagation parameters that can fundamentally contribute, possibly in combination to the global parameters derived by large-scale analysis, to the development of diagnostic and prognostic tools for uterine contraction monitoring and labor prediction.

The measurement of the electrohysterographic surface AP CV is here proposed for the first time. The use of an electrode matrix permits estimating the CV vector in two dimensions. This is an important aspect in electrohysterographic measurements because, differently from electromyographic CV measurements, the EHG CV direction is not known *a priori*. For the signal analysis we propose a ML method, which is implemented in two dimension and comprises the use of weights in the cost function. The weight values depend on the estimated SNR.

Results on simulated signals show that the estimate accuracy is significantly improved by the use of weights. Among the two different weighting strategies that were proposed, the use of the same weights for estimating the reference signal shape and for the cost function results in more accurate estimates. As compared to the ML method alone, on average, the error variance diminished by 56.70%, becoming up to less than 3% of the measured value.

In our previous study [36], the use of clustering in combination with weighting was successfully proposed, for the first time, to select a subset of electrodes for the CV estimation in one direction and to improve the estimate accuracy. In the present study, we tested the combined use of clustering and weighting by defining the cluster distance as the reciprocal of the weights a_{rc}^w. On our simulated signals, the combined use of clustering and weighting led to an estimate accuracy comparable to that of the best weighting strategy (i.e the use of the cost function $\widehat{E}_{a^w}^2(\tau_r, \tau_c)$) alone. As clustering can be viewed as a form of binary weighting, these results could be expected and are therefore not explicitly reported.

The method feasibility was confirmed by measurements on ten women at term with uterine contractions. Calculation of the CV amplitude led to values that are within the expected physiological range [8, 14, 21]. As for the incidence angle of propagating surface AP, differently from what is reported for the propagation of the whole electrical burst [12], we could not highlight a most frequent direction of the surface AP propagation pattern even within the same contraction. The same variability in both origin and direction of the surface AP propagation pattern has been previously observed in *in-vivo* and *in-vitro* studies on the uterus, and, at least during labor [21], it seems physiological.

For practical reasons, the real signal analysis was conducted on APs that were previously selected around the contraction peak in order to exclude waves originating within the electrode area and then propagating in two different directions below the

electrode grid. Noteworthy, the proposed method for the CV estimation is not limited by this assumption. In fact, if the surface AP originates within the region covered by the electrode grid and then propagate in two different directions [21], an additional step is required for detecting the pacemaker electrode (i.e the first electrode recording the burst). The CV can be estimated for the two directions of propagation by applying the proposed method separately on the two subsets of electrodes in which the grid can be divided by the pacemaker electrode.

Additional exclusion criteria for the surface AP selection were circulating excitation, re-entries, and partial propagation along the electrode grid. These phenomena have been previously observed for the myometrium activity in animal studies. In particular, in rats circulating excitation had an occurrence of 22% [38]. Partial propagation of the surface AP along the electrode grid are common events especially at the beginning or at the end of a burst as highlighted in [40], where only in 25% of the bursts the mapped area was completely activated by the first AP. As confirmed in the literature, the high probability of these events, which we all excluded from the real signal analysis, imposed a limitation to the amount of analyzed signals.

The advantage of using a HD two-dimensional grid for the EHG signal recording is highlighted by the reported sequence of propagation maps. Furthermore, the example of surface AP in the maps satisfies the planar wave approximation that we assumed in our propagation model.

In conclusion, our results show that the proposed ML method is suitable for the two dimensional estimation of the EHG surface AP conduction velocity. Moreover, the use of weights for both the reference shape and the cost function leads to more accurate estimates than the use of the ML alone and should therefore be preferred. However, even if conceived for estimating the CV of surface AP extracted from the EHG signal, the proposed method can be employed for the analysis of other types of signal, in particular of those whose direction of propagation is *a priori* unknown.

For EHG surface AP analysis, the method, as currently presented, requires an accurate detection of the surface AP as prerequisite for the signal analysis. Future research will focus on implementation and clinical evaluation aspects such as the possibility of automatically selecting surfaceAPs. In general, this work opens new possibilities for future clinical studies aimed at assessing the CV-vector dynamics and its value for analysis of the pregnancy course and, most importantly, for prediction of preterm delivery.

Bibliography

[1] F.E. Peters, *Greek Philosophical Terms: A Historical Lexicon*, NYU Press, 1967.

[2] R.L. Goldenberg, J.F. Culhane, J.D. Jams, and R. Romero, "Epidemiology and causes of preterm birth," *Lancet*, vol. 371, pp. 75–84, 2008.

[3] R.E. Behrman and A.S Butler, *Preterm Birth: Causes, Consequences, and Prevention*, The National Academy Press, Washington, DC, 2007.

[4] R.E. Garfield, H. Maul, L. Shi, W. Maner, C. Fittkow, G. Olsen, and G.R. Saade, "Methods and devices for the management of term and preterm labor," *Ann. NY Acad.Sci.*, vol. 943, pp. 203–224, 2001.

[5] C. Rabotti, M. Mischi, J.O.E.H. van Laar, S.G. Oei, and J.W.M. Bergmans, "Estimation of internal uterine pressure by joint amplitude and frequency analysis of electrohysterographic signals," *Physiol. Meas.*, vol. 29, pp. 829–41, 2008.

[6] M.D. Skowronski, J.G. Harris, D.E. Marossero, R.K. Edwards, and T.Y. Euliano, "Prediction of intrauterine pressure from electrohysterography using optimal linear filtering," *IEEE Trans. Biomed. Eng.*, vol. 53, pp. 1983–1989, 2006.

[7] J. Jezewski, K. Horoba, A.Matonia, and J. Wrobel, "Quantitative analysis of contraction patterns in electrical activity signal of pregnant uterus as an alternative to mechanical approach," *Physiol. Meas.*, vol. 26, pp. 753–767, 2005.

[8] D. Devedeux, C. Marque, S. Mansour, G. Germain, and J. Duchêne, "Uterine electromyography: a critical review," *Am. J. Obstet. Gynecol.*, vol. 169, pp. 1636–1653, 1993.

[9] W.L. Maner, R.E. Garfield, H. Maul, G. Olson, and G. Saade, "Predicting term and preterm delivery with transabdominal uterine electromyography," *Obstet. Gynecol.*, vol. 101, pp. 1254–1260, 2003.

[10] M.P.G.C. Vinken, C. Rabotti, S.G. Oei, and M. Mischi, "Accuracy of frequency-related parameters of the electrohysterogram for predicting preterm delivery: a review of the literature," *Ob. Gyn. Survey*, vol. 64, pp. 529–541, 2009.

[11] T.Y. Euliano, D. Marossero, M.T. Nguyen, N.R. Euliano, J. Principe, and R.K. Edwards, "Spatiotemporal electrohysterography patterns in normal and arrested labor," *Am. J. Obstet. Gynecol.*, pp. 54.e1–54.e7, 2009.

[12] C. Rabotti, M. Mischi, J.O.E.H. van Laar, S.G. Oei, and J.W.M. Bergmans, "Inter-electrode delay estimators for electrohysterographic propagation analysis," *Physiol. Meas.*, vol. 30, pp. 745–761, 2009.

[13] R.E. Garfield, S. Sims, E.E. Daniel, et al., "Gap junctions: their presence and necessity in myometrium during parturition," *Science*, vol. 198, pp. 958–960, 1977.

[14] S.M. Miller, R.E. Garfield, and E.E. Daniel, "Improved propagation in myometrium associated with gap junctions during parturition," *Am. J. Physiol. Cell. Physiol.*, vol. 256, pp. C130–C141, 1989.

[15] R.C. Young, "Tissue-level signaling and control of uterine contractility: The action potentialcalcium wave hypothesis," *J. Soc. Gynecol. Invest.*, vol. 7, pp. 146–152, 2000.

[16] T. Chard and J. Grudzinskas, *The uterus*, Cambridge University Press, 1994.

[17] R.E. Garfield, W.L. Maner, L.B. MacKay, D. Schlembach, and G.R. Saade, "Comparing uterine electromyography activity of antepartum patients versus term labor patients," *Am. J. Obstet. Gynecol.*, vol. 193, pp. 23–29, 2005.

[18] H. Leman, C. Marque, and J. Gondry, "Use of the electrohysterogram signal for characterization of contractions during pregnancy," *IEEE Trans. Biomed. Eng.*, vol. 46, pp. 1222–1229, 1999.

[19] C. Marque, J. Duchêne, S. Leclercq, G. Panczer, and J. Chaumont, "Uterine EHG processing for obstetrical monitoring," *IEEE Trans. Biomed. Eng.*, vol. BME-33, pp. 1182–1187, 1986.

[20] C. Rabotti, M. Mischi, L. Beulen, S.G. Oei, and J.W.M. Bergmans, "Modeling and identification of the electrohysterographic volume conductor by high-density electrodes," *IEEE Trans. Biomed. Eng.*, vol. 57, pp. 519–527, 2010.

[21] W.J.E.P. Lammers, H. Mirghani, B. Stephen, S. Dhanasekaran, A. Wahab, and M.A.H. Al Sultan, "Patterns of electrical propagation in the intact guinea pig uterus," *Am. J. Physiol. Regul. Integr. Comp. Physiol.*, vol. 294, pp. R919–R928, 2008.

[22] M.J. Zwarts and D.F. Stegeman, "Multichannel surface EMG: basic aspects and clinical utility," *Muscle Nerve*, vol. 28, pp. 1–17, 2003.

[23] J.P. van Dijk, D.F. Stegeman, and M.J. Lapatki, B.G.and Zwarts, "Evidence of potential averaging over the finite surface of a bioelectric electrode using high-density EMG," in *XVI Congr. of the ISEK*, 2006, p. 62.

[24] G.M.J.A. Wolfs and M. van Leeuwen, "Electromyographic observations on the human uterus during labour," *Acta Obstet. Gynecol. Scand.*, vol. 58, pp. 1–61, 1979.

[25] D. Farina and R. Merletti, "Methods for estimating muscle fibre conduction velocity from surface electromyographic signals," *Med. Biol. Eng. Comput.*, vol. 42, pp. 432–445, 2004.

[26] P.A. Parker and R.N. Scott, "Statistics of the myoelectric signal from monopolar and bipolar electrodes," *Med. Biol. Eng.*, vol. 11, pp. 591–596, 1973.

[27] I.W. Hunter, R.E. Kearney, and L.A. Jones, "Estimation of the conduction velocity of muscle action potentials using phase and impulse response function techniques," *Med. Biol. Eng.*, vol. 25, pp. 121–126, 1987.

[28] D. Farina, W. Muhammad, E. Fortunato, O. Meste, R. Merletti, and H. Rix, "Estimation of single motor unit conduction velocity from surface electromyogram signals detected with linear electrode arrays," *Med. Biol. Eng. Comput.*, vol. 39, pp. 225–236, 2001.

[29] P.A. Lynn, "Direct on-line estimation of muscle fiber conduction velocity by surface electromyography," *IEEE Trans. Biomed. Eng.*, vol. 26, pp. 564–571, 1979.

[30] D. Farina and F. Negro, "Estimation of muscle fiber conduction velocity with a spectral multidip approach," *IEEE Trans. Biom. Eng.*, vol. 54, pp. 1583–1589, 2007.

[31] D. Farina and R. Merletti, "Estimation of average muscle fiber conduction velocity from two-dimensional surface EMG recordings," *J. Neuroscience Methods*, vol. 134, pp. 199–208, 2004.

[32] A.C. Metting van Rijn, A. Peper, and C.A. Grimbergen, "High-quality recording of bioelectric events. part 1 interference reduction, theory and practice," *Med. Biol. Eng. Comput.*, vol. 28, pp. 389–397, 1990.

[33] W.L. Maner and R.E. Garfield, "Identification of human term and preterm labor using artificial neural networks on uterine electromyography data," *Ann. NY Acad. Sci.*, vol. 35, pp. 465–473, 2007.

[34] C.M. Bishop, *Pattern Recognition and Machine Learning*, Springer, 2006.

[35] D.G. Manolakis, V.K. Ingle, and S.M. Kogon, *Statistical and Adaptive Signal Processing*, Artech house, Norwood, MA, 2005.

[36] M. Mischi, C. Rabotti, L.P.J. Vosters, S.G. Oei, and J.W.M. Bergmans, "Electrohysterographic conduction velocity estimation," in *IEEE EMBS Proc. Int. Conference*, 2009, pp. 6934–6939.

[37] J.C. Lagarias, J.A. Reeds, M.H. Wright, and P.E. Wright, "Convergence properties of the Nelder-Mead simplex method in low dimensions," *SIAM J. Optim.*, vol. 9, pp. 112–147, 1998.

[38] W.J.E.P. Lammers, "Circulating excitations and re-entry in the pregnant uterus.," *Eur. J. Physiol.*, vol. 433, pp. 287–293, 1997.

[39] L Spätling, F Fallenstein, R Danders, and A. Hasenburg, "External four-channel tocography during delivery," *Int. J. Gynaecol. Obstet.*, vol. 46, pp. 291–295, 1994.

[40] W.J.E.P. Lammers, K. Arafat, A. El-Kays, and T.Y. El-Sharkawy, "Spatial and temporal variation in local spike propagation in the myometrium of the 17-day pregnant rat," *Am. J. Physiol. Cell. Physiol.*, vol. 267, pp. C1210–C1223, 1994.

Chapter 7

Conclusions and future directions

...un pianoforte. I tasti iniziano. I tasti finiscono. Tu sai che sono 88,
su questo nessuno può fregarti. Non sono infiniti, loro. Tu sei infinito, e
dentro quei tasti, infinita è la musica che puoi suonare. (A. Baricco) [1].

For timely recognition of complications and proper medical intervention when acute risks are detected, quantitative assessment of uterine activity can be important throughout pregnancy and delivery. Unfortunately, assessment methods currently employed in clinical practice for contraction monitoring are either inaccurate or invasive.

Electrohysterography is the noninvasive measurement of the root cause of a uterine contraction. Therefore, the electrohysterographic (EHG) signal has great potential for routine uterine contraction monitoring both during pregnancy, for instance, for timely predictions of preterm labor, and during delivery, for accurate detection of complications like poor labor progress.

There are several important aspects related to the EHG signal interpretation, measurement, and analysis that have not been studied yet. In particular, the possibility of accurately estimating the internal uterine pressure (IUP) from noninvasive EHG recordings has not been previously investigated. Moreover, important issues like the effect of the tissues interposed between the uterus and the skin (volume conductor) on EHG recordings have not been studied. Furthermore, EHG signal interpretation has been typically based on single-channel measurements, while the use of multiple electrodes conveys additional information that can possibly be predictive of delivery.

This thesis aims at contributing to the technical basis for a comprehensive characterization of uterine activity by electrohysterography, as a prerequisite for introduction of electrohysterography in clinical practice. In this work, dedicated EHG signal analysis techniques were developed that, exploiting the underlying physiol-

---

[1] Literally '... a piano. The keys start. The keys end. You know that they are 88, nobody can cheat you about that. The keys are not infinite. You are infinite, and within those keys, infinite is the music that you can play'. From 'Novecento: un monologo' (Published also in English as 'Novecento: pianist')

ogy, aim at improving the current accuracy of EHG measurement and interpretation in the perspective of clinical applications.

One of the major issues addressed in this thesis is the possibility of replacing invasive IUP catheters, which are currently the golden standard for contraction monitoring, by EHG signal analysis. In the first part of this thesis, we demonstrated that the joint use of amplitude and frequency parameters derived from the EHG signal, combined with a nonlinear model of the relation between the electrical activity and the mechanical contraction of the myometrium (electromechanical activation), can provide, noninvasively, an accurate estimate of the IUP. Validation during delivery by comparison with the invasively recorded IUP showed that the proposed method outperforms the previous methods proposed in the literature, with an accuracy that is comparable to the golden standard. These results, due to the physiology-based approach, can also support the formulation of hypotheses on the mechanism underlying the uterine contraction. An example is provided by the hypothesis of the nonlinear electromechanical activation of the myometrium (see Chapter 3). In the perspective of introducing the proposed method for noninvasive IUP measurements in everyday clinical practice, due to the limited amount of analyzed data, further clinical validation is required to assess the robustness of the method with respect to the physiological differences among patients.

It is well established that the EHG signal is representative of the root cause of a uterine contraction and can therefore be predictive of labor or indicative of contraction efficiency. In this context, differently from the previous literature focused on the frequency analysis of the EHG signal, we studied the spreading of electrical activity in the myometrium as the first cause of a coordinated and effective contraction. We designed a method for analyzing the spatial distribution and dynamics of the EHG propagation vector on a large scale (cm). This method is based on the delay by which the signal is detected at multiple locations over the abdomen. Time-delay estimators based on cross-correlation function (CCF) maximization and spectral matching were implemented. Furthermore, we proposed a dedicated interelectrode time-delay estimator that, relative to existing methods, improves the robustness to noise in measurements performed in a clinical environment. The electrode configuration employed in these experiments was chosen to maximize the coverage of the uterine surface with a limited number of electrodes in order to test the robustness and the feasibility of the estimators on real data and in a clinical setting.

The results of the large-scale propagation study in labor suggested that poor values of interchannel correlation might affect the accuracy of time-delay estimators based on spectral matching and on the maximization of the CCF. Besides, although the assessment of the conduction velocity (CV) was not the aim of this propagation study, the estimated values of velocity were in the range reported in the literature for EHG bursts. Most of the contractions recorded in this study were first detected by the

uppermost electrodes, suggesting a preferred top-down propagation of the myometrial electrical burst during delivery. Since the mechanical contraction of the uterine muscle acts towards the expulsion of the fetus, this propagation pattern could be expected during labor and it might be associated with the effectiveness of the contractile activity.

The design of the dedicated interelectrode time-delay estimator was based on the assumption that the shape variations between the signals recorded by different electrodes are mainly due to the inhomogeneous structure and properties of the biological tissues interposed between the myometrium and the recording site on the skin. In order to further investigate this assumption and improve the interpretation accuracy of clinically relevant EHG parameters, a mathematical model of the EHG volume conductor was designed and validated. The intracellular AP at the myometrium was also analytically modeled in the spatial domain by a 2-parameter exponential in the form of a Gamma variate function.

The EHG signal was recorded by an electrode matrix on women. To validate the volume conductor model, a 64-channel (8×8) high-density (HD) electrode grid was employed to record the EHG signal. The use of electrodes with a reduced surface and smaller interelectrode distance with respect to previous studies resulted in an increased spatial resolution of the EHG measurements and reduced geometrical and electrical differences among the tissues below the recording locations. The volume conductor model parameters were estimated from the recorded EHG signal by a least mean square method. The volume conductor model is validated by comparing the thickness of the biological tissues recorded by echography to the values estimated using the model. The agreement between the estimated parameters and the echographic measurements suggested that the proposed model of the volume conductor is in agreement with the human anatomy and it can provide an accurate description of the physiology underlying the EHG signal.

The specific assumptions made for modeling the EHG volume conductor allowed developing a relatively simple one-dimensional model that leads to an accurate description of the data with a limited number of parameters. This model is therefore particularly suitable to support future physiological studies on the mechanism of EHG AP propagation in humans, the design of specific experimental protocols for future clinical investigations, and the interpretation of the relevant parameters. On the other hand, as the role played by the complex three-dimensional anatomical structure of the myometrium in the conduction of the electrical activity needs to be understood, future studies might suggest the need for integration of additional parameters into the model as well as extension of the model to more dimensions.

Based on the developed volume conductor model, the small-scale propagation properties of the EHG signal were then investigated for the first time in patients. The CV of the a single propagating surface AP was estimated by a 64-channel HD

electrode grid placed on the mother's abdomen. The use of an electrode matrix permits estimation of the CV vector in two dimensions. This is an important aspect in EHG measurements because, differently from electromyography (EMG) CV measurements, the direction of the EHG AP CV is not known *a priori*. Furthermore, the use of a HD electrode grid allows an increased resolution of the measurement relative to previous studies on EHG. For the signal analysis, we designed a maximum likelihood (ML) method, which was implemented in two dimensions and comprises the use of weights in the cost function. The weight values depend on the estimated channel signal-to-noise (SNR) ratio. Results on dedicated simulations showed that the estimate accuracy is significantly improved by the introduction of weights relative to the standard ML method. Among the two different weighting strategies that were proposed, the use of the same weights for estimating the reference signal shape and for the cost function (see Chapter 6) resulted in the most accurate estimates.

The feasibility of the method for small-scale propagation analysis was again confirmed by measurements on women at term with uterine contractions. These measurements led to CV values within the expected physiological range. Furthermore, analysis of the EHG signals recorded by the HD electrode grid suggested that also for the myometrium, similarly to the skeletal muscle, it is possible to observe a linear propagation of the surface APs, i.e., the surface APs detected by the different electrodes are the delayed and possibly scaled version of the same signal.

The proposed methods for EHG propagation analysis both on a large scale and on small scale has been conceived on the basis of the physiological background and specifically tailored to the analysis of EHG signals. Nevertheless, the methods proposed in this thesis can be extended for use to other applications related to the detection of propagating electrophysiological signals (e.g., the EMG).

More in general, this thesis provides a quantitative characterization of the uterine activity during pregnancy and delivery by analysis of the EHG signal aiming at an accurate measurement and interpretation of parameters with clinical relevance. Therefore, in view of the medical challenges faced everyday by obstetricians and the sever limitations of current technologies, this work opens the way to clinical applications and studies, that, based on these results, aim at understanding the processes underlying the onset of labor, advancing obstetrical monitoring technologies, and, ultimately, reducing the incidence of preterm birth and improving the perinatal outcome.

Acknowledgments

This PhD thesis represents for me the completion of a work that I have carried out with passion and determination, but not without moments of difficulties and discouragements, that I managed to overcome thanks to the many exceptional people I have been surrounded and supported by. For their contribution to the completion of my PhD and to the good time I had in last years, I wish to express my gratitude to these people.

First of all, I would like to thank my promotors, prof. Jan Bergmans and prof. Guid Oei, for giving me the possibility of joining this project and believing in my capabilities to complete this thesis. In particular, I would like to thank Jan for being always available to help, for his valuable suggestions, and for his challenging critiques, which, I believe, made me significantly grow both personally and scientifically. I am very grateful to him for his fundamental contribution to this thesis, whose quality has sensibly improved at each iteration and discussion I had with him. I thank Guid for his support, his enthusiasm, and his stimulating ideas. His clinical expertise was essential for the completion of my PhD. I take the chance of thanking Guid also for the very pleasant moments we shared during conferences and trips and for his patience for all the times I misspelled his initials in our publications.

This thesis could have never been done without the contribution of my copromotor and friend dr. Massimo Mischi. Massimo, thank you so much, for your excellent guidance, spiritual support, and fundamental help. I am grateful to you for trusting me, for the time you invested in this thesis, for your infinite patience in correcting the numerous mistakes of my texts, and for the kindness and understanding you have always shown towards me and my numerous help requests. I have learnt a great deal from you! Besides the very nice time we spent together during conferences and lunch, I also have to thank you (and Susan), for all the enjoyable moments we shared during football matches, dinners, and parties. Grazie!

Prof. Catherine Marque, prof. Sergio Cerutti, and Prof. Pieter Wijn are thanked for their contribution to the final version of this thesis and for sitting on my core committee at the defense. Prof. Joris van Der Post is thanked for joining the extended defense committee. A special thank goes also to prof. Piero Tortoli, 'il Grande Capo', because without him I would never have even started this PhD.

This PhD was part of the project 'electrophysiologic monitoring of fetal condition', supported by STW. I would like to thank all the members of the user committee

for their valuable feedbacks and inputs during our regular meetings. In particular, I would like to express my gratitude to Jan Peusher and Leo Hoogendoorn for their infinite kindness and for giving me the unique opportunity of being part of their team.

All the experimental data of this thesis have been recorded at the Máxima medical Centre in Veldhoven, and I feel indebted towards a bunch of people who struggled to find patients, attached an infinite number of electrodes, and coped with new and sometimes very bulky devices. Judith van Laar, Maartje Vinken, Lean Beulen, hartelijk bedankt! I really do not know how I could have done without you. I would like also to thank Barbara Vermeulen, Chris Peters, and, for the time she spent in my 'new electrodes', Lena Gourmelon from Philips.

I would also like to express my gratitude to prof. Rob Sluijter and prof. Yutaka Tomita for our fruitful discussions and to dr. Jeremy Terrien, for our fervid debates on electrohysterography and for his companionship. I also had the fortune to work with several students, whom I wish to thank for their contribution to this thesis, in particular, Paul Aalen, Marco Gamba, Jesse Kavelaars, and Luc Vosters.

Many thanks to the whole SPS group! To the staff members, Diana, Anja, Harrie, Sjoerd, to the other PhD students, Hongming, Yan, Maarten, Joep, Brian, to the regular participants of the 'fake' and 'NOISE' SPS events, Harald, Andrei, Joep K., and Arijit, to the officemates I had in the last years, Jamal, Steven, C.K., Suzanne, Iman, and Rik, I would like to express my gratitude for the help, companionship, and inspiring discussions! Speaking of officemates, I cannot forget my friend Tanya, whose company I had the chance to enjoy away from the office as well. Tanya, thanks, because since you moved into our current office, the quality of my long days at the TU/e dramatically improved! I really enjoy having you around and I wouldn't know how to do without your precious suggestions and tips: you definitely know one more than the devil! I would like to take the chance of thanking another friend, Tamara, for her support and the pleasant talks during our *tête-à-tête* dinners.

Besides my colleagues, there is a number of people whom it is impossible not to mention, because they made my life in Eindhoven wonderful, even when my research was depressing me, and contributed to make the last years memorable. For this, my thanks go to: Blanca, David, the karaoke, the innumerable laughs, and lovely moments I had with them; to Ben, his kindness, and confusing English; to Chris and his patience in listening to my terrible Dutch; to Kim, Misha, and their hospitality; to Carlos (the Spanish oracle), Maria, and Zaragozaaaaa; to Lorenzo and his sumptuous dinners; to Brett and his Cosmos; to Cees and our painful squash matches; to Thierry and the Fox Brulee; to Reinhard, Andrea, and the Gulash; to Joost, Irina, and the recipe that I always forgot to give them; to Mari, her sweetness, and the cauliflower. Furthermore, I would like to thank Emilie, Dani, Judit, Monica, Johan, Jose Ramon, Maurizio, Shanna, Matt, Dana, and Erik for the wonderful evening, dinners, and parties.

Even being far away, I still have many good friends back in Italy whom I wish to thank because they have been always close to me: in the good times to celebrate and in the bad times to support. Moreover, I am grateful to them because they have warmly welcomed me whenever I got back and have often visited me over here. Grazie mille a Gigia, Checca, Laura, Francesca, Paola, la Rossa, Marì, Antonello, Renzo, Olga, e Bice.

Un grazie di cuore va alla mia famiglia, a mio padre, alle mie sorelle, Maria Teresa e Francesca, e a Luca per essermi sempre stati vicini e avermi calorosamente sostenuto in ogni mia scelta. Un grazie speciale va ai miei nipoti, in particolare a Ginevra, Emma, e Filippo perchè l'affetto e l'ammirazione che hanno sempre dimostrato nei miei confronti sono stati uno stimolo eccezionale a fare sempre meglio e non deludere le loro aspettative. Infine vorrei ringraziare la famiglia Balzano per la generosità e l'accoglienza (nonchè per i favolosi medaglioni e le pizze di grano). Grazie!

Last but not least I would like to thank Luigi, my 'better half' and best friend, for the fun we had, his love, his support, his patience, and for his exceptionally positive nature that even in the worst moments made me feel serene and confident that any difficulty could have been overcome and, eventually, everything would have been alright.

C.

Curriculum Vitae

Chiara Rabotti was born in Florence (Italy) in 1977. In 2004 she received the M.Sc. degree in electrical engineering from the University of Florence, Italy, with a master thesis on the analysis of carotid artery blood flow by ultrasound echo-Doppler. Since 2005 she is a PhD student at the Signal Processing Systems Group of the Eindhoven University of Technology in the Netherlands. Her research concerns the characterization of the uterine activity by electrohysterography. Since September 2009 she is an employee of TMS International on a project aiming at the development of a telemedicine system for pregnancy monitoring. She is a member of the IEEE Engineering in Medicine and Biology Society.